A Study on Nonlinear Static Deflection and Free Vibration Behaviour of Functionally Graded Timoshenko Micro-Beam Based on Modified Couple Stress Theory

Thesis Submitted in Partial Fulfillment of the Requirements for the Degree of

Master of Engineering in Mechanical Engineering

By

SAMRAT

[Examination Roll No: M4MEC24008]

[University Registration No: 163710 of 2022-2023]

Under the Guidance of

Dr. DEBABRATA DAS

DEPARTMENT OF MECHANICAL ENGINEERING

FACULTY OF ENGINEERING & TECHNOLOGY

JADAVPUR UNIVERSITY

KOLKATA – 700032

MAY 2024

FACULTY OF ENGINEERING AND TECHNOLOGY

JADAVPURUNIVERSITY

CERTIFICATE OF APPROVAL*

This foregoing thesis is hereby approved as a credible study of an engineering subject carried out and presented in a manner satisfactory to warrant its acceptance as a prerequisite to the degree for which it has been submitted. It is understood that by this approval the undersigned do not endorse or approve any statement made, opinion expressed or conclusion drawn therein but approve the thesis only for the purpose for which it has been submitted.

COMMITTEE ----------

ON FINAL EXAMINATION FOR

EVALUATION OF THE THESIS ----------

***Only in case the thesis is approved**

FACULTY OF ENGINEERING AND TECHNOLOGY

JADAVPURUNIVERSITY

CERTIFICATE OF RECOMMENDATION

I hereby recommend that the thesis presented under my supervision by ***SRI SAMRAT*** *entitled* "**A Study on Nonlinear Static Deflection and Free Vibration Behaviour of Functionally Graded Timoshenko Micro-Beam Based on Modified Couple Stress Theory**" *be accepted in partial fulfillment of the requirements for the degree of* ***Master of Engineering in Mechanical Engineering***.

Countersigned

Thesis Supervisor

Head of the Department
Department of Mechanical Engineering

Dean
Faculty of Engineering and Technology

DECLARATION OF ORIGINALITY AND COMPLIANCE OF ACADEMIC ETHICS

I hereby declare that the thesis contains literature survey and original research work by the undersigned candidate, as a part of his ***MASTER OF ENGINEERING IN MECHANICAL ENGINEERING*** studies. All information in this document have been obtained and presented in accordance with the academic rules and ethical conduct.

I also declare that, as required by these rules of conduct, I have fully cited and referenced all the material and results that are not original to this work.

Name: **SAMRAT**

Examination Roll Number: **M4MEC24008**

Class Roll Number: **002211202015**

University Registration No: **163710 of 2022-2023**

Thesis Title: ***A Study on Nonlinear Static Deflection and Free Vibration Behaviour of Functionally Graded Timoshenko Micro-Beam Based on Modified Couple Stress Theory***

Signature with Date:

ACKNOWLEDGEMENT

First and above all, I praise God, the almighty for providing me this opportunity and granting me the capability to proceed successfully. This thesis appears in its current form due to the assistance and guidance of several people. I would therefore like to offer my sincere thanks to all of them.

The author expresses his deep sense of gratitude to his supervisor, Dr. Debabrata Das, Professor, Department of Mechanical Engineering, Jadavpur University, for his inspiration, support, academic and personal guidance throughout the course work. I'm grateful to him for being very supportive in letting me pursue my interests outside of academics, and encouraging me to learn and read widely. I'm grateful for this opportunity and look forward to continue my interactions with him in future.

I'm happy to be a part of the Applied Mechanics Laboratory, Mechanical Engineering Department, Jadavpur University and my thanks also goes to all laboratory assistants for providing excellent working experience.

My thanks also goes to all my batch mates who have made the atmosphere in my classes lively. The excellent cooperation and support by research scholars, namely Mr. S. Pal and Mr. B. Sikder are thankfully acknowledged.

Last, but most importantly, I'm grateful to my parents, brother, sister and family for their love, blessings and support throughout this endeavor. This thesis, a fruit of the combined efforts of my family members, is dedicated to them as a token of love and gratitude.

Date: May 2024

(SAMRAT)

Contents

List of Symbols

E	Young's modulus of elasticity
E_f	Effective elastic modulus
f_i	Body force
G	Shear modulus
G_f	Effective shear modulus
k	Material gradation index
$\left[k_{cl}^{\ l}\right]$	Stiffness matrix due to classical strain energy containing only linear terms
$\left[k_{cl}^{\ nl}\right]$	Stiffness matrix due to classical strain energy containing only nonlinear terms
$\left[k_{ncl}\right]$	Stiffness matrix due to non-classical strain energy
$\left(k_{cl}^{\ l}\right)^T$	Tangent stiffness matrix due to classical strain energy containing only linear terms
$\left(k_{cl}^{\ nl}\right)^T$	Tangent stiffness matrix due to classical strain energy containing only nonlinear terms
$\left(k_{ncl}\right)^T$	Tangent stiffness matrix due to non-classical strain energy
k_s	Shear correction factor
$\left[K_T\right]$	Tangent stiffness matrix
L, h, b	Length, thickness, width of the beam respectively
l	Material length scale parameter
$\left[M\right]$	Mass matrix
m	Couple stress tensor
M_f	Effective material property
$\left\{P\right\}$	Load vector
p	Intensity of the uniformly distributed load

T	Kinetic energy
T_i	Surface Traction
U	Strain energy
u, v, w	Displacement in x, y, z direction respectively
U_o	Strain energy density
U_1	Classical strain energy
U_2	Non-classical strain energy
V	Potential of the external loads
χ	Curvature tensors
δ	Variational operator
$\varepsilon_{ij}, \varepsilon$	Strain tensor
$\phi(x)$	Rotation angle of the beam cross-sections around y-axis
φ_i^w, φ_i^u, φ_i^ϕ	Set of orthogonal admissible functions for w, u, ϕ respectively
γ	Shear strain
μ_f	Effective Poisson's ratio
Π	Potential energy
θ	Rotation vector
ρ_f	Effective density
σ_{ij}, σ	Stress tensor
τ	Shear stress
ω	Frequency of the free vibration
ζ	Lagrangian

List of Figures

List of Tables

Chapter 1

INTRODUCTION

1.1 Introduction

Thin beams are common structural elements used in micro-electro-mechanical systems (MEMS) that have garnered a lot of attention because of their high-precision measurement capabilities (Kong et al. (2008)). Owing to their numerous advantages, they are extensively employed in micro- and nanoscale technologies, including micro-electro-mechanical transducers and atomic force microscopy (AFM), which serve as the foundation for chemical and biological sensors (Abbasion et al. (2009)).

Micro-beams, function at micron and submicron scales, where behaviour is greatly influenced by small-scale effects. Experimental studies have shown that size-dependent static and vibration behaviours observed in micro-structures are poorly captured by traditional continuum theories. As a result, nonclassical continuum theories have gained popularity in the study of micro-scaled structures. Examples of these theories include nonlocal, strain gradient, and couple stress theories. Classical couple stress theory was founded by Mindlin and Tiersten (1962) and other scholars, including Toupin (1962). In comparison to Lame constants for isotropic elastic materials, their formulations incorporate higher-order rotation gradients as the anti-symmetric element of second-order deformation gradients, resulting in the introduction of four material constants.

Modified couple stress theory (MCST) was proposed by Yang et al. (2002) by introducing a new, higher-order equilibrium equation while considering the equilibrium equation of moments of couples. Unlike the classical couple stress theory, this modification includes only one internal material length scale parameter and employs a symmetric couple stress tensor. The inclusion of an asymmetric couple stress tensor and the involvement of a single length scale

parameter are the two primary benefits of the MCST over the classical couple stress theory, as noted by Ma et al. (2008). This is because the strain energy density function is solely dependent on the strain and the symmetric part of the curvature tensor. The effect of micro-structural elements on the overall mechanical response of the material is taken into account by the internal material length scale parameter (l). By adding this parameter to the theory, MCST aims to include size-dependent effects that are ignored by classical continuum mechanics. This internal material length scale is a critical parameter in MCST. Several experimental investigations were carried out by researchers to ascertain this material length scale parameter for a particular material. The micro-bend test was one of several common techniques, along with the micro-torsion and micro-/nano-indentation tests, that Stolken and Evans used back in 1998 to measure this crucial parameter, Additionally, scientists have discovered that a material's material length scale parameter varies depending on how it is measured rather than having a fixed value. For instance, Park and Gao's (2006) research on epoxy micro-beams discovered a value of 17.6 micrometers (μm), but only for beams with a thickness of 20-115 μm. The investigation of vibrations in thin copper micro-beams by Li et al. (2018) yielded a value of 1.422 μm for its material length scale parameter. So, in addition to being a material constant, the material length scale parameter used in couple stress theories also depend on the size of the structure (Khorshidi (2018)).

Functionally graded materials (FGMs) have special thermo-mechanical properties that make them a revolutionary development in material engineering. Because of their microscopically diverse compositions, FGMs exhibit a continuously varying mechanical profile in contrast to traditional composites. The problem of high transverse shear stresses that are generally present when bonding dissimilar materials with notable differences in properties is lessened by this gradient compositional variation. FGMs avoid issues related to stress concentration by smoothly varying the volume fractions of component materials, such as metals and ceramics, guaranteeing the maintenance of continuous stress fields throughout their structure. This novel micro-structural design creates new opportunities in several engineering and scientific domains. FGMs exhibit potential for use in AFM, micro- and nano-structures, micro-sensors and micro-actuators, as well as MEMS (Ke and Wang (2011)). Component design for these systems can be made with an unprecedented degree of flexibility due to their ability to precisely tune material properties at the microscopic level. Modern developments in material

processing methods have improved the viability and usefulness of FGMs even more. In micro-systems, FGMs of thin films containing shape memory alloys have shown impressive potential (Fu et al. (2003)). The combination of material science and structural design represents a paradigm shift in the way we approach materials and structures in a variety of applications, as well as an extension of engineering possibilities.

The goal of the current work is to determine the nonlinear static deflection and natural frequency of a Timoshenko beam under uniformly distributed loading for four different types of boundary conditions, namely, Clamped-Clamped (CC), Clamped-Hinged (CH), Hinged-Hinged (HH) and Clamped-Free (CF). The formulation takes into account the moderate rotation of the transverse normal through the von Kármán nonlinear strain and the through-thickness power-law variation of a two-constituent material for four different combinations. The formulation is based on Timoshenko beam theory, the von Kármán geometric nonlinearity, power-law variation of the material, and a modified couple stress theory. The governing equations for the static deflection are derived using principle of minimum potential energy, whereas the governing equations for free vibration are derived using Hamilton's principle. The solutions of the governing equations are obtained using Ritz method.

1.2 Literature Review

For the past few decades, a large number of researchers have focused on the static, dynamic and buckling analysis of homogeneous and non-homogeneous micro-beams using a range of analysis techniques. In this section, very brief review of those works is provided.

1.2.1 Static, Dynamic and Buckling Behaviour of Homogeneous Beams

We've selected a few recent papers in which the researchers reported very high-quality work on the mechanical behaviour of homogeneous beams, including their static, dynamic and buckling behaviour. Hariz et al. (2022) presented buckling solutions for a quasi-static Timoshenko beam subjected to longitudinal force and an elastic wall. It analysed Haringx and Engesser models, derives buckling stress and shape expressions, establishes wall rigidity relations, and introduces a yield limit. Loya et al. (2022) examined the dynamic behaviour of cracked Timoshenko beams in a Winkler elastic medium, focusing on obtaining their natural

frequencies of bending vibration. The beam was modeled as two segments connected by massless springs, with stiffnesses proportional to shear force and bending moment. The methodology calculated natural frequencies based on various parameters. Li et al. (2023) examined the vibration modes of thin web gears in aerospace transmission systems, focusing on their impact on system stability. It suggested instability in out-of-plane vibration, with discrete springs worsening it. Frequency veering was observed, and a Timoshenko gear pair model with a coupling mesh stiffness matrix provided valuable insights for designing thin web gear transmission systems in aerospace applications. Cannizzaro et al. (2023) introduced a distributional model that considers both flexural and shear concentrated flexibilities in Timoshenko beams, enhancing their governing equations. It used generalized function theory to provide a closed-form solution for vibration modes and frequency equations, offering insights for structural analysis and design.

Rodríguez-Cruz et al. (2023) demonstrated that degenerate states of a beam with free ends, with anti-symmetrical transverse mode shape, tended asymptotically to the thickness-shear mode in the infinitely long beam limit. Wriggers (2023) explored the use of the virtual element method (VEM) to develop Timoshenko beam elements, a straightforward and exact formulation that can be integrated into classical finite element codes. This method was particularly useful for nonlinear structural problems involving large deflections and rotations. The Theory of Functional Connections (TFC) was used by Yassopoulos et al. (2023) to analyze static beams, incorporating von Kármán nonlinearity and Timoshenko–Ehrenfest beam theory. The authors compared TFC results with Finite Element Method (FEM) solutions, highlighting its advantages for stress analysis and solving buckling and free vibration problems. TFC offered more accurate solutions and faster solution times. Sabzehzar et al. (2024) introduced the equivalent beam approach for assessing truss structures strength and deflection. It revealed that the Euler-Bernoulli beam model was inadequate and had a high error rate. The Timoshenko beam method's accuracy depended on the selection of the Timoshenko shear coefficient. The paper proposed an exponential relationship for optimizing this coefficient. Torres-Guzmán et al. (2024) obtained closed-form expressions for the transfer matrix of free oscillations in finite periodic Timoshenko-Ehrenfest beams. It used the Cayley-Hamilton theorem to derive a fourth-order recursive relation for matrix coefficients, leading to the definition of Tetranacci Polynomials. The recursive

relation allowed for computing the N^{th} power of the transfer matrix without requiring the matrix product. The formalism can be extended to waves propagating in finite periodic layers.

1.2.2 Static, Dynamic and Buckling Behaviour of FGM Beams

In addition, we have chosen a few recent papers where the researchers have conducted excellent research on the static, dynamic and buckling behaviours of FGM beams. Rahimi et al. (2013) examined post-buckling behaviour of functionally graded (FG) beams using an exact solution method. It employed nonlinear strain-displacement relationships and Hamilton's principle. The study also analyses linear vibration, examining the influence of parameters like power-law exponent, boundary conditions, and beam geometry on static deflection and vibration frequencies. Mohanty et al. (2023) examined the parametric stability of a Timoshenko non-uniform sandwich beam on a Pasternak foundation, using extended Hamilton's principle, Galerkin method, and Hills equations. The results were visualized through plots and analyzed using MATLAB programming. Yee et al. (2023) presented a new theoretical approach to model the free vibrations of FG graphene platelets reinforced thick beams with a single-edge crack. The crack was modelled using strain-displacement, strain-stress, velocity-momentum, and dynamic equilibrium equations, resulting in complex coupled motion equations. The methodology was verified through simplified models and comparisons with literature and finite element software results. Patil et al. (2023) investigated the influence of porosity and temperature on the buckling and vibration properties of FG sandwich beams in a thermal environment. It used finite element (FE) analysis and FE solutions to analyze buckling and vibration. Shan et al. (2023) proposed a Timoshenko-beam FE model for shear-wall structures to accurately capture shear-flexure coupling behaviour for long-term structural health monitoring. Parametric identification framework and particle swarm optimization were used to update the model using vibration data. The model's accuracy is validated using data from the Walnut Creek building, showing good performance in predicting the building's response. Comparisons with shear-beam and Euler-Bernoulli-beam models further supported its superiority.

Zhang et al. (2023) presented a numerical method for analyzing the static, dynamic, and buckling behaviour of FG beams reinforced with graphene platelets. It used micro-scale homogenization and structural analysis to predict the elastic moduli of nanocomposite layers and

develop composite finite elements. The method was validated against existing literature and 3D printing results, showing good agreement. The study also examined the effects of boundary conditions, gradient distributions of graphene platelets and pores, microscopic parameters, and structural geometric dimensions on the static and dynamic performance of FG beams. Bi-directional gradient distribution patterns showed significant improvements in bending and dynamic performance. Xu et al. (2024) investigated FG beams reinforced with graphene platelets, porosity, and origami inclusions. It develops analytical solutions for static, dynamic, and buckling responses. A theoretical framework is established, including the principle of virtual work, reciprocal theorem of work, minimum potential, and complementary energies. The Ritz method is applied to derive expressions for transverse bending, rotation, frequencies and critical loads. Micromechanics approaches like the Halpin-Tsai expression were used to predict mechanical responses. Liu et al. (2024) introduced a variational framework based on Timoshenko-Ehrenfest beam theory and Hamilton's principle was used to study the dynamics of the Langevin transducer. By comparing computed resonance frequencies to 3D finite element models and laser Doppler vibrometry data, the framework's application using the FEM was validated. This approach provided a fast and accurate analysis of the free vibrations and dynamics of the transducer by taking into account the axial vibrations of the piezoelectric ceramic stack. Molina-Villegas et al. (2024) introduced the Green's Functions Stiffness Method (GFSM), a versatile approach for analyzing linear elastic static problems in non-uniform Timoshenko beams and frames, demonstrating its effectiveness in analyzing non-uniform structures under various loads.

1.2.3 Static Behaviour of Homogeneous Micro-/Nano-Beams

Ma et al. (2008) presented a microstructure-dependent Timoshenko beam model that considerd bending and axial deformations, including the Poisson effect, and incorporates a material length scale parameter. When normalcy was restored, the model became a microstructure-dependent Bernoulli-Euler beam model. The model predicted smaller deflection and rotation than the classical Timoshenko model, especially for very thin beams. The static and dynamic problems of Bernoulli-Euler beams were analysed by Kong et al. (2009) using the strain gradient elasticity theory. For cantilever beams, it evaluated the effects of size on bending response and natural frequencies and solved boundary value problems. Asghari et al. (2010)

presented a nonlinear Timoshenko beam model, incorporating MCST for size effects. It analyzed hinged-hinged beams, demonstrating nonlinear size-dependent static and free-vibration behaviours, using numerical and analytical methods. Karparvarfard et al. (2015) presented a non-linear differential equation of motion for small-scale Euler-Bernoulli beams using the second strain gradient theory, a non-classical continuum theory that accurately assesseed behaviour in structures, using a hinged-hinged beam. A microscale Timoshenko beam model for surface effects and flexoelectricity in piezoelectricity was presented by Yue et al. (2016). It resolved the issues of free vibration and static bending in a piezoelectric nano-beam under uniform load. The model showed that surface effects and flexoelectricity had a major impact on beam deformations, underscoring the significance of taking material properties into account when analysing piezoelectric nano-beams. A modified semi-continuum Euler beam model was developed by Shen and Li (2017) to study bending deformation of extremely thin beams at micro-/nano-scale thicknesses. The model considered external loads and boundary constraints, and its normalization was refined. The model also introduced a nonlinear semi-continuum model to predict elastic carrying capacity and analyse nonlinear bending deflections in extreme-thin beams. Comparisons with classical and nonlocal continuum models showed good agreement. Sobhy and Zenkour (2020) utilised MCST to investigate the bending behaviour of viscoelastic nano-beams on visco-Pasternak elastic foundations. The model included a material length scale coefficient and used Hamilton's principle. The study investigated how strains, damping structure, and material length scale affected nano-beam deflection and stresses, and it compared the expected outcomes with earlier studies.

1.2.4 Static Behaviour of FGM Micro-/Nano-Beams

Asghari et al. (2011) used MCST to provide a size-dependent formulation for FG Timoshenko beams that took thickness-related changes in beam attributes into account. The process yielded closed-form analytic formulations for static response parameters and generated governing differential equations. Chen et al. (2011) developed a model for composite laminated beams with first-order shear deformation using MCST. Compared to standard beam models, the model reduced deflections and stresses by properly capturing microstructure size effects. The MCST was applied by Salamat-talab et al. (2012) to analyse third-order shear deformation in FG

micro-beams. It applied Hamilton's principle to the analysis of bending and free vibration. The research deviated from the accepted models and revealed a significant size-dependency as the beam thickness got closer to the material length scale parameter. Mao et al. (2013) examined a mixed hardening plastic model, based on mechanism-based strain gradient plasticity, to dynamically assess FGM micro-beams. The model incorporated the effects of plastic strain gradients on flow stress, enabling both static and dynamic research. Utilising strain gradient theory, Tajalli et al. (2013) investigated a size-dependent formulation for FGM Timoshenko beams that captured the size-effects of micro-scaled structures. Five comparable length scale parameters were presented together with governing differential equations and boundary conditions. In this work, the results were evaluated using modified pair stress and classical theories. In order to evaluate micro- and macro-structural reactions, Romanoff et al. (2016) presented advanced non-local sandwich beam theories that included thick-faces beam, modified couple stress, and homogenization–localization. Convergence was demonstrated computationally, extending to different plates and microstructures. Yang et al. (2017) combined the zigzag and couple stress theories to provide a composite laminated beam model. By applying Reissner's Mixed Variational Theorem, it made precise displacement and stress predictions. Scale effects affected stiffness, displacements, and stresses, according to analytical solutions. Nguyen et al. (2018) investigated size-dependent behaviours in micro laminated composite beams. Ritz functions were presented in this article. It included the Lagrange equations, the displacement field, and the modified couple stress theory. The model offered effective solutions by forecasting size-dependent reactions in buckling, vibration, and bending. Sahmani et al. (2018) predicted nonlinear bending behaviour of porous micro-/nano-beams reinforced with graphene platelets using the nonlocal strain gradient theory of elasticity. It considered three different porosity distributions and Hamilton's principle. Using MCST, Babaei and Eslami (2022) examined nonlinear bending of functionally graded porous elastic tubes. The microtubes featured uniformly distributed porosity and temperature-dependent characteristics. Constitutive equations and nonlinear differential equations were derived using virtual displacement principle, uncoupled thermoelasticity theory, von Kármán kinematic assumptions, and higher-order shear deformation theory.

1.2.5 Dynamic Behaviour of Homogeneous Micro-/Nano-Beams

Kong et al. (2008) solved dynamic problems of FGM Bernoulli-Euler beams using MCST. It resolved two cantilever and simply supported beam boundary value issues. The new model predicted natural frequencies that showed size dependence. Ma et al. (2008) presented a microstructure-dependent Timoshenko FG beam model that considered bending and axial deformations, including the Poisson effect, and incorporated a material length scale parameter. When normalcy was restored, the model became a microstructure-dependent Bernoulli-Euler beam model. The model predicts smaller deflection and rotation than the classical Timoshenko model, especially for very thin beams. Abbasion et al. (2009) presented a model that considered surface elasticity and residual surface tension on the frequency of flexural vibrations in micro-beams. The study revealed that the frequency of micro and nano-scaled vibrations was size-dependent. The static and dynamic problems of Bernoulli-Euler beams were analysed by Kong et al. (2009) using the strain gradient elasticity theory. For cantilever beams, it evaluated the effects of size on bending response and natural frequencies and solved boundary value problems.

Asghari et al. (2010) presented a nonlinear Timoshenko beam model, incorporating modified couple stress theory for size effects. It analysed hinged-hinged beams, demonstrating nonlinear size-dependent static and free-vibration behaviours, using numerical and analytical methods. Sharma and Grover (2011) investigated the effects of surface conditions, beam dimensions, relaxation times, voids, and thermomechanical coupling on energy dissipation in thermoelastic damping in resonators of micro- and nano-electromechanical systems. It offered numerical outcomes from MATLAB simulations as well as analytical expressions. Using an Euler-Bernoulli model, Hendou and Mohammadi (2014) analysed the vibration of micro-beams with significant transverse deflection. Thermoelastic damping, integrated as imaginary stiffness, was the predominant damping mechanism. Using the Galerkin procedure and nonlinear normal mode theory, the equation of motion wass analysed. It was found that nonlinear modal analysis predicted extreme points in parameters such as frequency shift and inverse quality factor. Using Euler-Bernoulli theory, Sharma and Kaur (2014) examined transverse vibrations in a homogeneous isotropic, thermoelastic-diffusive thin beam. It looked at thermoelastic-diffusion-related deflection, thermal moment, mass moment, frequency shift, and damping.

In order to provide insights for the sensitivity design of resonant micro-gas sensors, Xu and Yang (2015) presented a multi-field coupled dynamics equation for a micro-beam and examined its natural frequencies, amplitude-frequency relationship, and system parameters. Karparvarfard et al. (2015) presented a non-linear differential equation of motion for small-scale Euler-Bernoulli beams using the second strain gradient theory, a non-classical continuum theory that accurately assessed behaviour in structures, using a hinged-hinged beam. Noori et al. (2016) explored the free vibration of micro-beams using three beam models, focusing on the first five natural frequencies, considering three length-scale-parameter/height ratios and five different boundary conditions, and solving equations using Hamilton's principle. A microscale Timoshenko beam model for surface effects and flexoelectricity in piezoelectricity was presented by Yue et al. (2016). It resolved the issues of free vibration and static bending in a piezoelectric nano-beam under uniform load. The model showed that surface effects and flexoelectricity had a major impact on beam deformations, underscoring the significance of taking material properties into account when analysing piezoelectric nano-beams. Habibi et al. (2019) investigated the size-dependent free vibration characteristics of magneto-electro-elastic nano-beams in a thermal environment, using MCST and Euler–Bernoulli beam model. Results showed increased length and decreased thickness decrease nano-beam natural frequencies. Using MCST, Ghasemi and Mohandes (2020) analysed the frequencies of cylindrical shells made of micro- and nano-fiber-metal laminate. It examined composites made of glass/epoxy, aramid/epoxy, and carbon/epoxy, with aluminium serving as the metal component. The micro and nano cylinders made of aramid reinforced aluminium laminate exhibited higher frequencies, and the results exhibited excellent agreement with previous research. Esen (2020) investigated the dynamic behaviour of size-dependent Timoshenko micro-beams under moving loads using the FEM. It focused on the interaction between the load and the beam, considering mass inertia effects. The study explored various parameters' effects on beam dynamics across various scenarios.

1.2.6 Dynamic Behaviour of FGM Micro-/Nano-Beams

Asghari et al. (2011) used MCST to provide a size-dependent formulation for Timoshenko FGM beams that took thickness-related changes in beam attributes into account. The process yielded closed-form analytic formulations for static response parameters and generates governing differential equations. Ke and Wang (2011) investigated the dynamic

stability of micro-beams made of FGM using MCST and Timoshenko beam theory. Using differential quadrature, Hamilton's concept, Bolotin's approach, and Mori-Tanaka homogenization, it examined free vibration. Ke et al. (2012) investigated the nonlinear free vibration of FGM micro-beams by the use of von Kármán geometric nonlinearity and MCST. To find vibration frequencies under various boundary conditions, it used Hamilton principle, a non-classical Timoshenko beam model, the Mori-Tanaka homogenization technique, and a numerical approach. A MCST based approach was applied by Salamat-talab et al. (2012) to analyse third-order shear deformation in FG microbeams. It applied Hamilton's principle to the analysis of bending and free vibration. The research deviated from the accepted models and reveals a significant size dependency as the beam thickness got closer to the material length scale parameter. Using Euler–Bernoulli beam theory and von Kármán geometric nonlinearity, Jia et al. (2015) examined the impacts of size effects on the free vibration of FG micro-beams under coupled forces such as electrostatic force, temperature changes, and Casimir force. The study emphasized how these elements interact significantly. Nguyen et al. (2016) used the Micro Genetic Algorithm (micro-GA) in conjunction with conventional beam theory to optimise vibration and lateral buckling in laminated composite beams. The ideal solution is strongly influenced by geometric factors, and micro-GA outperformed ordinary GA in terms of convergence rate and optimal solution.

Shafiei et al. (2016) integrated the MCST, von-Kármán geometric nonlinearity, and Euler-Bernoulli beam theory to investigate the nonlinear vibration of axially functionally graded (AFG) micro-beams. The model takes Hamilton's principle and a number of boundary conditions into account. According to the study, fundamental and second frequencies are impacted by the rate of cross-section change, which has implications for microstructure design. Simsek (2016) presented a new size-dependent beam model for analyzing the nonlinear free vibration of a FG nano-beam. It integrated nonlocal strain gradient theory (NLSGT) and Euler-Bernoulli beam theory, considering geometric nonlinearity. The model addressed coupling effects from unsymmetrical material variation and used Hamilton's principle to derive motion equations. The study presented a closed-form solution for nonlinear frequency. Using MCST, Ghasemi and Mohandes (2020) investigated the frequency of micro and nano fiber-metal laminate (FML) cylindrical shells. It studied vibrations in composites such as carbon/epoxy, glass/epoxy, and

aramid/epoxy using Love's first approximation shell theory and beam modal functions. Al-shujairi and Mollamahmutoğlu (2018) examined the dynamic stability of a FG sandwich micro-beam under parametric axial excitation and boundary conditions, including thermal effects. It used nonlocal strain gradient theory, first-order shear deformation beam theory, Hamilton's principle, and differential quadrature method to derive governing equations and solve differential equations. The study contributed to the field by providing insights into parametric instability regions. Nguyen et al. (2018) investigated size-dependent behaviours in micro laminated composite beams using Ritz functions. It included the Lagrange equations and the MCST. The model offered effective solutions by forecasting size-dependent reactions in buckling, vibration, and bending. Using a sophisticated mathematical model, Bhattacharya and Das (2019) investigated the free vibration behaviour of a spinning micro-beam. It dealt with Coriolis acceleration, geometric non-linearity, spin-softening, and high operating temperatures. In order to gain an understanding of the behaviour of the system in the non-dimensional speed vs frequency plane, the model was examined for different parameters and verified using the Ritz approach. Gul and Aydogdu (2021) investigated the free vibration analysis of FG periodic structure nano-beams via doublet mechanics theory, where the periodic FG nano-beams are modelled as a simple crystal lattice type. They derived micro strains and strains by expanding in Taylor series and obtained micro relations transformed to macro stress-strain relations. Saimi et al. (2023) examines the free vibratory behaviour of defective bidirectionally graded micro-beams with fractures using the MCST, and the Quasi-3D shear and normal deformation beam idea. It constructed mass and stiffness matrices using Gauss-Lobatto node architecture, DQ and Gauss-Lobatto quadrature techniques, and Lagrange's rule. The results offer a numerical basis for porous FG microstructure design.

1.2.7 Buckling Behaviour of Homogeneous and FGM Micro-/Nano-Beams

Akgöz and Civalek (2011) applied couple stress theories and strain gradient elasticity to study the stability of micro-sized beams. It used Bernoulli-Euler beam theory to present analytical solutions for nano-sized beams that are axially loaded. The research advanced the mechanical modelling of structures at the micro- and nanoscale. Using MCST and considering the theories of Euler-Bernoulli and Timoshenko beams as well as minimum potential energy, Abadi and Daneshmehr (2014) examined buckling in composite laminated beams. Size effects

and Fourier series expansions were included. The study examined the effects of material length, beam thickness, and length on the behaviour of micro composite laminated beams and compared its findings with previous research. Using MCST, Mohammadabadi et al. (2015) investigated the effect of temperature on size-dependent buckling in micro composite laminated beams. It used different cross-ply laminates to examine lamination, boundary conditions, and shear deformation. For hinged-hinged conditions, the governing equations and boundary conditions were solved analytically, and the generalised differential quadrature (GDQ) method was utilised to solve them numerically. Nguyen et al. (2016) used the Micro Genetic Algorithm (micro-GA) in conjunction with conventional beam theory to optimise vibration and lateral buckling in laminated composite beams. The ideal solution was strongly influenced by geometric factors, and micro-GA outperformed ordinary GA in terms of convergence rate and optimal solution. Shafiei and Kazemi (2017) investigated the nonlinear buckling behaviour of FG micro- and nano-beams composed of porous materials. It used MCST, Eringen's nonlocal theory, von Kármán geometric nonlinearity, and Euler-Bernoulli beam theory. Zandekarimi et al. (2018) investigated a circular microplate's thermal buckling and post-buckling behaviour under clamped boundary conditions and a uniform temperature rise. It analysed the behaviour in terms of length scale parameter, power law index, and thickness ratio using variational method, differential quadrature method, and iterative analysis. Under thermo-mechanical loading and boundary conditions, Taati (2018) provided an exact solution for the size-dependent buckling and post-buckling behaviour of FG micro-beams. It solved nonlinear equations by applying the minimum total potential energy principle and MCST. The study also emphasized how the lack of consideration for the stiffness of the flexural-extensional coupling limited the predictive power of Fourier series solutions in post-buckling behaviour.

1.3 Mathematical Background

` The mathematical formulation of the current thesis work is based on two energy principles of structural mechanics: minimum total potential energy principle and Hamilton's principle. The governing equations for the static deflection are derived using principle of minimum potential energy, whereas the governing equations for free vibration are derived using Hamilton’s principle. The solutions of the governing equations are obtained using Ritz method.

The solutions to the governing equations are obtained by approximating the displacement fields using the Ritz method. The displacement fields are approximated by using the orthogonal admissible functions that are produced by the Gram-Schmidt algorithm. In the end, the governing equations of the free vibration problem are transformed into an eigenvalue problem. A brief summary of the many principles and methods applied in the current thesis work is given in this section.

1.3.1 Minimum Total Potential Energy Principle

The principle of Minimum Potential Energy (MPE), states that: For conservative structural systems, of all the kinematically admissible deformations, those corresponding to the equilibrium state extremize (i.e., minimize or maximize) the total potential energy. If the extremum is a minimum, the equilibrium state is stable. In other words, the potential energy is stationary, and it could be maximum or minimum (Shames and Dym (2009)). For stable structures, it undergoes minimum value with respect to displacements.

The principle of virtual work, in variational form (first variation), is given as:

$$\int_s T_i \delta u_i ds + \int_v f_i \delta u_i dv = \int_v \sigma_{ij} \delta \varepsilon_{ij} dv. \tag{1.1}$$

Here δu is the virtual displacement; $\int_s T_i \delta u_i ds$ and $\int_v f_i \delta u_i dv$ are the virtual work by those vectors which are present in the surface and by body force respectively; $\int_v \sigma_{ij} \delta \varepsilon_{ij} dv$ is the internal virtual work. For elastic materials, the expression for stress is given by:

$$\sigma_{ij} = \frac{\partial U_0}{\partial \varepsilon_{ij}}, \tag{1.2}$$

where U_o is the strain energy density. Putting σ_{ij} in the Eq. (1.1), we get,

$$\int_s T_i \delta u_i ds + \int_v f_i \delta u_i dv = \int_v \frac{\partial U_0}{\partial \varepsilon_{ij}} \delta \varepsilon_{ij} dv. \tag{1.3}$$

The variation in strain energy density is given by

$$\delta U_0 = \frac{\partial U_0}{\partial \varepsilon_{ij}} \delta \varepsilon_{ij}. \tag{1.4}$$

Putting it in Eq. (1.3), we get,

$$\int_s T_i \delta u_i ds + \int_v f_i \delta u_i dv = \int_v \delta U_0 dv \tag{1.5}$$

By the properties of the calculus of variation, we can write,

$$\delta\left(\int_s T_i u_i ds + \int_v f_i u_i dv\right) = \delta\left(\int_v U_0 dv\right)$$

$$\Rightarrow \delta(-V) = \delta(U)$$

$$\Rightarrow \delta(U+V) = 0. \tag{1.6}$$

Here V is the potential of the external loads. It is negative of the external load acting on the structure. The strain energy U is the elastic energy stored in deformed structure. So, the potential energy (Π) of a structural system is defined as the sum of the strain energy (U) and the work potential (V), i.e.,

$$\Pi = U + V. \tag{1.7}$$

At equilibrium, we know that the potential energy is minimum (extremum). Hence,

$$\delta(\Pi) = \delta(U+V) = 0 \tag{1.8}$$

This expression only says that Π is stationary with respect to variations in the displacement field when the body is in equilibrium. So in structural problems, variational approach is used to find the displacement (dependent) functions that make the potential energy value stationary and this principle is only valid for elastic materials.

1.3.2 Hamilton's Principle

Hamilton's principle states that, of all the paths of admissible configurations that the body can take as it goes from configuration 1 at time t_1 to configuration 2 at time t_2, the path that satisfies Newton's law at each instant during the interval is the path that extremizes the time integral of the Lagrangian during the interval (Shames and Dym (2009)).

$$\delta\left(\int_{t_1}^{t_2} \zeta dt\right) = 0, \tag{1.9}$$

where ζ is the Lagrangian which is given by, $\zeta = T - \Pi$, i.e., $\zeta = T - U - V$.

Here T is the kinetic energy. Putting the value of ζ in Eq. (1.9), the final expression of Hamilton's principle is given as follows

$$\delta\left(\int_{t_1}^{t_2}\left(T-U-V\right)dt\right)=0\,. \tag{1.10}$$

1.3.3 Ritz Method

The Ritz method is an approximation method for solving variational problems (Shames and Dym (2009)). Instead of focusing on the differential equation, the Ritz method looks for a solution to the variational problem directly on the functional of the form given below:

$$I\left[y(x)\right]=\int_{x_a}^{x_b}F\left(x,y(x),y(x)'\right)dx. \tag{1.11}$$

The fundamental concept in Ritz method is to use a linear combination of n known functions $\phi_i(x)$ to approximate the solution function $y(x)$, i.e.,

$$\tilde{y}(x)=\sum_{i=1}^{n}C_i\phi_i(x); \tag{1.12}$$

Here $\phi_i(x)$ must satisfy the essential boundary conditions for $y(x)$. $\tilde{y}(x)$ indicates that the solution is approximate solution and the coefficients C_i are unknown scalars. These scalars are determined by substituting the linear combination $\tilde{y}(x)$ into the functional (1.11). Since the functions $\phi_i(x)$ are known, so their derivatives are $\phi_i'(x)$. The derivative of $\tilde{y}(x)$ can therefore be written as

$$\tilde{y}(x)'=\sum_{i=1}^{n}C_i\phi_i(x)', \tag{1.13}$$

Substituting the expression $\tilde{y}(x)$ and $y(x)$ into Eq. (1.11), we get the functional depending on $y(x)$ which is converted into a function Ψ of the n variables $\phi_i(x)$ given as below:

$$\Psi\left(C_1,C_2,...C_n\right)=\int_{x_a}^{x_b}F\left(x,\sum_{i=1}^{n}C_i\phi_i(x),\sum_{i=1}^{n}C_i\phi_i(x)',\right)dx. \tag{1.14}$$

Here the functions $\phi_i(x)$ are known, and the integration can be carried out with respect to the variable *x*. The variational problem has been reduced to finding the coefficients C_i for which the function attains an extreme value, subject to the boundary conditions.

In structural mechanics problems, this functional is the potential energy Π, which has to be minimized to get stable equilibrium state. From Eq. (1.14), to extremize Ψ, i.e., minimizing or maximizing the Ψ, we can write $\delta(\Psi)=0$. It implies:

$$\frac{\partial \Psi}{\partial C_1}=0,\frac{\partial \Psi}{\partial C_2}=0,\frac{\partial \Psi}{\partial C_3}=0,\frac{\partial \Psi}{\partial C_4}=0,...=\frac{\partial \Psi}{\partial C_n}=0. \tag{1.15}$$

Solution of equation (1.15) results in a series of *n*-equations, which can be solved to determine the parameters C_i. Putting the value of C_i along with $\phi_i(x)$ in Eq. (1.12) yields the final approximate solution of $\tilde{y}(x)$.

1.3.4 Modified Couple Stress Theory (MCST)

The MCST presented by Yang et al. (2002) evolved from the classical couple stress theory proposed by Mindlin (1964). The leading advantage of the MCST over the classical couple stress theory is the involvement of only one additional material length scale parameter *l*. According to the MCST, the strain energy density is a function of both strain tensor (conjugated with stress tensor) and curvature tensor (conjugated with couple stress tensor) (Yang et al. (2002)). So the strain energy in an isotropic linear elastic material is given as below:

$$U=U_1+U_2, \tag{1.16}$$

where U_1 is the classical strain energy, U_2 is the non-classical strain energy. The expression for U_1 and U_2 are given as follows:

$$U_1=\frac{1}{2}\int_V(\sigma:\varepsilon)dV \tag{1.17}$$

$$U_2=\frac{1}{2}\int_V(m:\chi)dV \tag{1.18}$$

Here V denotes volume, σ and ε are classical stress and strain tensors respectively; m and χ are couple stress and curvature tensors respectively. Their forms are given as follows:

$$\varepsilon = \frac{1}{2}\left(\nabla u + (\nabla u)^T\right), \tag{1.19}$$

$$\sigma = E\varepsilon, \tag{1.20}$$

$$m = 2Gl^2\chi, \tag{1.21}$$

$$\chi = \frac{1}{2}\left(\nabla\theta + (\nabla\theta)^T\right). \tag{1.22}$$

Here $\nabla = i\frac{\partial}{\partial x} + j\frac{\partial}{\partial y} + k\frac{\partial}{\partial z}$; u is the displacement vector; E and G are Young's modulus and shear modulus respectively; l is the material length scale parameter and θ is the rotation vector which is given as follows:

$$\theta = \frac{1}{2}curl(u) \tag{1.23}$$

1.4 Description of the Problem

In the present thesis work, we have studied the static deflection and free vibration behaviour of FG Timoshenko micro-beam for four different boundary conditions namely Clamped-Clamped (CC), Clamped-Hinged (CH), Hinged-Hinged (HH) and Clamped-Free (CF). It is assumed that the beam is subjected to uniformly distributed loading. In all these problems, metal-ceramic FGM compositions are considered, for which the through-thickness continuous material gradation is assumed following power law variation of volume fraction of the constituents. The size effect has been incorporated into the formulation using modified couple stress theory (MCST).

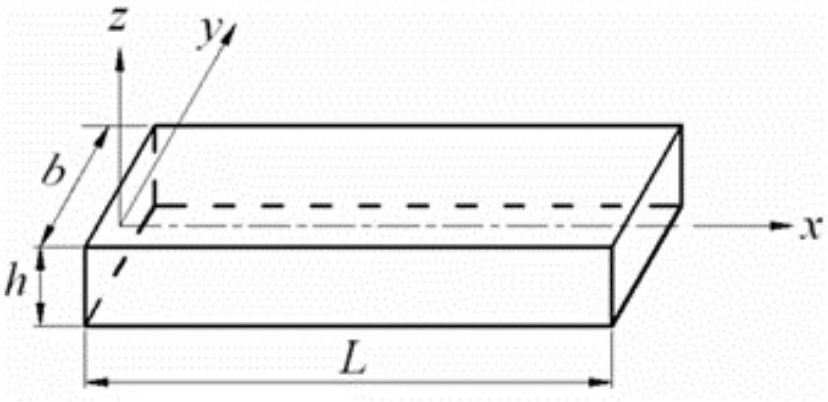

Fig. 1.1: Beam with dimensions and coordinate axes.

For the present study, a beam (Fig.1.1) having length L, thickness h and width b is considered. The axial, width and thickness coordinates are denoted by x, y and z respectively, where the origin lies at the left end in the mid-plane of the beam. The mathematical formulation is based on Timoshenko Beam theory (TBT). The governing equations for static deflection are derived using minimum potential energy principle. These governing equations are non-linear in nature as von Kármán type non-linearity has been incorporated in the expression of classical strain. For the free vibration problem, small amplitude free vibration behaviour of the pre-loaded beam is studied using Hamilton's principle. In both these problems, the governing equations are solved by approximating the displacement fields following Ritz method. The main objective of the thesis work is to determine static deflection and the free bending vibration frequencies of FG micro-beam. The model is successfully validated with the available results. An extensive set of results are presented for predicting the static deflection and free vibration frequency of the FGM micro-beam. The results are presented to show the effects of size-dependent thickness, material gradation index, FG composition and boundary conditions.

1.5 Chapter Summary

The introduction outlines the increasing use of thin beams in micro-electro-mechanical systems (MEMS) and nano-scale technologies, highlighting their significance in various applications. It also emphasizes the importance of non-classical continuum theories in capturing the size-dependent static and vibration behaviours observed in microstructures, leading to the development of the modified couple stress theory (MCST). The literature review provides a detailed overview of the research conducted on the static, dynamic, and buckling behaviour of both homogeneous and FG micro-/nano-beams. It covers the application of advanced theories such as strain gradient elasticity theory, modified couple stress theory, and nonlocal sandwich beam theories in analysing the behaviour of micro-beams. Additionally, the chapter delves into the mathematical background, describing the principles of minimum total potential energy, Hamilton's principle and the Ritz method. Furthermore, it introduces the MCST, outlining its formulation and the strain energy density function. The problem description section outlines the specific focus of the thesis work, detailing the investigation of the static deflection and free vibration behaviour of FG micro-beams under various boundary conditions. In summary, the

chapter provides a comprehensive overview of the study's background, literature review, mathematical formulation, and the specific problems addressed, offering a clear and structured insight into the research focus and objectives.

Chapter 2

MATHEMATICAL FORMULATION

2.1 Introduction

We have studied the static deflection and free vibration behaviour of FG Timoshenko micro-beams for four different boundary conditions namely Clamped-Clamped (CC), Clamped-Hinged (CH), Hinged-Hinged (HH) and Clamped-Free (CF). It is assumed that the beam is subjected to uniformly distributed loading. Metal-ceramic FGM compositions are considered, for which the through-thickness continuous material gradation is assumed following power law variation of volume fraction of the constituents. The size effect has been incorporated into the formulation using modified couple stress theory (MCST).

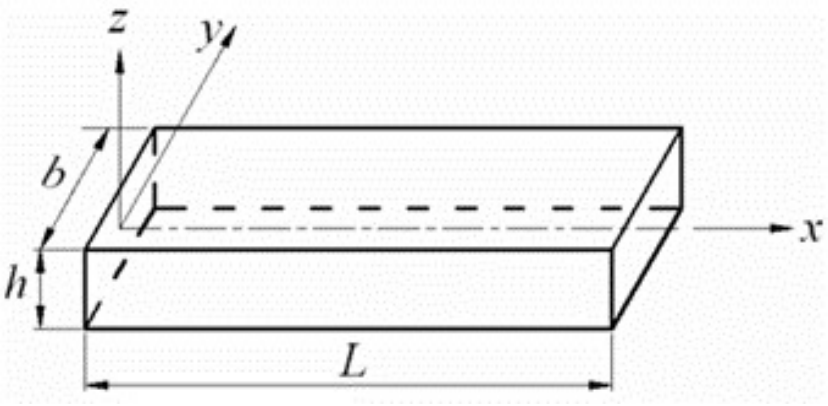

Fig. 2.1: Beam with dimensions and coordinate axes.

For the present study, a beam (Fig.2.1) having length L, thickness h and width b is considered. The axial, width and thickness coordinates are denoted by x, y and z respectively, where the origin lies at the left end in the mid-plane of the beam.

2.2 FGM Modeling

The beam material is assumed to be functionally graded along the z direction. The power law variation of the volume fraction of the metallic and ceramic phases is considered. Hence, any effective material property M_f, following Voigt model (Shen (2009)) is given as follows:

$$M_f(z) = M_m + \left(M_c - M_m\right)\left(\frac{z}{h} + \frac{1}{2}\right)^k \tag{2.1}$$

where, k $\left(0 \le k \le \infty\right)$ is the volume fraction index, and the subscripts c and m denote the ceramic and metallic constituents respectively. The top layer $\left(z = +h/2\right)$ is purely ceramic and the bottom layer is pure metallic $\left(z = -h/2\right)$. The effective elastic modulus (E_f), effective Poisson's ratio (μ_f), effective density (ρ_f) and effective shear modulus (G_f) are therefore given by the following equations.

$$E_f(z) = E_m + \left(E_c - E_m\right)\left(\frac{z}{h} + \frac{1}{2}\right)^k, \tag{2.2a}$$

$$\mu_f(z) = \mu_m + (\mu_c - \mu_m)\left(\frac{z}{h} + \frac{1}{2}\right)^k, \tag{2.2b}$$

$$\rho_f(z) = \rho_m + (\rho_c - \rho_m)\left(\frac{z}{h} + \frac{1}{2}\right)^k, \tag{2.2c}$$

$$G_f = E_f / 2(1 + \mu_f). \tag{2.2d}$$

It is to be noted that k =0 implies a purely ceramic beam, and as the value of k increases, the volume fraction of the metal increases. In the present work, we have taken four FG materials. They are given as follows: Stainless Steel/Alumina (SUS304/Al_2O_3) [FGM1], Stainless Steel/Silicon Nitride (SUS304/Si_3N_4) [FGM2], Stainless Steel/Zirconia (SUS304/ZrO_2) [FGM3] and Titanium Alloy/Zirconia (Ti-6Al-4V/ZrO_2) [FGM4]. Table 2.1 shows the material properties of different constituents at room temperature i.e., 300 K.

Table 2.1: Material properties of FGM constituents at 300 K.

Property	Stainless Steel (SUS304)	Titanium Alloy (Ti-6Al-4V)	Silicon Nitride (Si_3N_4)	Zirconia (ZrO_2)	Alumina (Al_2O_3)
E (GPa)	207.79	105.70	322.27	168.06	320.24
μ	0.318	0.298	0.240	0.298	0.260
ρ (kg/m^3)	8166	4429	2370	3000	3750

2.3 Displacement Fields

The displacements fields $\{u, w\}$ along the axial and transverse directions for the Timoshenko beam model are given as follows,

$$u(x,z,t) = u_0(x,t) - z\,\phi(x,t), \tag{2.3a}$$

$$w(x,t) = w_0\,. \tag{2.3b}$$

Here $u_0(x,t)$ is the axial displacement of the mid-plane and $\phi(x)$ is the rotation of the transverse normal.

2.4 Strain and Curvature Fields

2.4.1 Strain Fields

Strain in the *x*-direction with von Kármán non-linearity is given by

$$\varepsilon_{xx} = \frac{\partial u}{\partial x} + \frac{1}{2}\left(\frac{\partial w}{\partial x}\right)^2. \tag{2.4}$$

Putting Eqs. (2.3a) and (2.3b) into Eq. (2.4), the final expression of strain in *x*-direction is given as follows,

$$\varepsilon_{xx} = \frac{\partial u_0}{\partial x} - z\frac{\partial \phi}{\partial x} + \frac{1}{2}\left(\frac{\partial w_0}{\partial x}\right)^2. \tag{2.5}$$

The shear strain in *z*-direction and in *x*-plane is given as below,

$$\gamma_{xz} = \frac{\partial w}{\partial x} + \frac{\partial u}{\partial z} = \frac{\partial w_0}{\partial x} - \phi. \tag{2.6}$$

Due to symmetry, we can write,

$$\gamma_{xz} = \gamma_{zx} = \frac{\partial w_0}{\partial x} - \phi. \tag{2.7}$$

It is mentioned that the other components of the strain are zero.

2.4.2 Curvature Fields

Using the relations (1.22) and (1.23), and substituting the displacement fields given by Eqs. (2.3a) and (2.3b), the components of curvature tensor are given as below:

$$\chi_{xy} = \chi_{yx} = -\frac{1}{4}\left(\frac{\partial^2 w_0}{\partial x^2} + \frac{\partial \phi}{\partial x}\right), \tag{2.8a}$$

$$\chi_{xx} = \chi_{yy} = \chi_{zz} = \chi_{xz} = \chi_{zx} = \chi_{yz} = \chi_{zy} = 0. \tag{2.8b}$$

2.5 Stress and Couple Stress Fields

2.5.1 Stress Fields

The stress in the *x* direction and in plane normal to *x* is given by,

$$\sigma_{xx} = E_f \varepsilon_{xx}. \tag{2.9}$$

By putting the value of ε_{xx} from Eq. (2.4) into Eq. (2.9), we get,

$$\sigma_{xx} = E_f \left(\frac{\partial u_0}{\partial x} - z\frac{\partial \phi}{\partial x} + \frac{1}{2}\left(\frac{\partial w_0}{\partial x}\right)^2\right). \tag{2.10}$$

The shear stress in *x* plane and in *z* direction is same as in *z* plane along *x* direction. It is given by,

$$\tau_{xz} = \tau_{zx} = G_f k_s \gamma_{xz}. \tag{2.11}$$

Here k_s is the shear correction factor. By putting the value of γ_{xz} or γ_{zx} from Eq. (2.7), we get,

$$\tau_{xz} = \tau_{zx} = G_f k_s \left(\frac{\partial w_0}{\partial x} - \phi\right). \tag{2.12}$$

2.5.2 Couple Stress Fields

The nonzero component of couple stress tensor is given as below:

$$m_{xy} = 2G_f l^2 \chi_{xy} \tag{2.13}$$

By putting the value of χ_{xy}, which is given in Eq. (2.8a), the expression for m_{xy} is given as below:

$$m_{xy} = -\frac{G_f l^2}{2}\left(\frac{\partial^2 w_0}{\partial x^2} + \frac{\partial \phi}{\partial x}\right) \tag{2.14}$$

The components of couple stress tensor other than m_{xy} and m_{yx} are equal to zero, i.e.,

$$m_{xx} = m_{yy} = m_{zz} = m_{xz} = m_{zx} = m_{zy} = m_{yz} = 0 \tag{2.15}$$

2.6 Strain Energy, Work Potential and Kinetic Energy

2.6.1 Strain Energy

According to MCST, the strain energy in the combination of classical strain energy and non-classical strain energy is as given below:

$$U = U_1 + U_2 \tag{2.16}$$

Here U_1 and U_2 are the classical and non-classical strain energies respectively.

The expression for U_1 is derived as follows:

$$U_1 = \frac{1}{2}\int_V (\sigma : \varepsilon) dV$$

$$= \frac{1}{2}\int_V \left(\sigma_{xx}\varepsilon_{xx} + \tau_{xz}\gamma_{xz}\right) dV$$

$$= \frac{1}{2}\int_V \left(E_f {\varepsilon_{xx}}^2 + G_f k_s {\gamma_{xz}}^2\right) dV$$

$$= \frac{1}{2}\int_V \left(E_f \left(\frac{\partial u_0}{\partial x} - z\frac{\partial \phi}{\partial x} + \frac{1}{2}\left(\frac{\partial w_0}{\partial x}\right)^2 \right)^2 + G_f k_s \left(\frac{\partial w_0}{\partial x} - \phi \right)^2 \right) dV$$

$$= \frac{1}{2}\int_V \left\{ \begin{array}{l} E_f \left(\begin{array}{l} \left(\frac{du_0}{dx}\right) - 2z\left(\frac{d\phi}{dx}\right)\left(\frac{du_0}{dx}\right) + \left(\frac{du_0}{dx}\right)\left(\frac{dw_0}{dx}\right)^2 + z^2\left(\frac{d\phi}{dx}\right)^2 - \\ z\left(\frac{d\phi}{dx}\right)\left(\frac{dw_0}{dx}\right)^2 + \frac{1}{4}\left(\frac{dw_0}{dx}\right)^4 \end{array} \right) \\ +G_f k_s \left(\left(\frac{dw_0}{dx}\right)^2 - 2\phi\left(\frac{dw_0}{dx}\right) + \phi^2 \right) \end{array} \right\} dV$$

$$= \frac{1}{2}\int_0^L \int_A \left\{ \begin{array}{l} E_f \left(\begin{array}{l} \left(\frac{du_0}{dx}\right) - 2z\left(\frac{d\phi}{dx}\right)\left(\frac{du_0}{dx}\right) + \left(\frac{du_0}{dx}\right)\left(\frac{dw_0}{dx}\right)^2 + z^2\left(\frac{d\phi}{dx}\right)^2 \\ -z\left(\frac{d\phi}{dx}\right)\left(\frac{dw_0}{dx}\right)^2 + \frac{1}{4}\left(\frac{dw_0}{dx}\right)^4 \end{array} \right) \\ +G_f k_s \left(\left(\frac{dw_0}{dx}\right)^2 - 2\phi\left(\frac{dw_0}{dx}\right) + \phi^2 \right) \end{array} \right\} dA dx$$

$$= \frac{1}{2}\int_o^L \left\{ \begin{array}{l} \left(\begin{array}{l} EA\left(\frac{du_0}{dx}\right) - 2EQ\left(\frac{d\phi}{dx}\right)\left(\frac{du_0}{dx}\right) + EA\left(\frac{du_0}{dx}\right)\left(\frac{dw_0}{dx}\right)^2 + EI\left(\frac{d\phi}{dx}\right)^2 - \\ EQ\left(\frac{d\phi}{dx}\right)\left(\frac{dw_0}{dx}\right)^2 + \frac{1}{4}EA\left(\frac{dw_0}{dx}\right)^4 \end{array} \right) + \\ \left(GAk_s\left(\frac{dw_0}{dx}\right)^2 - 2GAk_s\phi\left(\frac{dw_0}{dx}\right) + GAk_s\phi^2 \right) \end{array} \right\} dx. \qquad (2.17)$$

Here $EA = \int_A E_f dA$, $EQ = \int_A E_f z dA$, $EI = \int_A E_f z^2 dA$, and $GA = \int_A G_f dA.$ (2.18)

The expression for U_2 is derived as follows:

$$U_2 = \frac{1}{2}\int_V (m : \chi) dV$$

$$= \frac{1}{2}\int_V \left(m_{xy}\chi_{xy} + m_{yx}\chi_{yx} \right) dV$$

$$= \frac{1}{2}\int_V \left(m_{xy}\left(-\frac{1}{4}\left(\frac{\partial^2 w_0}{\partial x^2} + \frac{\partial \phi}{\partial x} \right) \right) + m_{yx}\left(-\frac{1}{4}\left(\frac{\partial^2 w_0}{\partial x^2} + \frac{\partial \phi}{\partial x} \right) \right) \right) dV$$

$$= \frac{1}{2}\int_V \left\{ \begin{array}{l} \left(-\frac{G_f l^2}{2}\left(\frac{\partial^2 w_0}{\partial x^2} + \frac{\partial \phi}{\partial x} \right) \right)\left(-\frac{1}{4}\left(\frac{\partial^2 w_0}{\partial x^2} + \frac{\partial \phi}{\partial x} \right) \right) \\ +\left(-\frac{G_f l^2}{2}\left(\frac{\partial^2 w_0}{\partial x^2} + \frac{\partial \phi}{\partial x} \right) \right)\left(-\frac{1}{4}\left(\frac{\partial^2 w_0}{\partial x^2} + \frac{\partial \phi}{\partial x} \right) \right) \end{array} \right\} dV$$

$$= \frac{G_f l^2}{8} \int_0^L \iint_A \left(\left(\frac{\partial^2 w_0}{\partial x^2} \right)^2 + 2 \left(\frac{\partial^2 w_0}{\partial x^2} \right) \left(\frac{\partial \phi}{\partial x} \right) + \left(\frac{\partial \phi}{\partial x} \right)^2 \right) dA dx$$

$$= \int_0^L \left(\frac{GAl^2}{8} \left(\frac{\partial^2 w_0}{\partial x^2} \right)^2 + \frac{GAl^2}{4} \left(\frac{\partial^2 w_0}{\partial x^2} \right) \left(\frac{\partial \phi}{\partial x} \right) + \frac{GAl^2}{8} \left(\frac{\partial \phi}{\partial x} \right)^2 \right) dx. \quad (2.19)$$

2.6.2 Work Potential

The work potential of the uniformly distributed load (UDL) is given below,

$$V = -p \int_0^L w_0 dx,$$

(2.20)

where p is the intensity of the uniformly distributed load (N/m).

2.6.3 Kinetic Energy

The expression for kinetic energy (T) is derived as follows:

$$T = \frac{1}{2} \int_0^L \iint_A \left(\rho_f \left(\frac{\partial w}{\partial t} \right)^2 + \rho_f \left(\frac{\partial u}{\partial t} \right)^2 \right) dA dx$$

$$= \frac{1}{2} \int_0^L \iint_A \left(\rho_f \left(\frac{\partial w_0}{\partial t} \right)^2 + \rho_f \left(\frac{\partial u_0}{\partial t} - z \frac{\partial \phi}{\partial t} \right)^2 \right) dA dx$$

$$= \frac{1}{2} \int_0^L \iint_A \left(\rho_f \left(\frac{\partial w_0}{\partial t} \right)^2 + \rho_f \left(\left(\frac{\partial u_0}{\partial t} \right)^2 + z^2 \left(\frac{\partial \phi}{\partial t} \right)^2 - 2z \left(\frac{\partial u_0}{\partial t} \right) \left(\frac{\partial \phi}{\partial t} \right) \right) \right) dA dx$$

$$= \frac{1}{2} \int_0^L \left(RA \left(\frac{\partial w_0}{\partial t} \right)^2 + RA \left(\frac{\partial u_0}{\partial t} \right)^2 + RI \left(\frac{\partial \phi}{\partial t} \right)^2 - 2RQ \left(\frac{\partial u_0}{\partial t} \right) \left(\frac{\partial \phi}{\partial t} \right) \right) dx. \quad (2.21)$$

Here $RA = \int_A \rho_f dA$, $RQ = \int_A z \rho_f dA$ and $RI = \int_A z^2 \rho_f dA$. (2.22)

2.7 Determination of Static Deflection

The minimum potential energy principle can be expressed mathematically as,

$$\delta(\Pi) = \delta(U + V) = 0\,. \tag{2.23}$$

The displacement fields are approximated using Ritz method as follows:

$$w_0(x) = \sum_{i=1}^{nw} c_i \varphi_i^{\,w}(x), \tag{2.24a}$$

$$u_0(x) = \sum_{i=1}^{nu} c_{nw+i} \varphi_i^{\,u}(x), \tag{2.24b}$$

$$\phi(x) = \sum_{i=1}^{n\phi} c_{nw+nu+i} \varphi_i^{\,\phi}(x). \tag{2.24c}$$

Here $\varphi_i^{\,w}, \varphi_i^{\,u}$ and $\varphi_i^{\,\phi}$ are the set of orthogonal admissible functions, c_i is the set of generalized coordinates, and nw, nu and $n\phi$ are the number of the respective functions. The set of orthogonal functions $\varphi_i^{\,w}$, $\varphi_i^{\,u}$ and $\varphi_i^{\,\phi}$ are generated numerically from the lowest order admissible functions by Gram-Schmidt orthogonalization scheme.The selected lowest order functions satisfying different boundary conditions are given in Table 2.2.

Table 2.2: List of lowest order functions for different boundary conditions.

Boundary Condition	$\varphi_1^{\,w}$	$\varphi_1^{\,u}$	$\varphi_1^{\,\phi}$
CC	$\frac{x}{L}\left(1-\frac{x}{L}\right)$	$\frac{x}{L}\left(1-\frac{x}{L}\right)$	$\sin\left(\frac{\pi x}{L}\right)$
CH	$\frac{x}{L}\left(1-\frac{x}{L}\right)$	$\frac{x}{L}\left(1-\frac{x}{L}\right)$	$\sin\left(\frac{\pi x}{2L}\right)$
HH	$\frac{x}{L}\left(1-\frac{x}{L}\right)$	$\frac{x}{L}\left(1-\frac{x}{L}\right)$	$\cos\left(\frac{\pi x}{L}\right)$
CF	$\frac{x}{L}$	$\frac{x}{L}\left(1-\frac{x}{L}\right)$	$\sin\left(\frac{\pi x}{2L}\right)$

Substituting the assumed displacement fields given by Eqs. (2.24a)-(2.24c) into Eqs. (2.17), (2.19), (2.20), and using Eq. (2.23), the set of governing equations are given in the matrix form as follows:

$$\left(\left[k_{cl}^{\,l}\right] + \left[k_{cl}^{\,nl}\right] + \left[k_{ncl}\right]\right)\{c\} = \{P\}. \tag{2.25}$$

Here $\left[k_{cl}{}^{l}\right]$ is the stiffness matrix due to classical strain energy which contains the linear terms of the classical strain energy; $\left[k_{cl}{}^{nl}\right]$ is the stiffness matrix due to classical strain energy that contains the nonlinear terms of the classical strain energy; $\left[k_{ncl}\right]$ is the stiffness matrix due to non-classical strain energy; $\{P\}$ is the load vector.

The set of equations given by Eq. (2.25) is nonlinear. It is solved using a substitution method with successive relaxation (Das et al. (2008)). The solution yields $\{c\}$, which is used to calculate $\{w_0, u_0, \phi\}$ using Eqs. (2.24a)-(2.24c). The elements of the $\left[k_{cl}{}^{l}\right]$, $\left[k_{cl}{}^{nl}\right]$, $\left[k_{ncl}\right]$ and $\{P\}$ are given in the Appendix 2A.

2.8 Determination of Free Vibration

Hamilton principle is mathematically expressed as,

$$\delta\left(\int_{t_1}^{t_2}\left(T-U-V\right)dt\right)=0. \tag{2.26}$$

For the present problem involving free vibration, the work potential (V) is taken as zero.
It is assumed that the dynamic displacement fields for the free vibration problem are separable in both space and time. Assuming harmonic vibration for elastic system, the dynamic displacement fields are assumed as shown below:

$$w_0\left(x,t\right)=e^{\mathbf{i}\omega t}\sum_{i=1}^{nw}d_i\varphi_i{}^{w}\left(x\right), \tag{2.27a}$$

$$u_0\left(x,t\right)=e^{\mathbf{i}\omega t}\sum_{i=1}^{nu}d_{nw+i}\varphi_i{}^{u}\left(x\right), \tag{2.27b}$$

$$\phi\left(x,t\right)=e^{\mathbf{i}\omega t}\sum_{i=1}^{n\phi}d_{nw+nu+i}\varphi_i{}^{\phi}\left(x\right). \tag{2.27c}$$

Here $\mathbf{i}=\sqrt{-1}$, and ω is the frequency of the free vibration.

As the micro-beam executes small amplitude free vibration about its deformed configuration, its tangent stiffness is responsible for free vibratory motion that would occur in the neighborhood of the deformed configuration. Hence, in the final form of Eq. (2.26), the part

corresponding to the strain energy (U) is associated with the tangent stiffness of the deformed configuration. The tangent stiffness $\left[k^T\right]$ of the deformed beam is derived using the following relationship (Das (2018):

$$\left[\left(k_{ji}\right)^T\right]=\frac{\partial}{\partial c_i}\left\{P_j^r\right\}. \tag{2.28}$$

In Eq. (2.28), $\left\{P_j^r\right\}$ is the restoring force vector for the deformed configuration given by $\left\{P_j^r\right\}=\left(\left[k_{cl}{}^{l}\right]+\left[k_{cl}{}^{nl}\right]+\left[k_{ncl}\right]\right)_{ji}\left\{c_i\right\}$. The elements of $\left[k^T\right]$ in subscripted form are given in Appendix 2B. As the deformed configuration is already known from the previous static analysis, the elements of $\left[k^T\right]$ are fully known so that it can be used in the governing equations for the free vibration problem.

Substituting the dynamic displacement fields given by Eqs. (2.27a)-(2.27c) into Eq. (2.21), incorporating the tangent stiffness of the micro-beam, and applying the Hamilton's principle given by Eq. (2.26), an eigenvalue problem is obtained as follows:

$$\left[\left[k^T\right]-\omega^2\left[M\right]\right]\left\{d\right\}=\left\{0\right\}. \tag{2.29}$$

Here $\left[M\right]$ is the mass matrix, $\left[k^T\right]$ is the tangent stiffness matrix, ω^2 is the eigenvalue, and $\left\{d\right\}$ is the eigenvector. It is noted that the nonlinear tangent stiffness matrix $\left[k^T\right]$ appearing in Eq. (2.29) is linearized using the solution coefficients $\left\{\mathrm{c}\right\}$ of the deformed configuration of the micro-beam to take into the effect of pre-stress induced due to static loading. The square roots of the eigenvalues $\left(\omega^2\right)$ signify the frequencies of vibratory motion of the deformed micro-beam, and the eigenvectors i.e., $\left\{d\right\}$ represent the corresponding mode-shapes of vibration. These eigenvectors when used in Eqs. (2.27a)-(2.27c) generate the mode-shapes of vibration. Eq. (2.29) is solved using a standard eigen-solver of MATLAB.

2.9 Chapter Summery

The static and vibration behaviour of a FG Timoshenko micro-beam under various boundary conditions is mathematically formulated in this chapter, taking metal-ceramic FGM compositions into account and using the MCST to account for size effects. It starts by outlining

the FGM modelling and taking into account the power law variation of the volume fractions of the metallic and ceramic phases, which results in the effective material properties. The formulation of strain energy, work potential, and kinetic energy is presented in detail, as are the displacement, strain, curvature, stress, and couple stress fields. The governing equations for the static problem and vibration problem are derived. They are solved following Ritz method. Two appendices describing the non-zero components of different matrices and the load vector rounds off the chapter.

Appendix 2A

Non-zero components of $\left[k_{cl}{}^{l}\right]$

$$\left[\left(k_{cl}{}^{l}\right)_{ji}\right]_{\substack{j=1,nw\\ i=1,nw}} = GA\,k_s\int_0^L \frac{d\varphi_i{}^{w}}{dx}\frac{d\varphi_j{}^{w}}{dx}dx,$$

$$\left[\left(k_{cl}{}^{l}\right)_{ji}\right]_{\substack{j=1,nw\\ i=nw+nu+1,nw+nu+n\phi}} = -GA\,k_s\int_0^L \varphi^{\phi}_{i-nw-nu}\frac{d\varphi_j{}^{w}}{dx}dx,$$

$$\left[\left(k_{cl}{}^{l}\right)_{ji}\right]_{\substack{j=nw+1,nw+nu\\ i=nw+1,nw+nu}} = EA\int_0^L \frac{d\varphi^{u}_{i-nw}}{dx}\frac{d\varphi^{u}_{j-nw}}{dx}dx,$$

$$\left[\left(k_{cl}{}^{l}\right)_{ji}\right]_{\substack{j=nw+1,nw+nu\\ i=nw+nu+1,nw+nu+n\phi}} = EA\int_0^L \frac{d\varphi^{\phi}_{i-nw-nu}}{dx}\frac{d\varphi^{u}_{j-nw}}{dx}dx,$$

$$\left[\left(k_{cl}{}^{l}\right)_{ji}\right]_{\substack{j=nw+nu+1,nw+nu+n\phi\\ i=1,nw}} = -GA\,k_s\int_0^L \frac{d\varphi^{w}_{i}}{dx}\varphi^{\phi}_{j-nw-nu}\,dx,$$

$$\left[\left(k_{cl}{}^{l}\right)_{ji}\right]_{\substack{j=nw+nu+1,nw+nu+n\phi\\ i=nw+1,nw+nu}} = -EQ\int_0^L \frac{d\varphi^{u}_{i-nw}}{dx}\frac{d\varphi^{\phi}_{j-nw-nu}}{dx}dx,$$

$$\left[\left(k_{cl}{}^{l}\right)_{ji}\right]_{\substack{j=nw+nu+1,nw+nu+n\phi\\ i=nw+nu+1,nw+nu+n\phi}} = EI\int_0^L \frac{d\varphi^{\phi}_{i-nw-nu}}{dx}\frac{d\varphi^{\phi}_{j-nw-nu}}{dx}dx + GA\,k_s\int_0^L \varphi^{\phi}_{i-nw-nu}\varphi^{\phi}_{j-nw-nu}\,dx.$$

Non-zero components of $\left[k_{cl}{}^{nl}\right]$

$$\left[\left(k_{cl}^{nl}\right)_{ji}\right]_{\substack{j=1,nw\\ i=1,nw}} = EA\int_0^L \left(\frac{du_0}{dx}\right)\frac{d\varphi_i^w}{dx}\frac{d\varphi_j^w}{dx}dx - EQ\int_0^L \left(\frac{d\phi}{dx}\right)\frac{d\varphi_i^w}{dx}\frac{d\varphi_j^w}{dx}dx + \frac{EA}{2}\int_0^L \left(\frac{dw_0}{dx}\right)^2\frac{d\varphi_i^w}{dx}\frac{d\varphi_j^w}{dx}dx,$$

$$\left[\left(k_{cl}^{nl}\right)_{ji}\right]_{\substack{j=nw+1,nw+nu\\ i=1,nw}} = \frac{EA}{2}\int_0^L \left(\frac{dw_0}{dx}\right)\frac{d\varphi_i^w}{dx}\frac{d\varphi_{j-nw}^u}{dx}dx,$$

$$\left[\left(k_{cl}^{nl}\right)_{ji}\right]_{\substack{j=nw+nu+1,nw+nu+n\phi\\ i=1,nw}} = -\frac{EQ}{2}\int_0^L \left(\frac{dw_0}{dx}\right)\frac{d\varphi_i^w}{dx}\frac{d\varphi_{j-nw-nu}^\phi}{dx}dx.$$

Non-zero components of $\left[k_{ncl}\right]$

$$\left[\left(k_{ncl}\right)_{ji}\right]_{\substack{j=1,nw\\ i=1,nw}} = \frac{GAl^2}{4}\int_0^L \frac{d^2\varphi_i^w}{dx^2}\frac{d^2\varphi_j^w}{dx^2}dx,$$

$$\left[\left(k_{ncl}\right)_{ji}\right]_{\substack{j=1,nw\\ i=nw+nu+1,nw+nu+n\phi}} = \frac{GAl^2}{4}\int_0^L \frac{d\varphi_{i-nw-nu}^\phi}{dx}\frac{d^2\varphi_j^w}{dx^2}dx,$$

$$\left[\left(k_{ncl}\right)_{ji}\right]_{\substack{j=nw+nu+1,nw+nu+n\phi\\ i=1,nw}} = \frac{GAl^2}{4}\int_0^L \frac{d^2\varphi_i^w}{dx^2}\frac{d\varphi_{j-nw-nu}^\phi}{dx}dx,$$

$$\left[\left(k_{ncl}\right)_{ji}\right]_{\substack{j=nw+nu+1,nw+nu+n\phi\\ i=nw+nu+1,nw+nu+n\phi}} = \frac{GAl^2}{4}\int_0^L \frac{d\varphi_{i-nw-nu}^\phi}{dx}\frac{d\varphi_{j-nw-nu}^\phi}{dx}dx.$$

Components of Load Vector

$$\left\{p_j\right\}_{j=1,nw} = p\int_0^L \varphi_j^w dx,$$

$$\left\{p_j\right\}_{j=nw+1,nw+nu} = 0,$$

$$\left\{p_j\right\}_{j=nw+nu+1,nw+nu+n\phi} = 0.$$

Appendix 2B

Nonzero components of Mass Matrix

$$\left[M\right]_{\substack{j=1,nw\\ i=1,nw}} = RA\int_o^L \varphi_i^w\varphi_j^w\,dx,$$

$$\left[M\right]_{\substack{j=nw+1,nu+nw \\ i=nw+1,nw+nu}} = RA\int_o^L \varphi_{i-nw}^u \varphi_{j-nw}^u \, dx,$$

$$\left[M\right]_{\substack{j=nw+1,nu+nw \\ i=nw+nu+1,nu+nw+n\phi}} = -RQ\int_o^L \varphi_{i-nw-nu}^\phi \varphi_{j-nw}^u \, dx,$$

$$\left[M\right]_{\substack{j=nw+nu+1,nu+nw+n\phi \\ i=nw+1,nu+nw}} = -RQ\int_0^L \varphi_{i-nw}^u \varphi_{j-nw-nu}^\phi \, dx,$$

$$\left[M\right]_{\substack{j=nw+nu+1,nu+nw+n\phi \\ i=nw+nu+1,nu+nw+n\phi}} = RI\int_o^L \varphi_{i-nw-nu}^\phi \varphi_{j-nw-nu}^\phi \, dx.$$

Nonzero components of Tangent Stiffness Matrix

Linear Terms (Classical)

$$\left[\left(k_{cl}^{\,l}\right)^T_{ji}\right]_{\substack{j=1,nw \\ i=1,nw}} = GA\,k_s\int_0^L \frac{d\varphi_i^{\,w}}{dx}\frac{d\varphi_j^{\,w}}{dx}\,dx,$$

$$\left[\left(k_{cl}^{\,l}\right)^T_{ji}\right]_{\substack{j=1,nw \\ i=nw+nu+1,nw+nu+n\phi}} = -GA\,k_s\int_0^L \varphi_{i-nw-nu}^\phi \frac{d\varphi_j^{\,w}}{dx}\,dx,$$

$$\left[\left(k_{cl}^{\,l}\right)^T_{ji}\right]_{\substack{j=nw+1,nw+nu \\ i=nw+1,nw+nu}} = EA\int_0^L \frac{d\varphi_{i-nw}^u}{dx}\frac{d\varphi_{j-nw}^u}{dx}\,dx,$$

$$\left[\left(k_{cl}^{\,l}\right)^T_{ji}\right]_{\substack{j=nw+1,nw+nu \\ i=nw+nu+1,nw+nu+n\phi}} = EA\int_0^L \frac{d\varphi_{i-nw-nu}^\phi}{dx}\frac{d\varphi_{j-nw}^u}{dx}\,dx,$$

$$\left[\left(k_{cl}^{\,l}\right)^T_{ji}\right]_{\substack{j=nw+nu+1,nw+nu+n\phi \\ i=1,nw}} = -GA\,k_s\int_0^L \frac{d\varphi_i^{\,w}}{dx}\varphi_{j-nw-nu}^\phi \,dx,$$

$$\left[\left(k_{cl}^{\,l}\right)^T_{ji}\right]_{\substack{j=nw+nu+1,nw+nu+n\phi \\ i=nw+1,nw+nu}} = EA\int_0^L \frac{d\varphi_{i-nw}^u}{dx}\frac{d\varphi_{j-nw-nu}^\phi}{dx}\,dx,$$

$$\left[\left(k_{cl}^{\,l}\right)^T_{ji}\right]_{\substack{j=nw+nu+1,nw+nu+n\phi \\ i=nw+nu+1,nw+nu+n\phi}} = EI\int_0^L \frac{d\varphi_{i-nw-nu}^\phi}{dx}\frac{d\varphi_{j-nw-nu}^\phi}{dx}\,dx + GA\,k_s\int_0^L \varphi_{i-nw-nu}^\phi \varphi_{j-nw-nu}^\phi \,dx.$$

Nonlinear Terms (Classical)

$$\left[\left(k_{cl}^{nl}\right)^{T}{}_{ji}\right]_{\substack{j=1,nw\\ i=1,nw}} = 2EA\int_0^L \left(\frac{du_0}{dx}\right)\frac{d\varphi_i^{w}}{dx}\frac{d\varphi_j^{w}}{dx}dx - 2EQ\int_0^L \left(\frac{d\phi}{dx}\right)\frac{d\varphi_i^{w}}{dx}\frac{d\varphi_j^{w}}{dx}dx + \frac{3EA}{2}\int_0^L \left(\frac{dw_0}{dx}\right)^2\frac{d\varphi_i^{w}}{dx}\frac{d\varphi_j^{w}}{dx}dx,$$

$$\left[\left(k_{cl}^{nl}\right)^{T}{}_{ji}\right]_{\substack{j=1,nw\\ i=nw+1,nw+nu}} = \int_0^L EA\left(\frac{dw_0}{dx}\right)\frac{d\varphi_{i-nw}^{u}}{dx}\frac{d\varphi_j^{w}}{dx}dx,$$

$$\left[\left(k_{cl}^{nl}\right)^{T}{}_{ji}\right]_{\substack{j=1,nw\\ i=nw+nu+1,nw+nu+n\phi}} = -EQ\int_0^L \left(\frac{dw_0}{dx}\right)\frac{d\varphi_{i-nw-nu}^{\phi}}{dx}\frac{d\varphi_j^{w}}{dx}dx,$$

$$\left[\left(k_{cl}^{nl}\right)^{T}{}_{ji}\right]_{\substack{j=nw+1,nw+nu\\ i=1,nw}} = EA\int_0^L \left(\frac{dw_0}{dx}\right)\frac{d\varphi_i^{w}}{dx}\frac{d\varphi_{j-nw}^{u}}{dx}dx,$$

$$\left[\left(k_{cl}^{nl}\right)^{T}{}_{ji}\right]_{\substack{j=nw+nu+1,nw+nu+n\phi\\ i=1,nw}} = -EQ\int_0^L \left(\frac{dw_0}{dx}\right)\frac{d\varphi_i^{w}}{dx}\frac{d\varphi_{j-nw-nu}^{\phi}}{dx}dx.$$

Linear Terms (Nonclassical)

$$\left[\left(k_{ncl}\right)^{T}{}_{ji}\right]_{\substack{j=1,nw\\ i=1,nw}} = \frac{GAl^2}{4}\int_0^L \frac{d^2\varphi_i^{w}}{dx^2}\frac{d^2\varphi_j^{w}}{dx^2}dx,$$

$$\left[\left(k_{ncl}\right)^{T}{}_{ji}\right]_{\substack{j=1,nw\\ i=nw+nu+1,nw+nu+n\phi}} = \frac{GAl^2}{4}\int_0^L \frac{d\varphi_{i-nw-nu}^{\phi}}{dx}\frac{d^2\varphi_j^{w}}{dx^2}dx,$$

$$\left[\left(k_{ncl}\right)^{T}{}_{ji}\right]_{\substack{j=nw+nu+1,nw+nu+n\phi\\ i=1,nw}} = \frac{GAl^2}{4}\int_0^L \frac{d^2\varphi_i^{w}}{dx^2}\frac{d\varphi_{j-nw-nu}^{\phi}}{dx}dx,$$

$$\left[\left(k_{ncl}\right)^{T}{}_{ji}\right]_{\substack{j=nw+nu+1,nw+nu+n\phi\\ i=nw+nu+1,nw+nu+n\phi}} = \frac{GAl^2}{4}\int_0^L \frac{d\varphi_{i-nw-nu}^{\phi}}{dx}\frac{d\varphi_{j-nw-nu}^{\phi}}{dx}dx.$$

Chapter 3

RESULTS FOR STATIC DEFLECTION BEHAVIOUR

3.1 Introduction

A theoretical investigation examines the static deflection of a Timoshenko micro-beam made of functionally graded material (FGM), where the volume fraction varies according to a power law along the thickness direction. To capture geometric non-linearity, the von Kármán non-linear strain-displacement relationship is utilized. The governing equation is derived using the minimum potential energy principle. We explored four different boundary conditions namely Clamped-Clamped (CC), Clamped-Hinged (CH), Hinged-Hinged (HH) and Clamped-Free (CF). The study evaluates the static deflection of four different FGMs: Stainless Steel/Alumina ($SUS304/Al_2O_3$) [FGM1], Stainless Steel/Silicon Nitride ($SUS304/Si_3N_4$) [FGM2], Stainless Steel/Zirconia ($SUS304/ZrO_2$) [FGM3] and Titanium Alloy/Zirconia ($Ti\text{-}6Al\text{-}4V/ZrO_2$) [FGM4]. The mathematical formulation for static deflection is presented in Chapter 2 along with the mechanical properties of four FGMs.

3.2 Validation Study

We have compared our result with Paul and Das (2016). The validation plots for Stainless Steel/Zirconia [FGM3] Timoshenko micro-beam are presented in Figs. 3.1(a)–(c) where the plots of $\overline{p}$ vs. $\overline{w}$ for $k = 2.0$ are shown. Here $\overline{p}$ is the non-dimensional uniform transverse pressure and $\overline{w}$ is the normalized maximum transverse deflection. These are defined as follows: $\overline{p} = p\left(\frac{L}{h}\right)^4 \Big/ (E_m b)$ and $\overline{w} = w/h$, where p is the intensity of the uniformly distributed load in N/m, w is the maximum transverse deflection, L is the length of beam, h is the height of beam section and b is the width of the beam. The material properties for FGM3 are given as follows:

E_m=207.79GPa, E_c=168.06GPa, μ_m=0.318, μ_c=0.298, ρ_m=8166$\left(kg\,m^{-3}\right)$ and ρ_c=3000 $\left(kg\,m^{-3}\right)$. Figs. 3.1(a)-(c) show the plot of $\overline{p}$ vs. $\overline{w}$ for CC, CH and HH micro-beams respectively. Figs. 3.1(a)–(c) show excellent agreement with present model and thus it validates the present model.

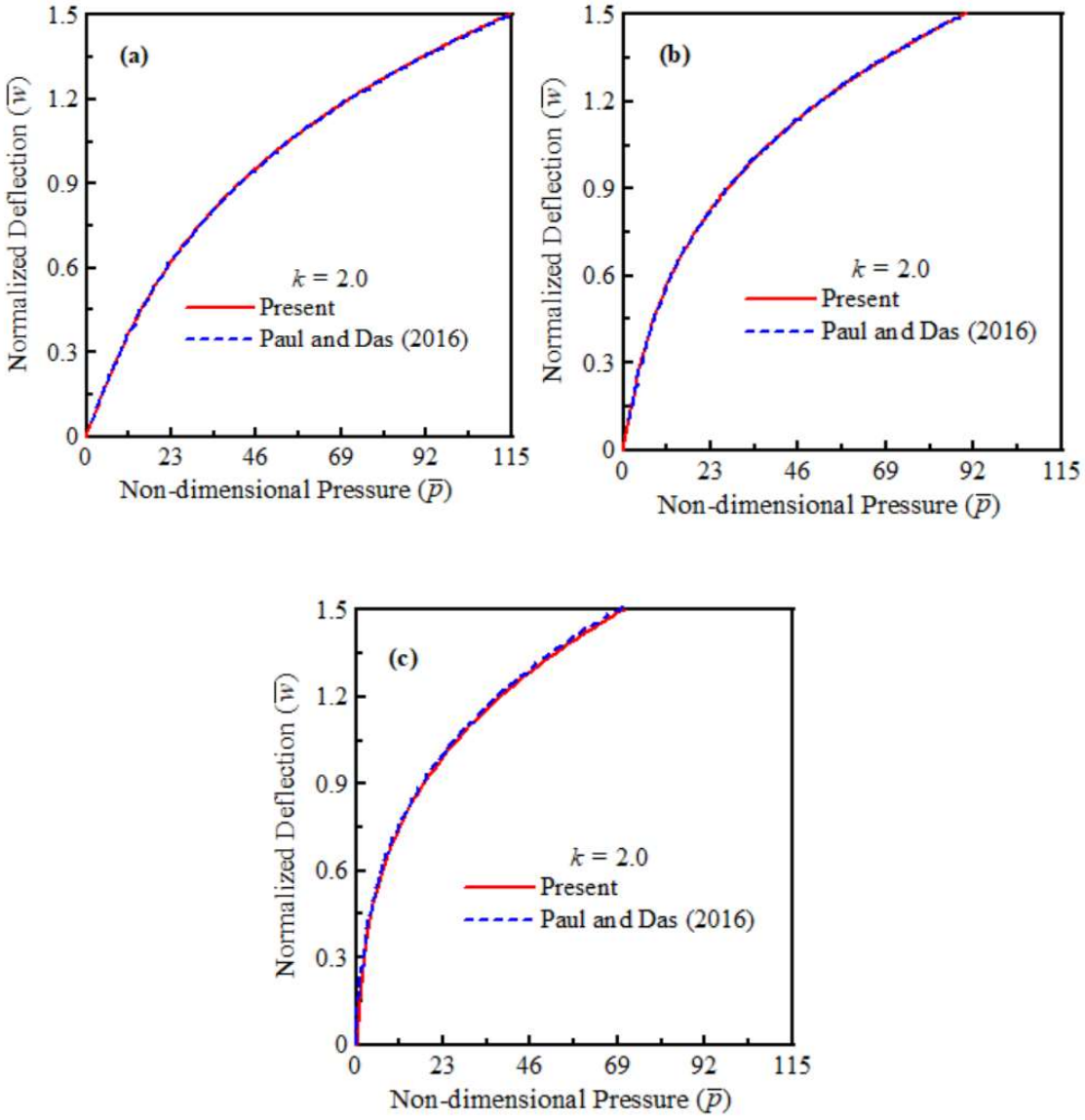

Fig. 3.1. Validation plots for static deflection for different boundary conditions: (a) CC, (b) CH, (c) HH.

We have also compared our model with Reddy (2011) for a homogeneous beam (k=0) for which the geometric and material properties are given as follows: $E_m = E_c = E$=1.44 GPa, $\mu_m = \mu_c = \mu$=0.38, $k_s = \left(5\left(1+\mu\right)/6+5\mu\right)$, b = 2h, L=20h and p=1.0 N/m. The validation details are given in the Tables 3.1 and 3.2 for uniformly distributed load and sinusoidal load respectively for different l/h values with its corresponding normalized central deflection $\overline{w} = w\left(EI/pL^4\right)\times 10^2$,where w is the maximum transverse deflection. Tables 3.1 and 3.2 show excellent agreement with present model and thus validate the present model.

Table 3.1: Comparison of normalized central deflection of a simply supported homogeneous (k=0) micro-beam under uniformly distributed load.

l/h	Reddy (2011)	Present
0.0	1.3103	1.3103
0.2	1.1162	1.1162
0.4	0.7731	0.7731
0.6	0.5116	0.5116
0.8	0.3475	0.3475
1.0	0.2464	0.2464

Table 3.2: Comparison of normalized central deflection of a simply supported homogeneous (k=0) micro-beam under sinusoidal load.

l/h	Reddy (2011)	Present
0.0	1.0333	1.033
0.2	0.8802	0.8802
0.4	0.6096	0.6096
0.6	0.4034	0.4034
0.8	0.2741	0.2741
1.0	0.1943	0.1943

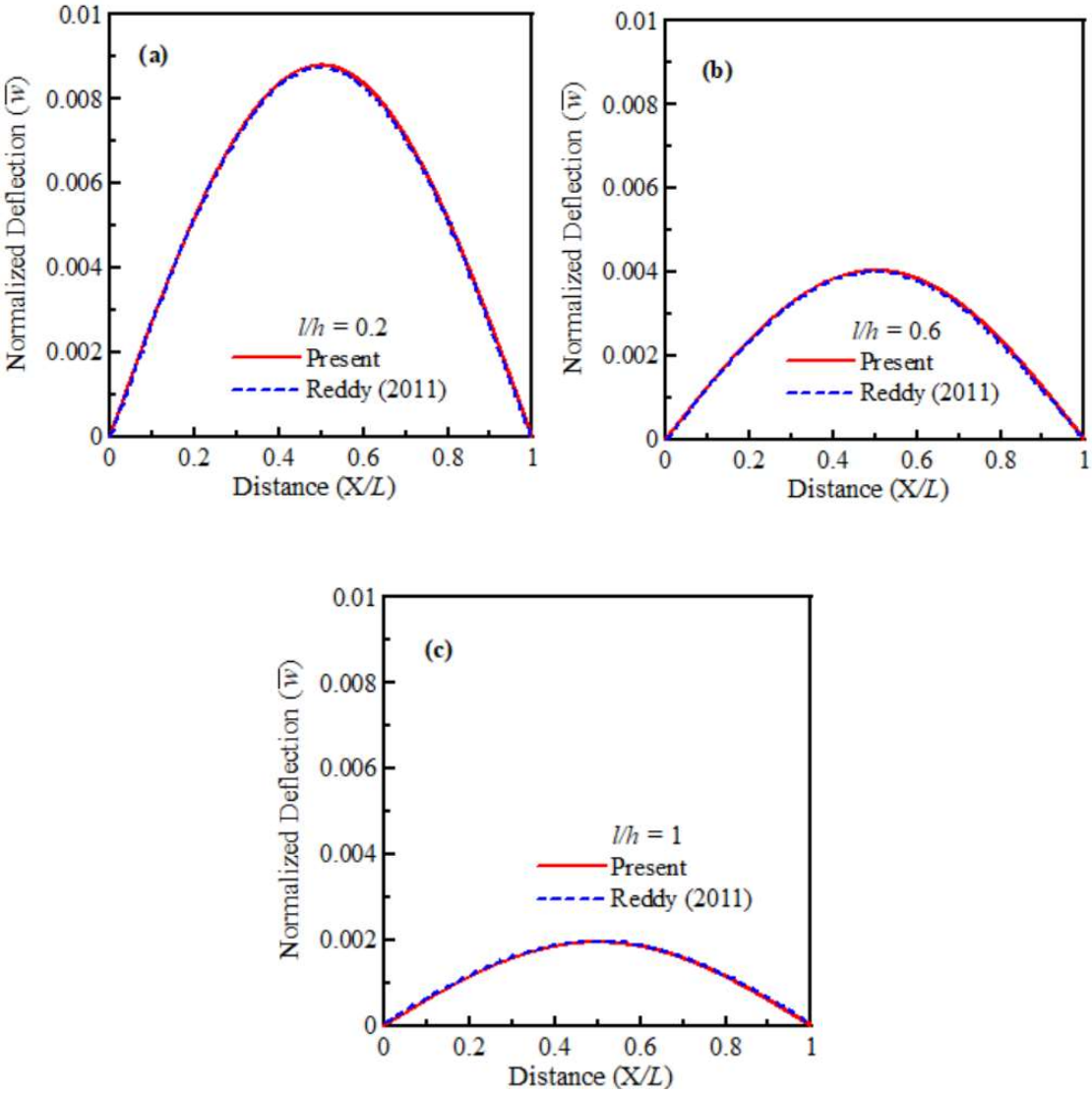

Fig. 3.2: Validation plots for static deflection for different size effect: (a) l/h = 0.2, (b) l/h = 0.6, (c) l/h = 1.

Figs. 3.2(a)-(b) show comparison of normalized deflection $\bar{w} = w\left(E\,I\,/\,pL^4\right)$ under sinusoidally distributed transverse load with Reddy (2011) for a homogeneous beam having given material properties: $E_c = E_m = E$=1.44 GPa, $\mu_m = \mu_c = \mu$=0.38, $k_s = \left(5\left(1+\mu\right)/\left(6+5\mu\right)\right)$, b=2h, L=20h and p=1.0 N/m. The deflection is shown as a function of the non-dimensional beam coordinate x/L for various l/h values which are 0.2, 0.6 and 1. Fig. 3.2 shows excellent agreement with present model and hence validates our model.

3.3 Results for Different Parameters

The present work is carried out to determine the static deflection of FGM micro beams. The static behaviour is presented graphically in non-dimensional $\bar{p}$ vs. $\bar{w}$ plane, where $\bar{p}$ is the non-dimensional uniform transverse pressure and $\bar{w}$ is the normalized maximum transverse deflection. The expression for $\bar{p}$ and $\bar{w}$ are as follows: $\bar{p} = p\left(L/h\right)^4 / \left(E_c b\right)$ and $\bar{w} = w_{\max} / h$, where p is the intensity of the UDL in N/m, L is the length of the beam which is related to thickness of beam h as follows L/h=25, E_c is the Young's modulus of ceramic, b is the width of the beam which is also related to h as follows b/h=2 and $w_{\max}$ is the maximum transverse deflection. To incorporate the size effect, the material length scale parameter l is taken as 17.6 micron.

The non-dimensional load-deflection curves for the CC, CH, HH and CF boundary conditions are shown in Figs. 3.3(a)–(f), 3.4(a)–(f), 3.5(a)–(f) and 3.6(a)–(f) respectively. These curves for figures (a)-(f) correspond to different values of the material gradation index which are: k=0.0, 0.1, 0.5, 1.0, 2.0, 5.0 respectively. Figs. 3.3-3.6 are presented for a Stainless Steel/Silicon Nitride [FGM2] micro-beam. Each figure in Figs. 3.3-3.6 shows how size affects the non-dimensional load-deflection behaviour by varying the size-dependent thickness (h/l) values as h/l=1.0, 2.0, 5.0, 10.0, and for classical FG beam (l = 0).

In Figs. 3.3–3.6 for different boundary conditions, the non-dimensional load-deflection curves for various values of the material gradation index, k =0.0, 0.1, 0.5, 1.0, 2.0, and 5.0 are shown. In each of the figures in Figs. 3.3-3.6, the size-dependent thickness (h/l) values are varied. It should be noted that the size-effect decreases as the h/l value increases. It is also to be noted that as k increases, the metal volume fractions in the beam increase. Because the metal component has a lower elastic modulus than its ceramic counterpart, the beam becomes more elastically flexible as k increases. For any particular boundary condition and for any given k value, it is observed that the micro-beam becomes more stiff with increasing size-effect, and that it is found to be maximum at h/l=1. At h/l=10, the micro-effect almost disappears as the curves at these values become almost coincident with the classical behaviour. When k increases for a given value of h/l, the curve becomes steeper, which indicates that the beam's stiffness decreases.

From Figs. 3.3-3.6, it is seen that the non-dimensional pressure is very less for CF boundary as compared to other boundary conditions, which means that the stiffness is very less for CF beams.

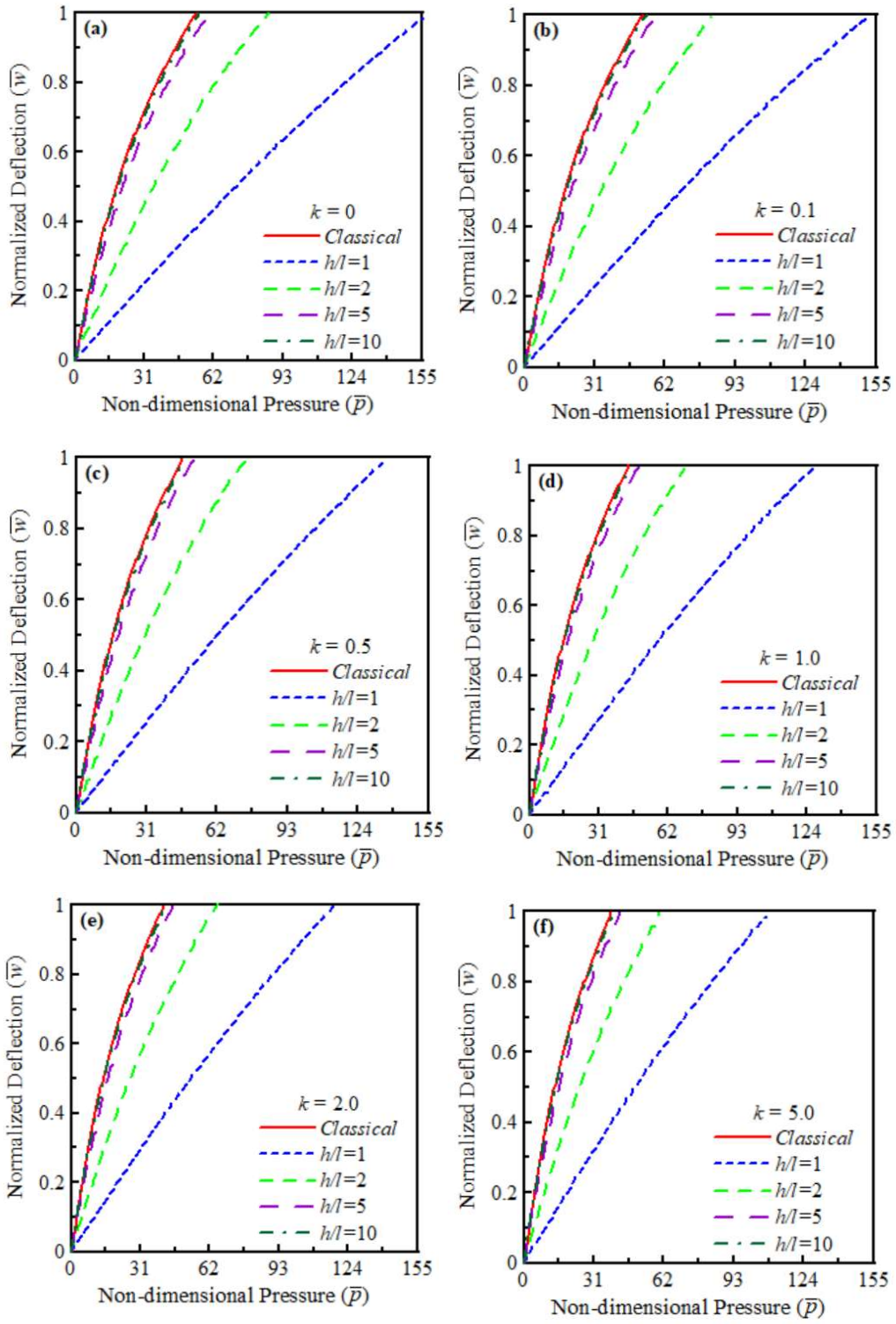

Fig. 3.3: Effect of size on non-dimensional load-deflection curves for CC micro-beams: (a) k=0, (b) k=0.1, (c) k=0.5, (d) k=1.0, (e) k=2.0, (f) k=5.0.

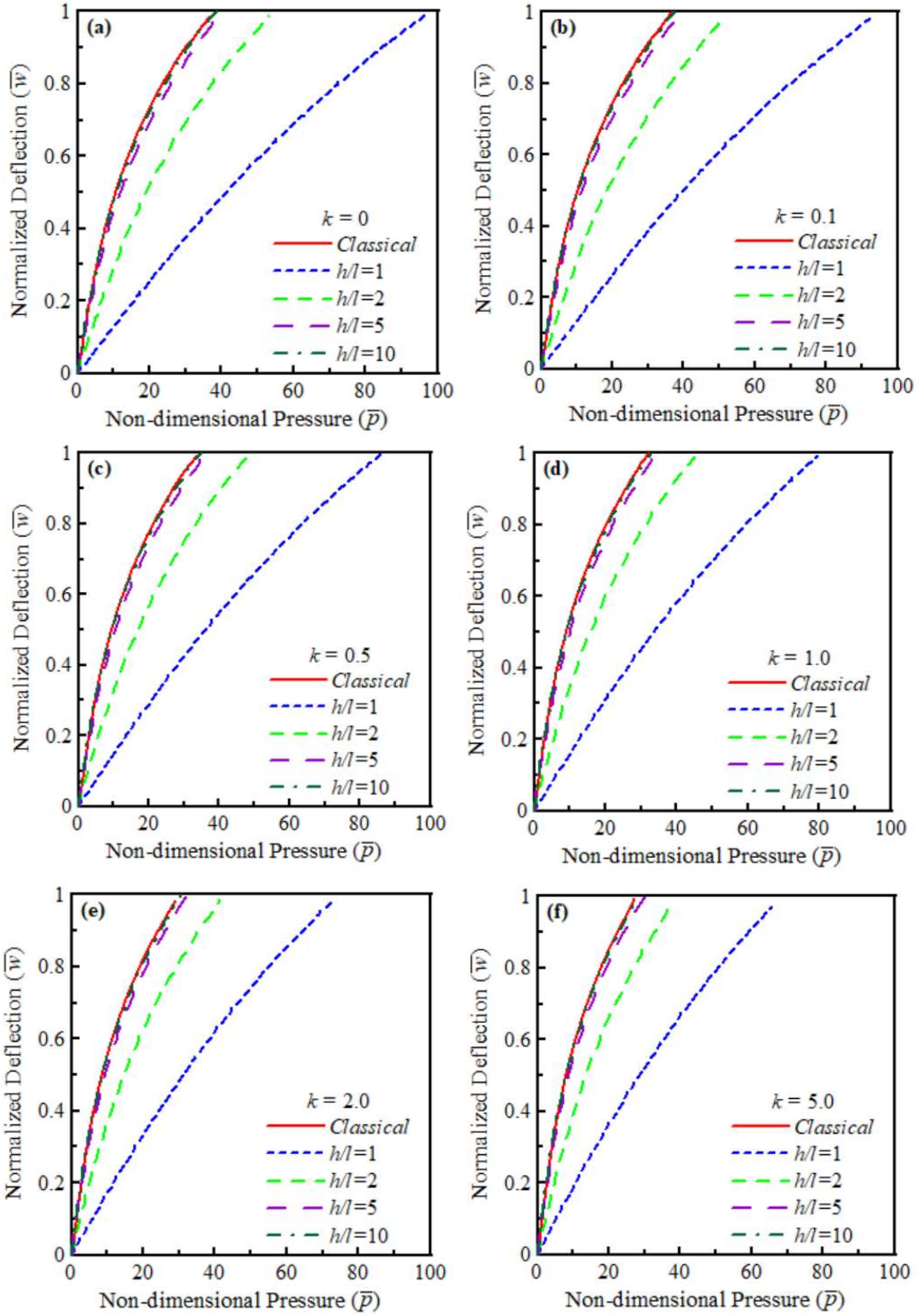

Fig. 3.4: Effect of size on non-dimensional load-deflection curves for CH micro-beams: (a) k=0, (b) k=0.1, (c) k=0.5, (d) k=1.0, (e) k=2.0, (f) k=5.0.

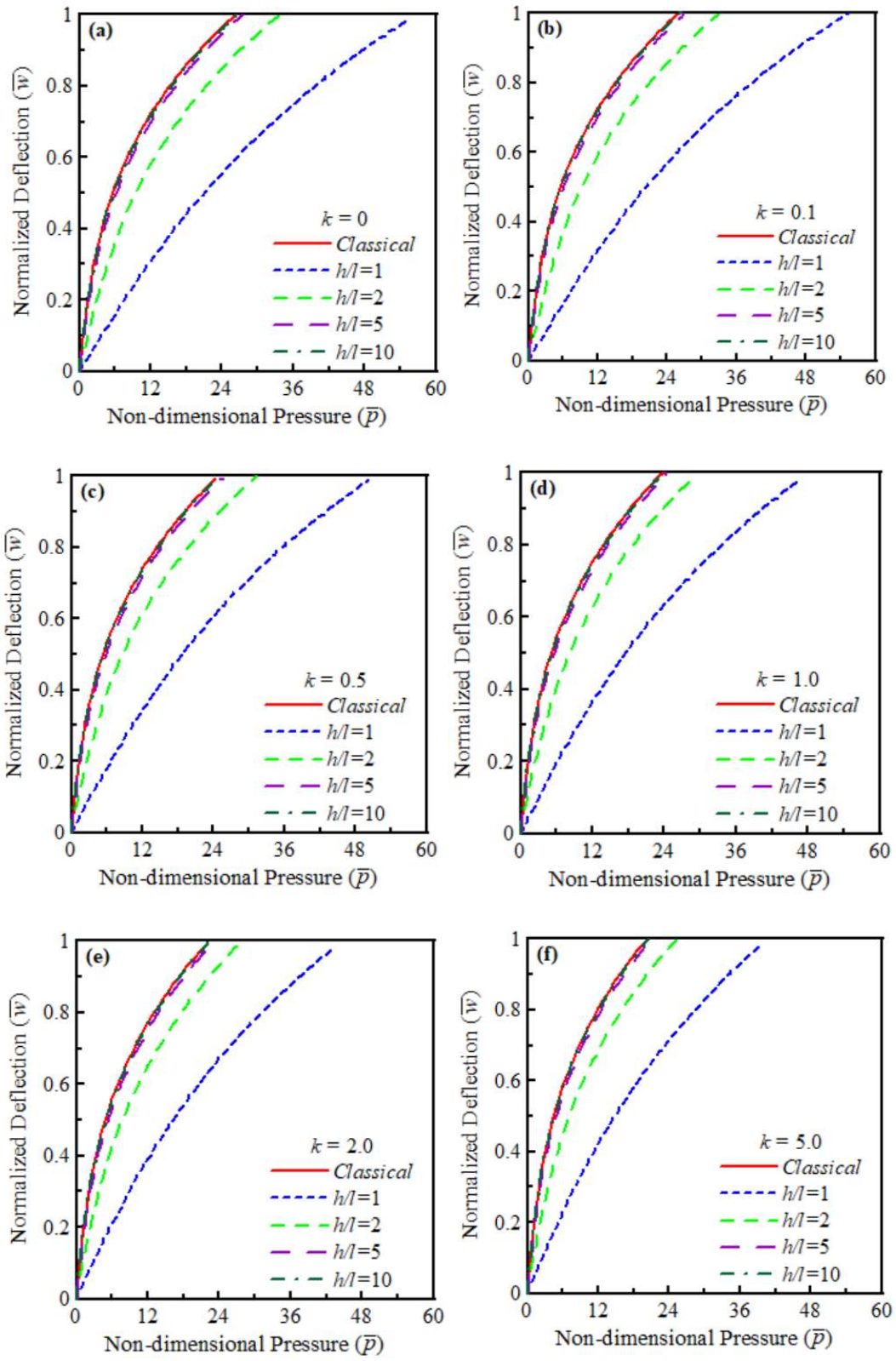

Fig. 3.5: Effect of size on non-dimensional load-deflection curves for HH micro-beams: (a) k=0, (b) k=0.1, (c) k=0.5, (d) k=1.0, (e) k=2.0, (f) k=5.0.

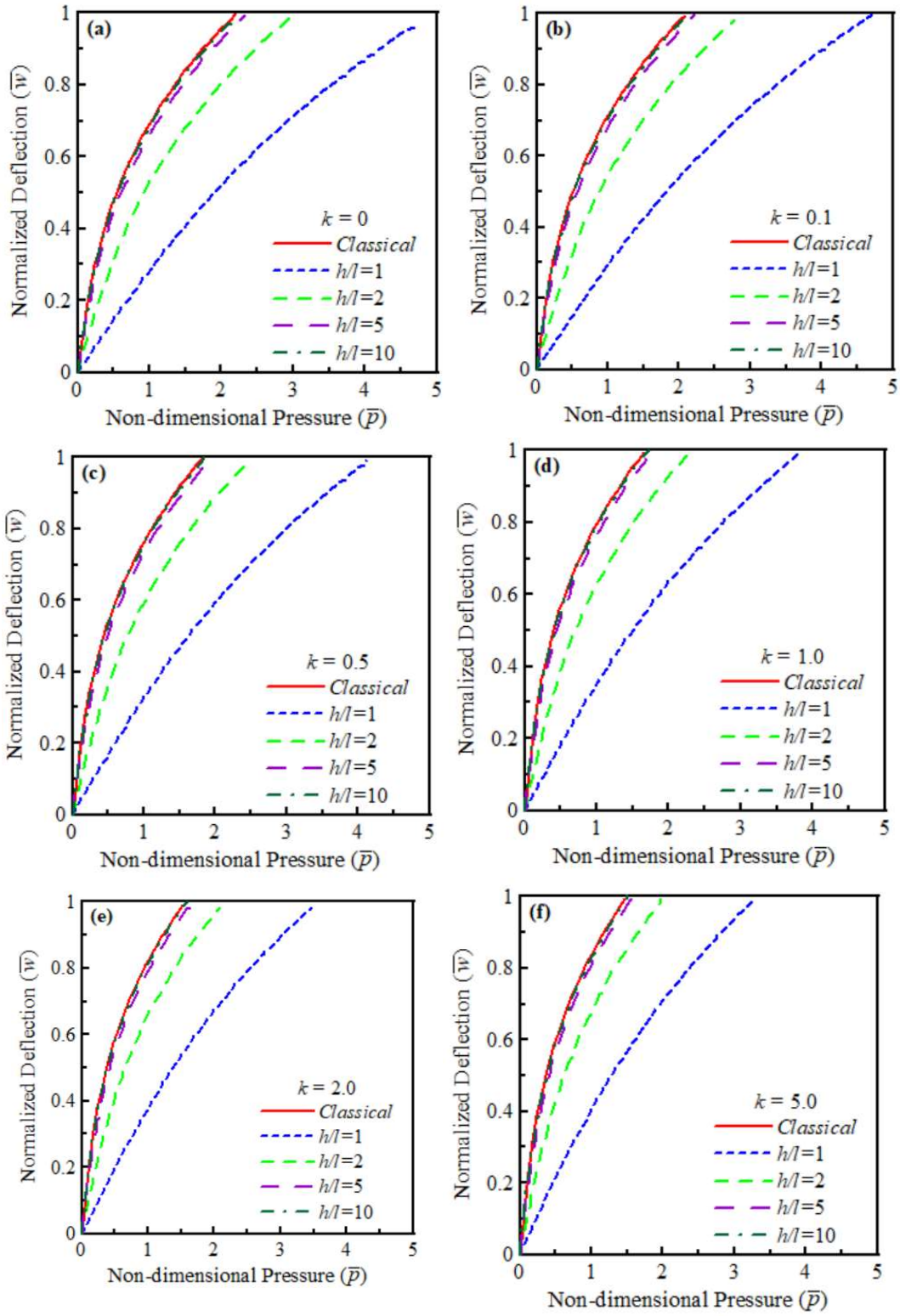

Fig. 3.6: Effect of size on non-dimensional load-deflection curves for CF micro-beams: (a) k=0, (b) k=0.1, (c) k=0.5, (d) k=1.0, (e) k=2.0, (f) k=5.0.

The non-dimensional load-deflection curves for the CC, CH, HH and CF boundary conditions are shown in Figs. 3.7(a)–(e), 3.8(a)–(e), 3.9(a)–(e) and 3.10(a)–(e) respectively. These curves for figures (a)-(e) correspond to different values of size-dependent thickness (h/l) which are: h/l=1.0, 2.0, 5.0, 10.0, and for classical FG micro-beam (l = 0) respectively. Figs. 3.7-3.10 are presented for a Stainless Steel/Silicon Nitride [FGM2] micro-beam. Each figure in Figs. 3.7-3.10 shows how material gradation index affects the non-dimensional load-deflection behaviour by varying the material gradation index, which are: k=0.0, 0.1, 0.5, 1.0, 2.0, 5.0.

In Figs. 3.7–3.10 for different boundary conditions, the non-dimensional load-deflection curves for various values of the size dependent thickness (h/l), that is h/l = 1, 2, 5, 10, and for classical beam (l = 0) are shown. In each of the figures in Figs. 3.7-3.10, the material gradation index (k) values are varied. With k = 0.0, 0.1, 0.5, 1.0, 2 and 5, it demonstrates the effect of material gradation index (k) on the non-dimensional load-deflection behaviour. For any given h/l value, it is observed that the steepness of the curve increases which means that the stiffness of the beam decreases so it becomes more flexible with increasing k. It is found to be maximum at k =5 whereas at k = 0.0, the beam rigidity is maximum as the curve is flat at k = 0.0. It is also observed from the figures that for any particular value of k, as the size effect increases that is value of h/l decreases, the stiffness of the beam increases and it is maximum for h/l = 1 and minimum for h/l = 10 as it approaches to same stiffness as a classical beam. From Figs. 3.7-3.10, the non-dimensional pressure is very less for CF beam as compared to other boundary conditions, which means that the stiffness is very less for CF micro-beams.

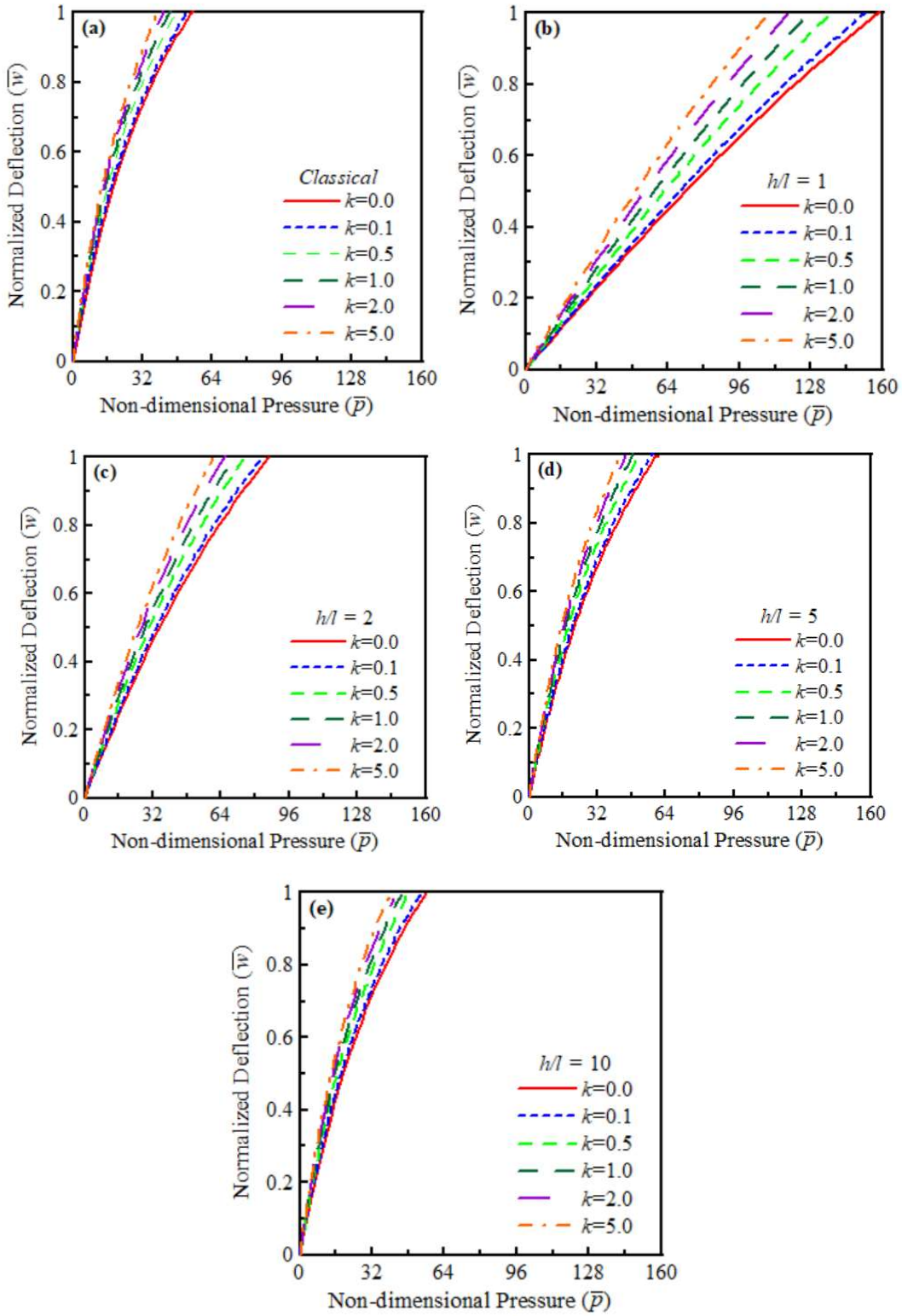

Fig. 3.7: Effect of material gradation index on non-dimensional load-deflection curves for CC micro-beams: (a) Classical (l=0), (b) h/l =1, (c) h/l =2, (d) h/l =5, (e) h/l =10.

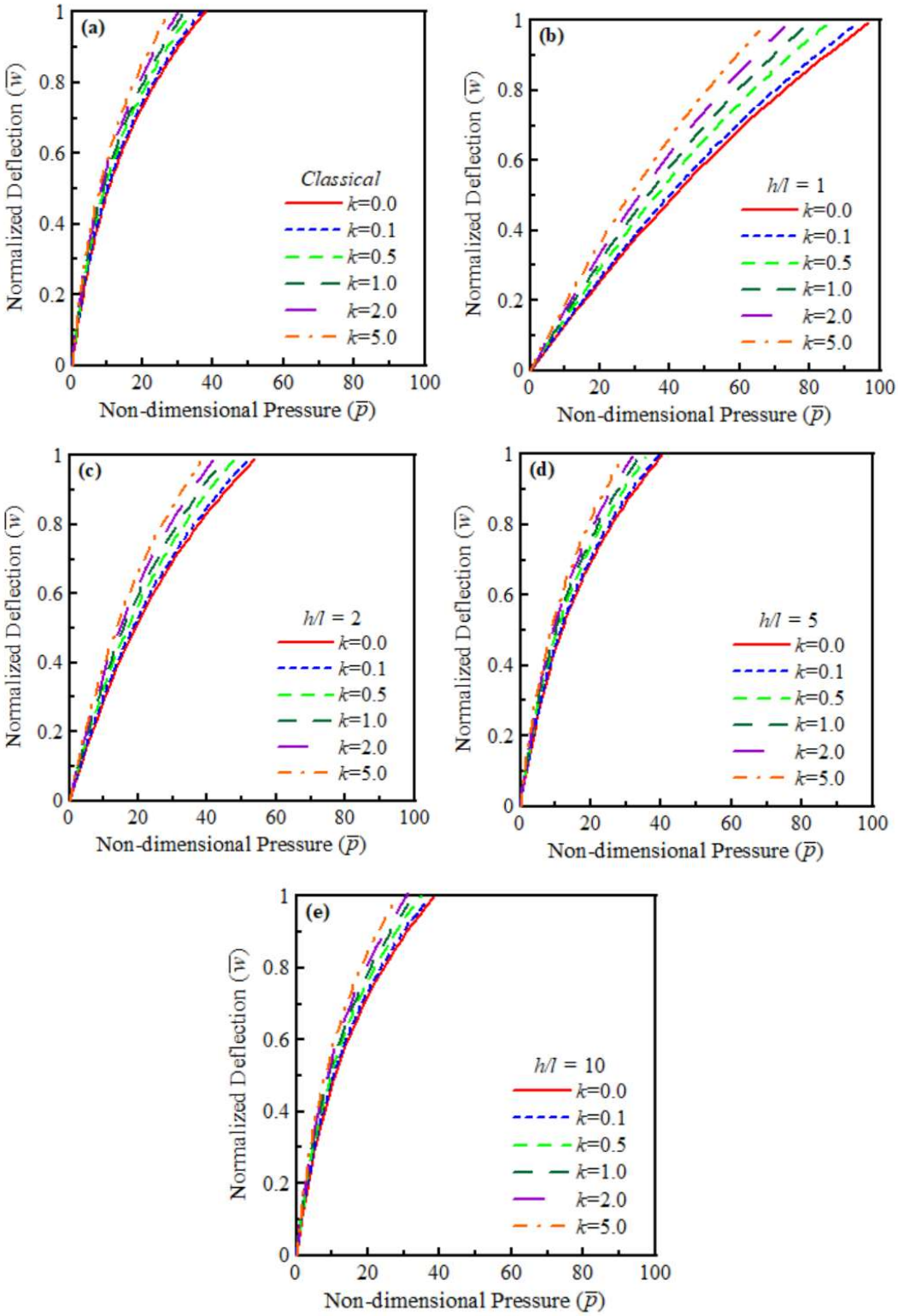

Fig. 3.8: Effect of material gradation index on non-dimensional load-deflection curves for CH micro-beams: (a) Classical (l=0), (b) h/l =1, (c) h/l =2, (d) h/l =5, (e) h/l =10.

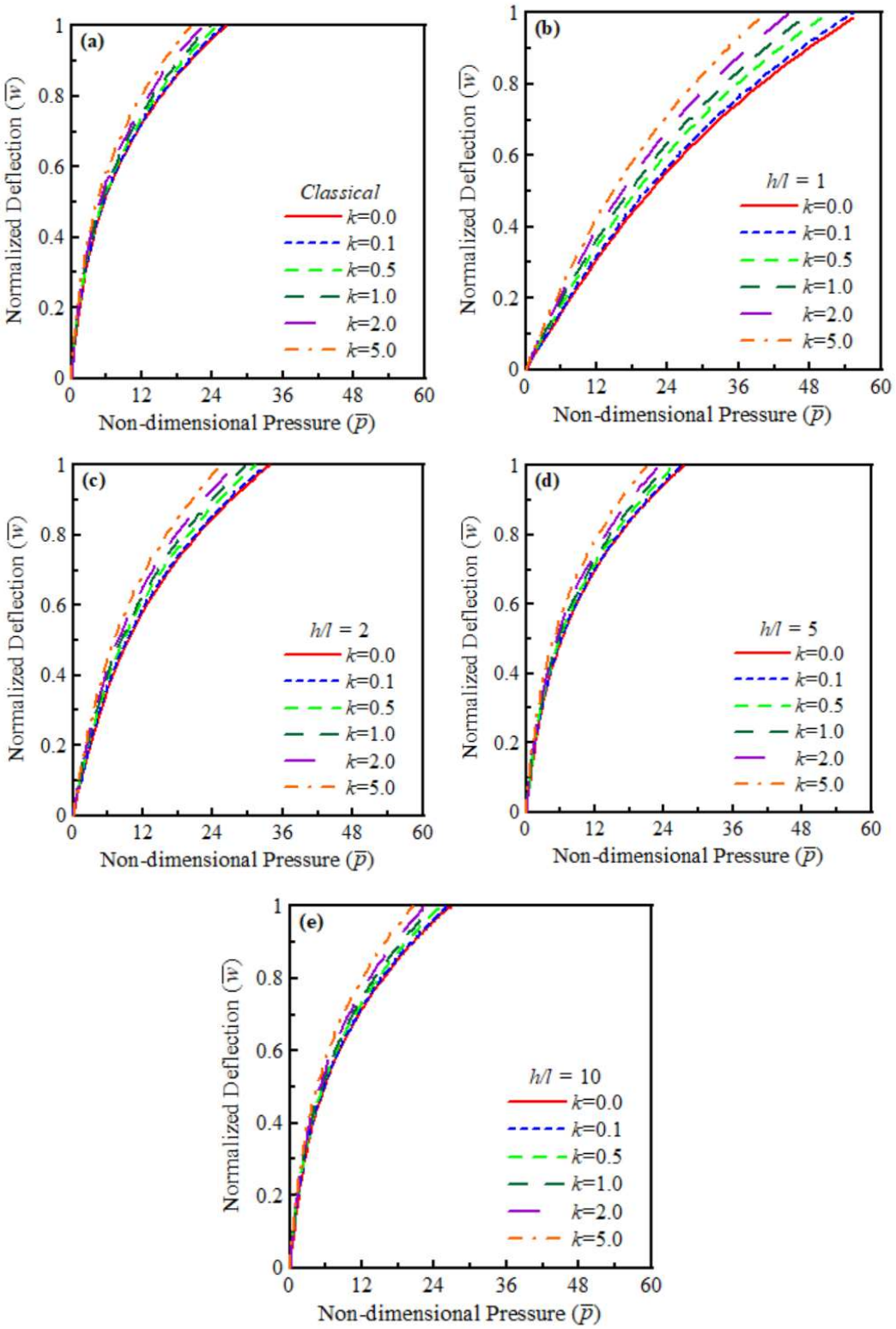

Fig. 3.9: Effect of material gradation index on non-dimensional load-deflection curves for HH micro-beams: (a) Classical (l=0), (b) h/l =1, (c) h/l =2, (d) h/l =5, (e) h/l =10.

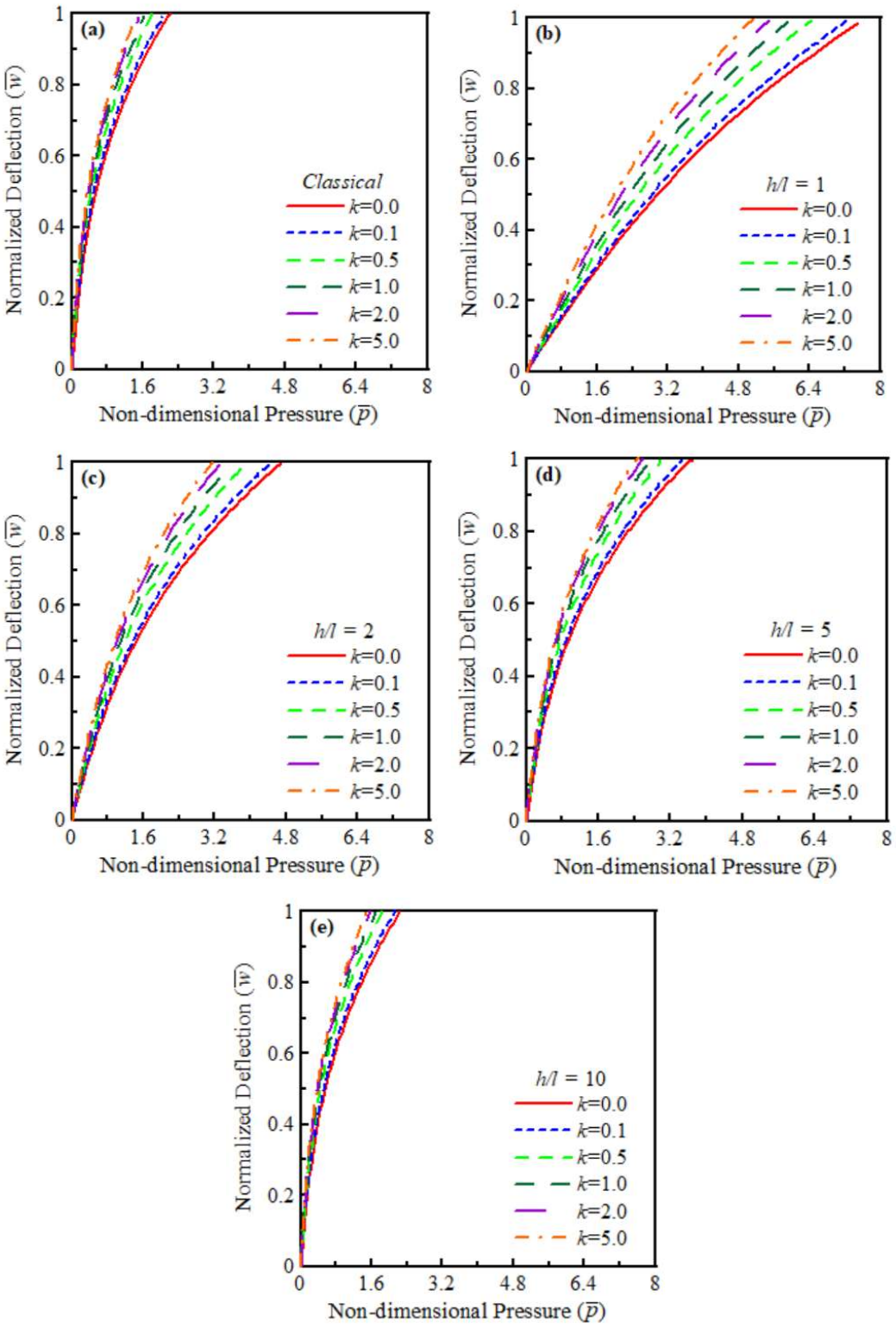

Fig. 3.10: Effect of material gradation index on non-dimensional load-deflection curves for CF micro-beams: (a) Classical (l=0), (b) h/l =1, (c) h/l =2, (d) h/l =5, (e) h/l =10.

The non-dimensional load-deflection curves for the CC, CH, HH and CF boundary conditions are shown in Figs. 3.11(a)–(f), 3.12(a)–(f), 3.13(a)–(f) and 3.14(a)–(f) respectively. These curves for figures (a)-(f) correspond to different values of material gradation index, i.e., k=0.0, 0.1, 0.5, 1.0, 2.0, and 5.0 respectively. Figs. 3.11-3.14 are presented for h/l=1. Each figure in Figs. 3.11-3.14 shows how different functionally graded material affects the non-dimensional load-deflection behaviour. The FGMs considered are as follows: Stainless Steel/Alumina [FGM1], Stainless Steel/Silicon Nitride [FGM2], Stainless Steel/Zirconia [FGM3] and Titanium Alloy/Zirconia [FGM4].

In Figs. 3.11–3.14 for different boundary conditions, the non-dimensional load-deflection curves for various values of the material gradation index (k), that is k = 0.0, 0.1, 0.5, 1, 2 and 5 are shown. Each of the Figs. 3.11-3.14 demonstrates the effect of different FGMs on the non-dimensional load-deflection behaviour. At k=0, almost all curves of different FGMs are coincident. As the value of k increases, the deviation of FGM 3 from other FGMs increases, and it is maximum at k = 5. So at k=5.0, the steepness of the curve corresponding to FGM 3 is lowest so its stiffness is maximum. But curves for other FGMs are coincident with each other, and have lower stiffness compared to FGM 3. For FGM 1, FGM 2 and FGM 4, as the material gradation index value (k) increases, the stiffness of the micro-beam decreases. But for FGM 3, as the value of material gradation index (k) increases, the stiffness of the micro-beam increases.

The non-dimensional load-deflection curves for the CC, CH, HH and CF boundary conditions are shown in Figs. 3.15(a)–(e), 3.16(a)–(e), 3.17(a)–(e) and 3.18(a)–(e) respectively. These curves for figures (a)-(e) correspond to different values of the size dependent thickness h/l, which are: h/l=1.0, 2.0, 5.0, 10.0, and for classical FG micro-beam (l = 0). Figs. 3.15-3.18 are presented for k=1. Each figure in Figs. 3.15-3.18 shows how different functionally graded material affects the non-dimensional load-deflection behaviour. The FGMs considered are as follows: Stainless Steel/Alumina [FGM1], Stainless Steel/Silicon Nitride [FGM2], Stainless Steel/Zirconia [FGM3] and Titanium Alloy/Zirconia [FGM4].

In Figs. 3.15–3.18 for different boundary conditions, the non-dimensional load-deflection curves for various values of the size dependent thickness (h/l), that is h/l=1, 2, 5, 10, and for classical beam (l = 0) are shown. Each of the figures of Figs. 3.15-3.18 demonstrate the effect of

different FGMs on the non-dimensional load-deflection behaviour. For any particular FG material, as the size effect increases, i.e., as *h/l* decreases, the stiffness of the beam increases.

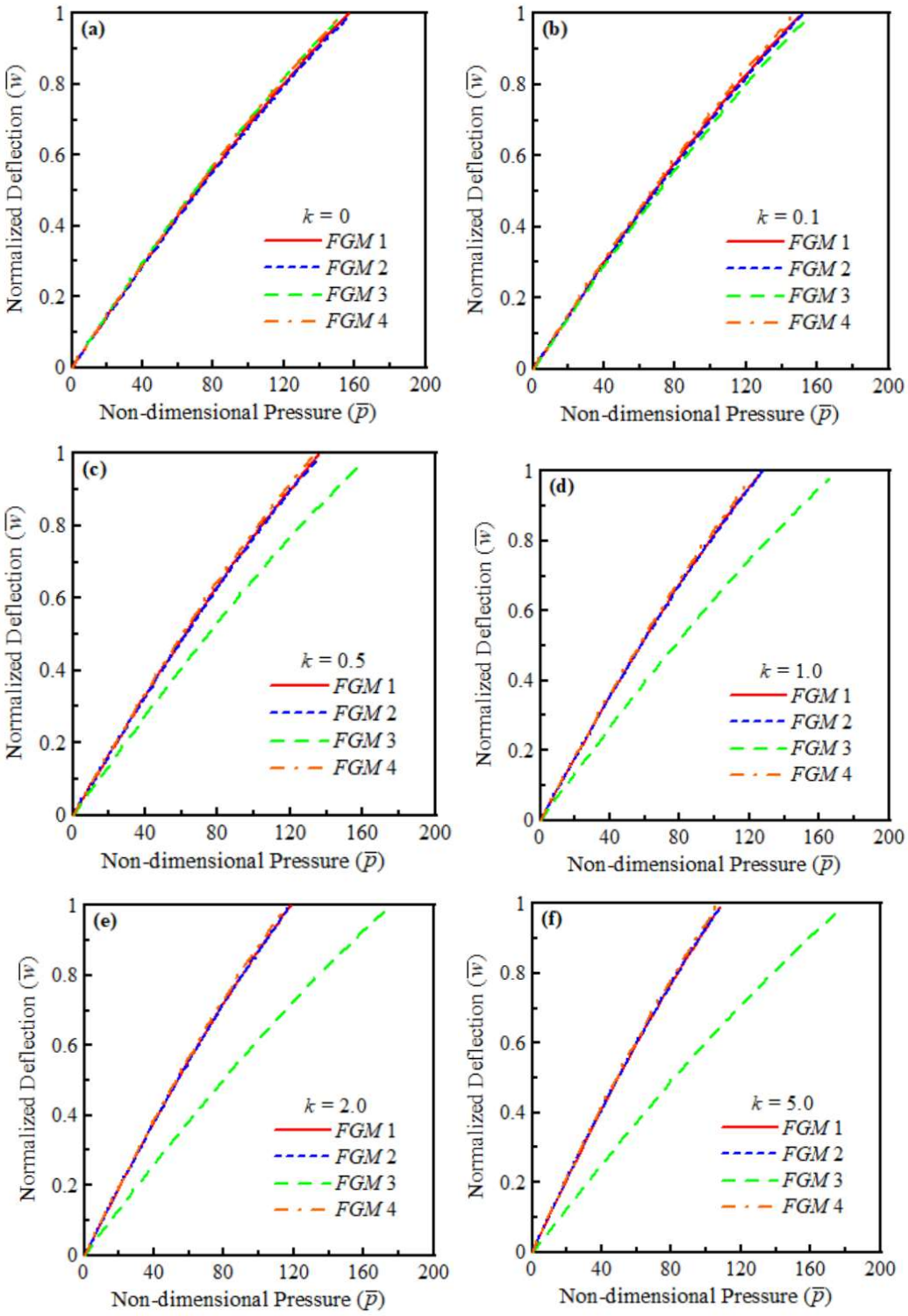

Fig. 3.11: Effect of different FGM compositions on non-dimensional load-deflection curves for CC micro-beams: (a) *k*=0, (b) *k*=0.1, (c) *k*=0.5, (d) *k*=1.0, (e) *k*=2.0, (f) *k*=5.0.

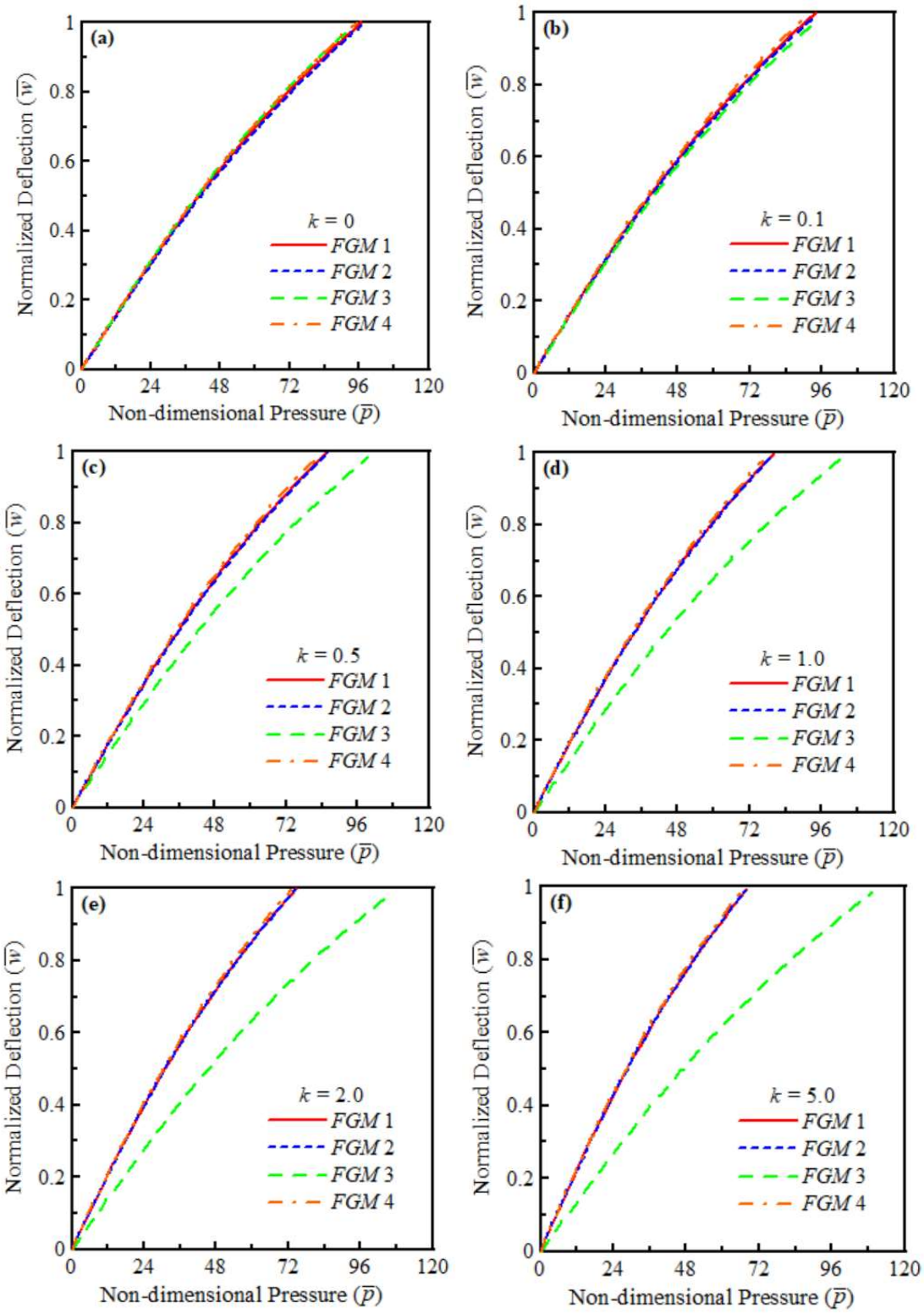

Fig. 3.12: Effect of different FGM compositions on non-dimensional load-deflection curves for CH micro-beams: (a) k=0, (b) k=0.1, (c) k=0.5, (d) k=1.0, (e) k=2.0, (f) k=5.0.

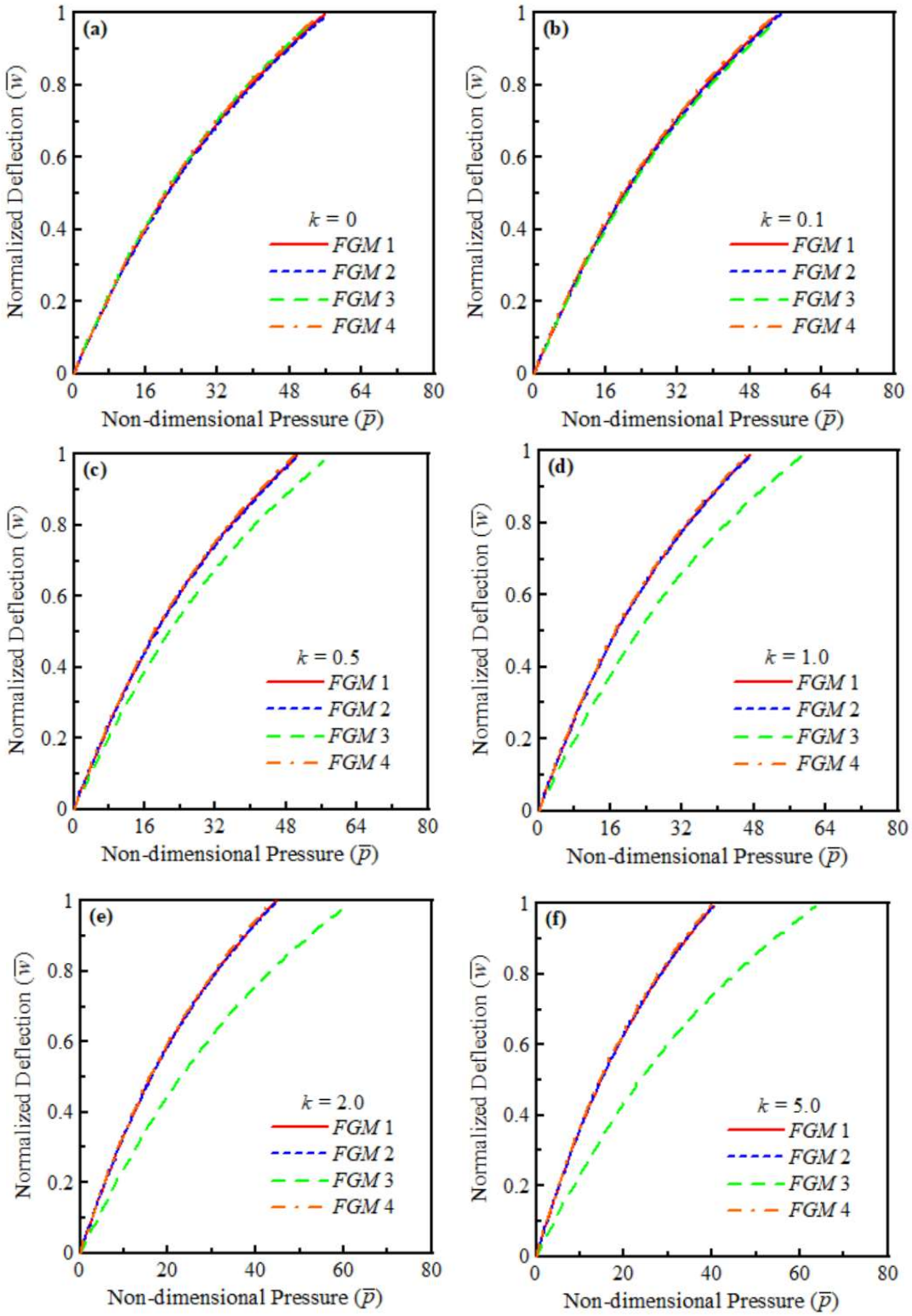

Fig. 3.13: Effect of different FGM compositions on non-dimensional load-deflection curves for HH micro-beams: (a) k=0, (b) k=0.1, (c) k=0.5, (d) k=1.0, (e) k=2.0, (f) k=5.0.

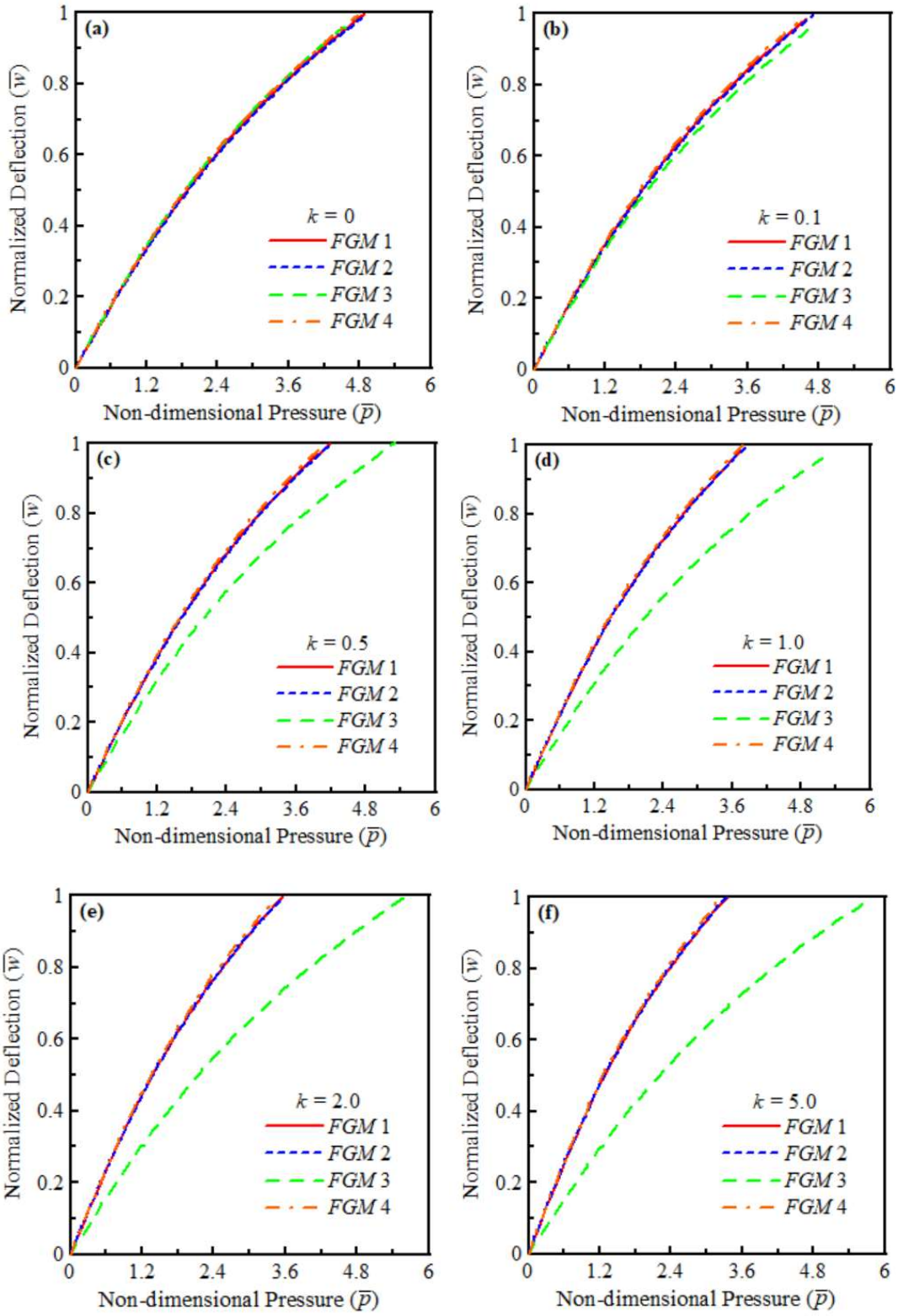

Fig. 3.14: Effect of different FGM compositions on non-dimensional load-deflection curves for CF micro-beams: (a) k=0, (b) k=0.1, (c) k=0.5, (d) k=1.0, (e) k=2.0, (f) k=5.0.

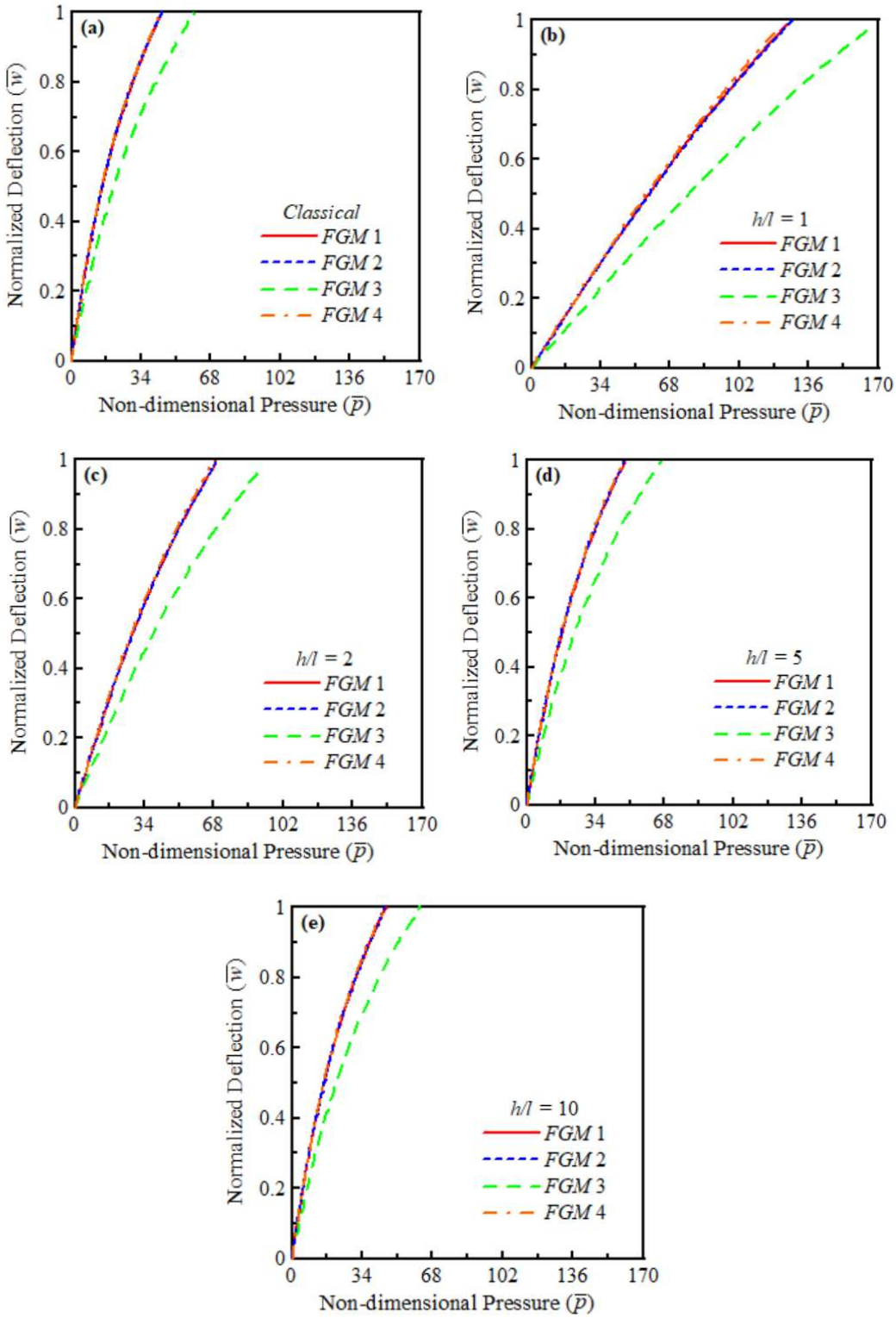

Fig. 3.15: Effect of different FGM compositions on non-dimensional load-deflection curves for CC micro-beams: (a) Classical (l=0), (b) h/l =1, (c) h/l =2, (d) h/l =5, (e) h/l =10.

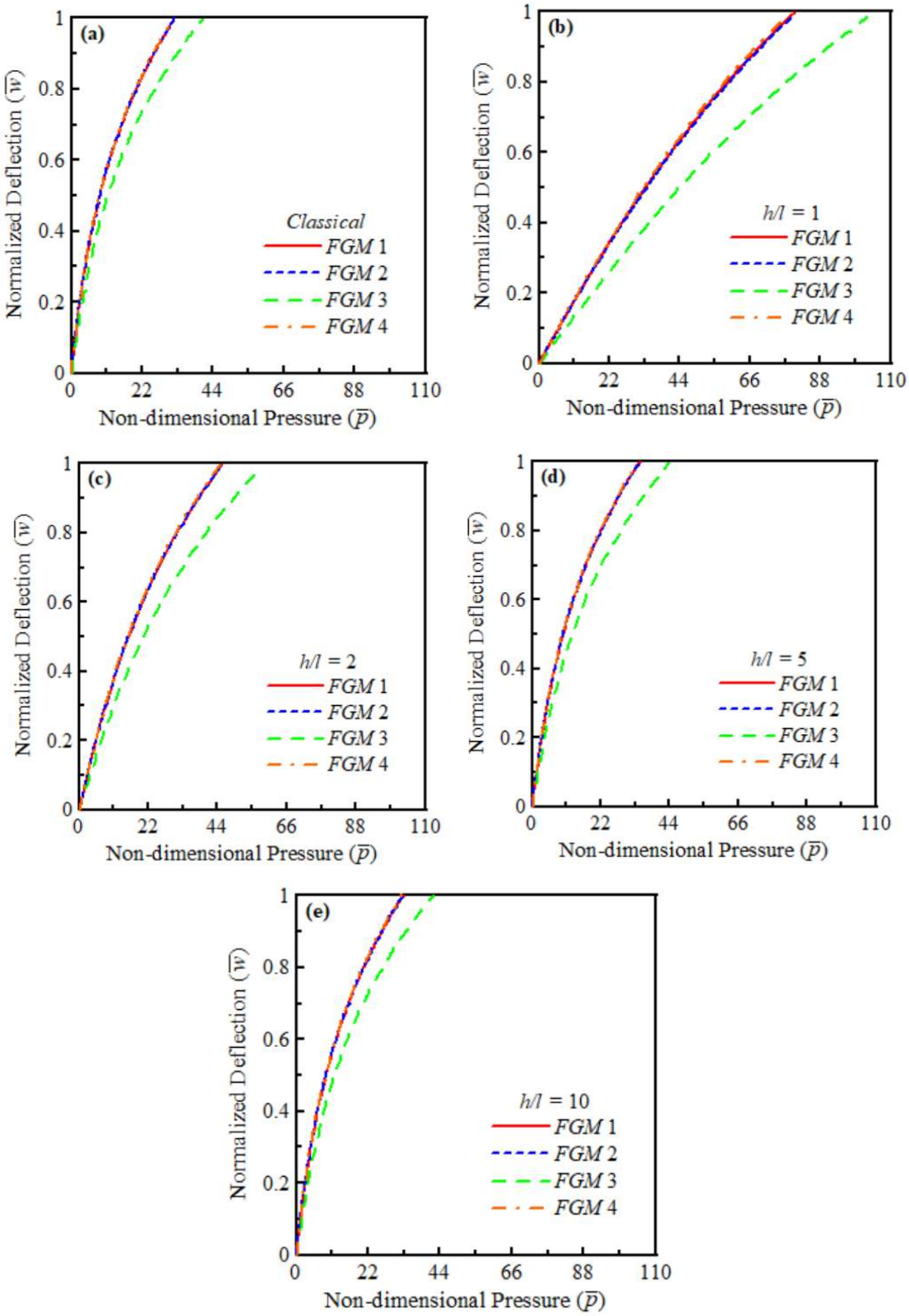

Fig. 3.16: Effect of different FGM compositions on non-dimensional load-deflection curves for CH micro-beams: (a) Classical (l=0), (b) h/l =1, (c) h/l =2, (d) h/l =5, (e) h/l =10.

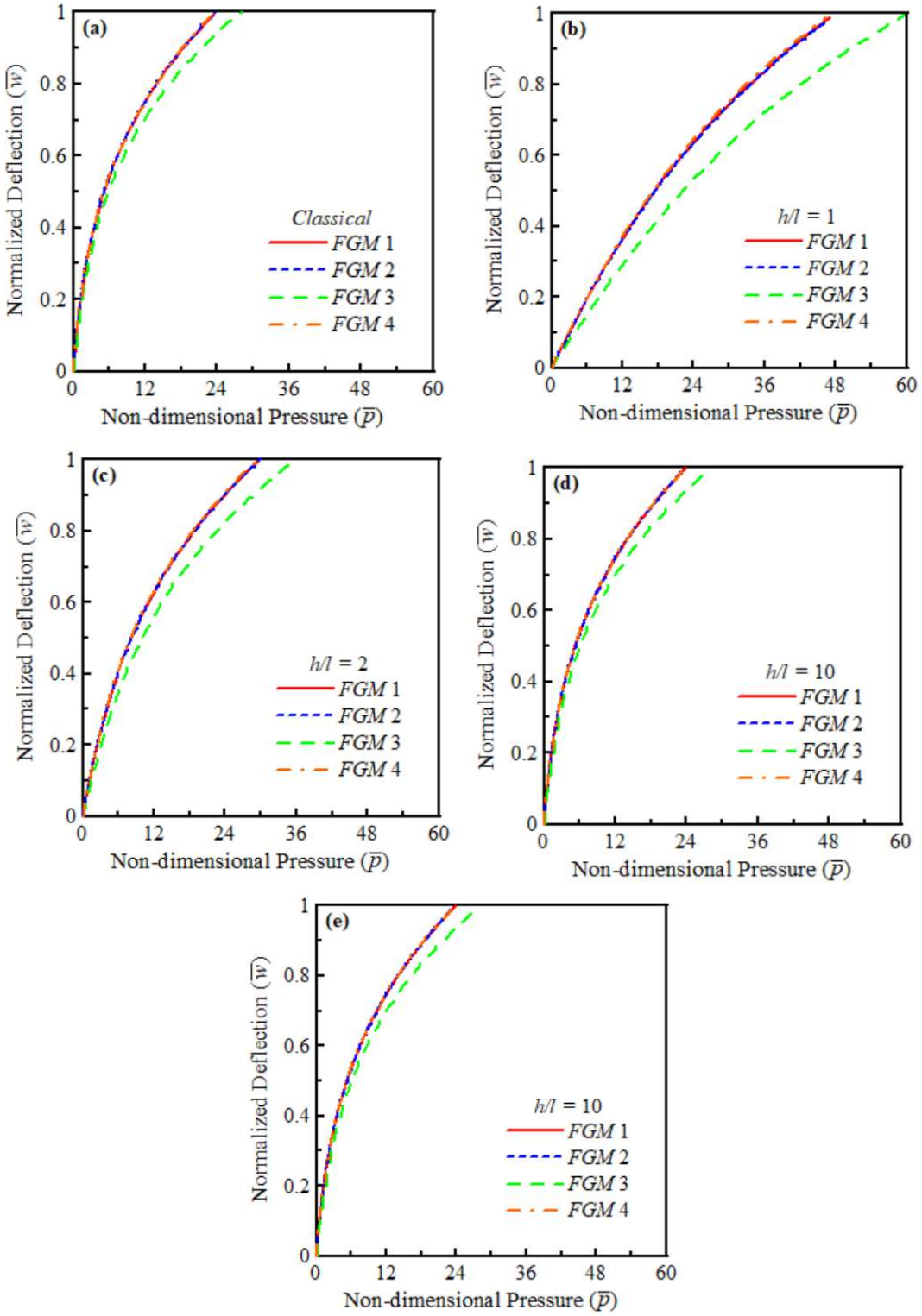

Fig. 3.17: Effect of different FGM compositions on non-dimensional load-deflection curves for HH micro-beams: (a) Classical (l=0), (b) h/l =1, (c) h/l =2, (d) h/l =5, (e) h/l =10.

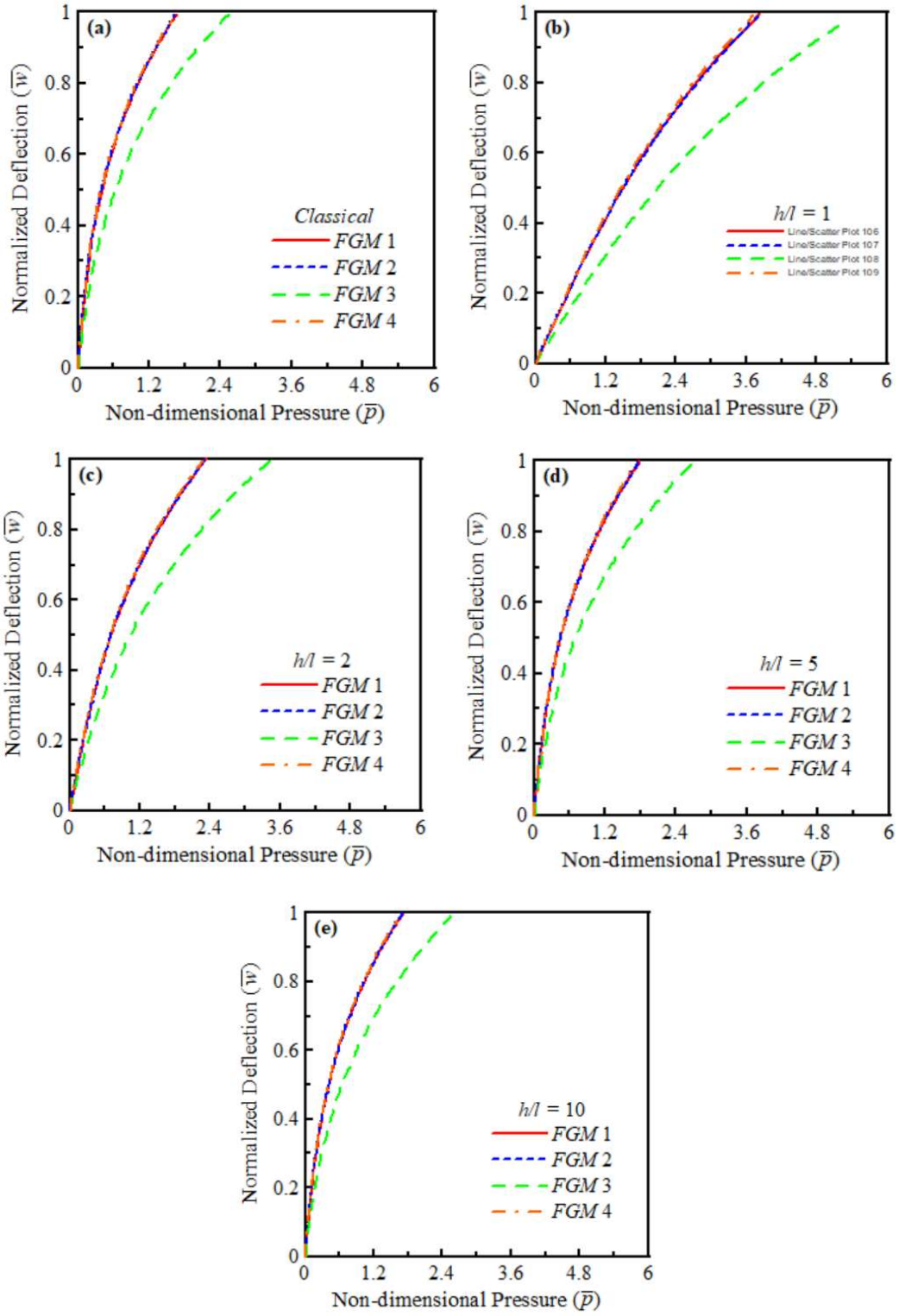

Fig. 3.18: Effect of different FGM compositions on non-dimensional load-deflection curves for CF micro-beams: (a) Classical (l=0), (b) h/l =1, (c) h/l =2, (d) h/l =5, (e) h/l =10.

3.4 Chapter Summary

In this chapter we discussed the static deflection behaviour of Timoshenko micro-beams made of functionally graded materials (FGMs). It presented theoretical investigation using the von Kármán non-linear strain-displacement relationship and the minimum potential energy principle to derive the governing equation for static deflection. The study evaluated four different FGMs under various boundary conditions. Validation of the model is conducted against previous studies, demonstrating excellent agreement and thereby validating the present model. The results are presented graphically as well as in tabulated form. The findings suggest that as the material gradation index increases, the stiffness of the micro-beam decreases for most FGMs, except for FGM 3, where stiffness increases with the material gradation index. Additionally, it is observed that the stiffness of the beam decreases as the size effect decreases, approaching the stiffness of a classical beam. Furthermore, for specific boundary conditions, the non-dimensional pressure is significantly lower for the CF beams, indicating lower stiffness compared to other boundary conditions. The study provides valuable insights into the static deflection behaviour of FGM micro beams, elucidating the influence of material gradation, size-dependent thickness, and boundary conditions on the non-dimensional load-deflection behaviour.

Chapter 4

RESULTS FOR FREE VIBRATION OF PRE-LOADED MICRO-BEAM

4.1 Introduction

A theoretical investigation examines the free vibration of pre-loaded Timoshenko micro-beam made of functionally graded material (FGM), where the volume fraction varies according to a power law along the thickness direction. To capture geometric non-linearity, the von Kármán non-linear strain-displacement relationship is utilized. The governing equation is derived using the Hamilton's principle. We explored four different boundary conditions namely Clamped-Clamped (CC), Clamped-Hinged (CH), Hinged-Hinged (HH) and Clamped-Free (CF). The study evaluates the free vibration of pre-loaded beam made of four different FGMs: Stainless Steel/Alumina (SUS304/Al_2O_3) [FGM1], Stainless Steel/Silicon Nitride (SUS304/Si_3N_4) [FGM2], Stainless Steel/Zirconia (SUS304/ZrO_2) [FGM3] and Titanium Alloy/Zirconia (Ti-6Al-4V/ZrO_2) [FGM4]. The mathematical formulation for free vibration presented in the Chapter 2 along with the mechanical properties of four FGMs.

4.2 Validation

We have compared our result with Paul and Das (2016). The validation plots for Stainless Steel/Zirconia (FGM3) Timoshenko beam are presented in Figs. 4.1(a)–(c), which show the plot of λ - $\overline{w}$ for k = 2.0 where λ is the non-dimensional loaded natural frequency and $\overline{w}$ is the normalized maximum transverse deflection which are defined as follows $\lambda = \omega L^2 \sqrt{(\rho_m A)/(E_m I)}$ and $\overline{w} = w/h$, where ω natural frequency of vibration of the beam, L is the length of the beam, w is the maximum transverse deflection, A is the cross sectional area (A=bh), I is the area moment of inertia about centroidal axis ($I = bh^3/12$), h is the thickness of

beam (h=0.01 m) and b is the width of the beam (b=0.02 m). The material properties for FGM3 are given as follows: E_m=207.79GPa, E_c=168.06 GPa, μ_m=0.318, μ_c=0.298, ρ_m=8166 $\left(kg\,m^{-3}\right)$and ρ_c =3000$\left(kg\,m^{-3}\right)$. Figs. 4.1(a)-(c) shows the plot of λ - $\overline{w}$ for CC, CH and HH beams respectively. Excellent agreement with the current model can be seen in Fig. 4.1, which validates the classical beam model for pre-loaded conditions.

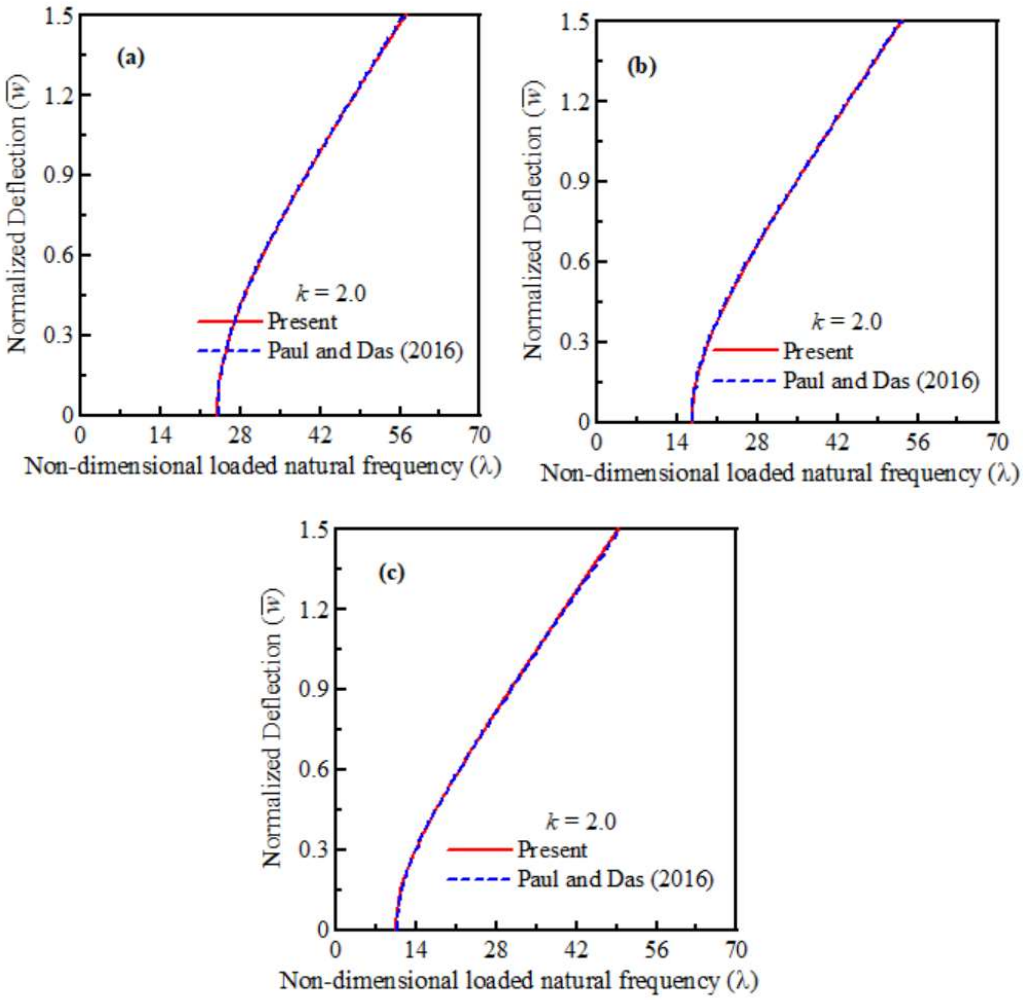

Fig 4.1: Validation plots for free vibration of preloaded beam for various boundary conditions: (a) CC, (b) CH, (c) HH.

Furthermore, we compared our model to that of Hemmatnezhad et al. (2013). The table presented below shows the non-dimensional frequency parameter λ of undeformed FGM beam, which is given as follows: $\lambda^2 = \omega L^2\sqrt{\left(\rho_s A\right)/\left(E_s I\right)}$,where ω is the natural frequency of

vibration of beam, L is the length of the beam, A is the cross sectional area ($A=bh$), I is the area moment of inertia about centroidal axis ($I = bh^3/12$), h is the thickness of beam (h=0.01 m) and b is the width of the beam (b=0.02 m). The comparison is made for various volume fraction indices (k) as well as various boundary conditions. Alumina–Steel FGM beams with varying length-to-thickness (L/h) ratios are compared. The following material properties were used for comparison: E_m=210 GPa, E_c = 390 GPa, μ_m = 0.29, μ_c = 0.22, ρ_m = 7800 $\left(kg\,m^{-3}\right)$ and ρ_c = 3960 $\left(kg\,m^{-3}\right)$. Table 4.1 provides evidence of a good agreement between the current findings and those of Hemmatnezhad et al (2013). This shows that the free vibration dynamic behaviour of the classical beam, as determined by the current methodology, is valid for the undeformed FGM beam.

Table 4.1: Comparison of frequency parameters for various L/h values.

L/h		Hemmatnezhad et al. (2013)	Present	Hemmatnezhad et al. (2013)	Present	Hemmatnezhad et al. (2013)	Present
		k = 0	k= 0	k= 0.5	k= 0.5	k= 5	k=5
20	HH	4.3371	4.3362	3.8554	3.8413	3.3803	3.3643
	CC	6.4971	6.4912	5.7575	5.7511	5.0390	5.0333
	CH	5.4086	5.4058	4.7951	4.7891	4.1990	4.1931
50	HH	4.3435	4.3433	3.8611	3.8476	3.3857	3.3703
	CC	6.5343	6.5333	5.7899	5.7878	5.0706	5.0691
	CH	5.4268	5.4263	4.8111	4.8071	4.2145	4.2105
100	HH	4.3444	4.3443	3.8619	3.8485	3.3864	3.3711
	CC	6.5397	6.5394	5.7946	5.7931	5.0752	5.0743
	CH	5.4295	5.4293	4.8134	4.8097	4.2167	4.2130

Additionally, we contrasted the analytical solutions provided by Ansari et al. (2011) with our current analysis. The comparison is carried out for a HH isotropic homogeneous Timoshenko micro-beam with k_s = 5/6, L/h = 10, μ = 0.38, ρ = 1220 kg/m3, E = 1.44 GPa and l = 17.6 μm, for various h/l ratios. Table 4.2 presents the initial two natural frequencies (MHz) for a range of

h/l values. It demonstrates a high degree of agreement with our current model, thereby validating our micro beam model.

Table 4.2: Comparison of first two natural frequencies (MHz) for isotropic homogeneous microbeams.

Mode	*h/l*=10		*h/l*=5		*h/l*=3.33	
	Present	Ansari et al. (2011)	Present	Ansari et al. (2011)	Present	Ansari et al. (2011))
1	0.0377	0.0376	0.0778	0.0778	0.1229	0.1229
2	0.1397	0.1397	0.2887	0.2888	0.4561	0.4561

Table 4.3: Comparison of the initial five natural frequencies (MHz) for isotropic homogeneous microbeams with respect to variation in *h/l* values.

Mode	*h/l*=3			*h/l*=1		
	Present	Ke et al. (2012)	Ma et al. (2008)	Present	Ke et al. (2012)	Ma et al. (2008)
1	0.1391	0.1391	0.1391	0.6723	0.6724	0.6723
2	0.5163	0.5163	0.5163	2.4529	2.4533	2.4530
3	1.0519	1.0519	1.0519	4.9368	4.9374	4.9374
4	1.6813	1.6814	1.6814	7.8606	7.8615	7.8606
5	2.3693	2.3677	2.3677	11.116	11.1057	11.1045

To validate our micro beam model, we have also compared our model with Ke et al. (2012) and Ma et al. (2008) for simply-supported isotropic homogeneous Timoshenko micro-beam with k_s = 5/6, *L/h* = 10, μ = 0.38, ρ = 1220 kg/m3, *E* = 1.44 GPa and $l = 17.6\,\mu m$ for various *h/l* ratios. Table 4.3 also shows good agreement and thus validates our micro-beam model.

Table 4.4: Comparison of first three non-dimensional natural frequency of functionally graded simply supported micro-beam.

k	l/h	Reddy (2011)	Present	Reddy (2011)	Present	Reddy (2011)	Present
		ϖ_1	ϖ_1	ϖ_2	ϖ_2	ϖ_3	ϖ_3
0	0.0	9.83	9.83	38.82	38.82	85.63	85.63
	0.2	10.65	10.65	42.06	42.06	92.78	92.78
	0.4	12.80	12.79	50.52	50.51	111.34	111.34
	0.6	15.73	15.73	62.01	62.01	136.39	136.39
	0.8	19.08	19.08	75.05	75.05	164.51	164.50
	1.0	22.66	22.66	88.84	88.84	193.82	193.82
1	0.0	8.67	8.66	34.29	34.27	75.79	75.56
	0.2	9.59	9.58	37.93	37.91	83.84	83.46
	0.4	11.93	11.92	47.16	47.14	104.15	110.94
	0.6	15.04	15.03	59.35	59.31	130.77	131.90
	0.8	18.52	18.51	72.91	72.83	160.69	160.84
	1.0	22.28	22.19	87.42	86.89	190.99	190.96
10	0.0	10.28	10.28	40.47	40.45	88.80	87.83
	0.2	11.07	11.06	43.56	43.53	95.58	93.96
	0.4	13.14	13.14	51.70	51.65	113.38	104.82
	0.6	16.00	16.00	62.88	62.80	137.66	139.42
	0.8	19.30	19.30	75.67	75.49	165.14	166.50
	1.0	22.92	22.84	89.57	88.83	194.63	195.18

To validate FGM Timoshenko micro-beam model, we compared our model with Reddy (2011). The comparison details are given in the Table 4.4. The material properties for FGM beam is given as follows: E_1=14.4 GPa, E_2=1.44 GPa, $\rho_1 = 12.2\times10^3\ kg/m^3$,

$\rho_2 = 1.22\times10^3\ kg/m^3$, $\mu = 0.38$, $k_s = \left(5(1+\mu)/6+5\mu\right)$, b = 2h, L=20h. Table 4.4 presents the first three non-dimensional natural frequencies which is given as follows: $\varpi_n = \omega_n L^2\sqrt{\rho_2 A / E_2 I}$, where ϖ_n is the non-dimensional natural frequency, ω_n is the natural frequency, L is the length, A is the area (A=bh) and I is the moment of inertia about centroidal axis ($I = b\,h^3/12$). The comparison is shown for a range of h/l values along with variation in material gradation index (k). The comparison of the first three non-dimensional natural frequencies shown in Table 4.4 demonstrates strong agreement with our current model, validating our micro-beam model.

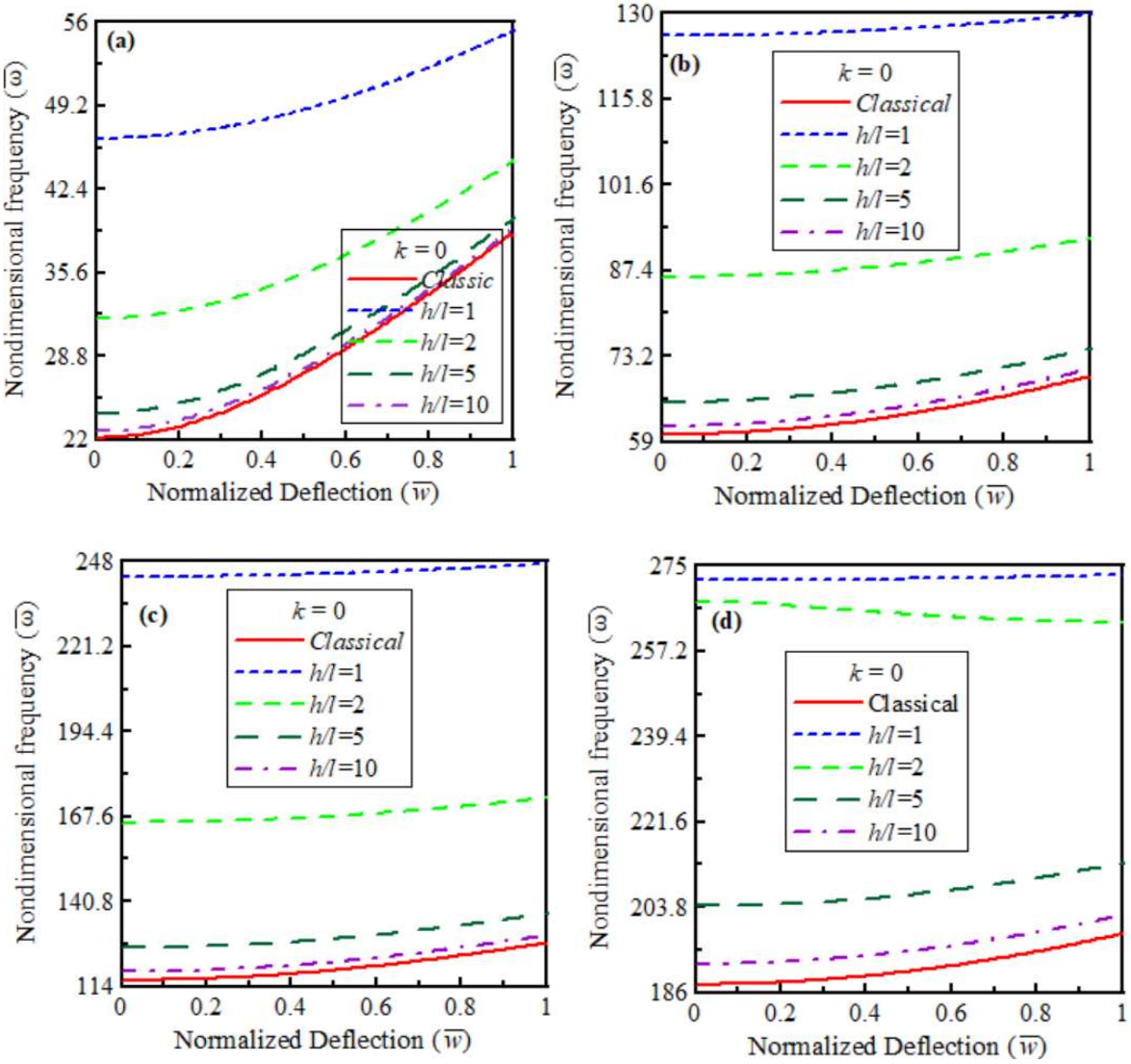

Fig. 4.2A: Effect of size on non-dimensional deflection-frequency curves for CC beams with k=0: (a) first mode, (b) second mode, (c) third mode, (d) fourth mode.

4.3 Results for Different Parameters

The present work is carried out to determine the free vibration frequencies of FGM micro beams. The dynamic behaviour is presented graphically in non-dimensional $\bar{w}$-$\bar{\omega}$ plane, where $\bar{w}$ is the normalized maximum transverse deflection and $\bar{\omega}$ is the non-dimensional frequency. The expression for $\bar{w}$ and $\bar{\omega}$ are as follows: $\bar{w} = w_{\max} / h$ and $\bar{\omega} = \omega L^2 \sqrt{\frac{\rho_c A}{E_c I}}$. Here ω is the natural frequency of vibration of micro-beam, L is the length of the beam which is related to thickness of beam h as follows: L/h=25, E_c is the Young's modulus of ceramic, A is the area of the beam (A= bh), b is the width of the beam which is also related to h as follows b/h=2 and $w_{\max}$ is the maximum transverse deflection. To incorporate the size effect, the material length scale parameter l is taken as 17.6 micron. Unless specified, the results are generated for a Stainless Steel/Silicon Nitride [FGM2] micro-beam.

The non-dimensional deflection-frequency curves for the first four modes of the CC, CH, HH and CF boundary conditions are shown in Figs. 4.2A-C, 4.3A-C, 4.4A–C and 4.5A–C respectively. Figures A-C correspond to different values of the material gradation index which are: k=0.0, 1.0, 5.0. In each of the figures A-C, plots are presented for the first four modes, indicated by (a)-(d) respectively. Each figure in Figs. 4.2-4.5 shows how size affects the non-dimensional deflection-frequency behaviour by varying the size-dependent thickness (h/l) values as h/l=1.0, 2.0, 5.0, 10.0, and for classical FG beam (l = 0).

The non-dimensional deflection-frequency curves for the first four modes of the CC, CH, HH and CF boundary conditions are shown in Figs. 4.6A-C, 4.7A-C, 4.8A–C and 4.9A–C respectively. Figures A-C correspond to different values of size-dependent thickness (h/l) such as: h/l=1.0, 5.0, and for classical FG beam (l = 0). In each of the figures A-C, plots are presented for the first four modes, indicated by (a)-(d) respectively. Each figure in Figs. 4.6-4.9 shows how the material gradation index affects the non-dimensional deflection-frequency behaviour by varying the material gradation index which are: k=0.0, 0.1, 0.5, 1.0, 2.0, and 5.0.

For a particular mode and particular material gradation index (k), natural frequency increases as size effect increases and it is maximum for h/l = 1, and deceases as size effect decreases and approaches to the natural frequency of the classical beam at h/l=10. We compared

the difference between $\bar{\omega}_{max}$ and $\bar{\omega}_{min}$, defined as $\Delta\bar{\omega} = \bar{\omega}_{max} - \bar{\omega}_{min}$, where $\bar{\omega}_{max}$ and $\bar{\omega}_{min}$ are defined as the maximum and minimum values of vibration frequencies at w_{max} = 0 and 1.5 respectively. This is highest for the classical beam and lowest for *h/l* = 1. As the size effect increases, $\Delta\bar{\omega}$ decreases and vice versa. For any particular mode, it is found that: $\bar{\omega}_{C-C} > \bar{\omega}_{C-H} > \bar{\omega}_{H-H} > \bar{\omega}_{C-F}$. For any particular mode, it is found that: $\Delta\bar{\omega}_{H-H} > \Delta\bar{\omega}_{C-H} > \Delta\bar{\omega}_{C-C} > \Delta\bar{\omega}_{C-F}$.

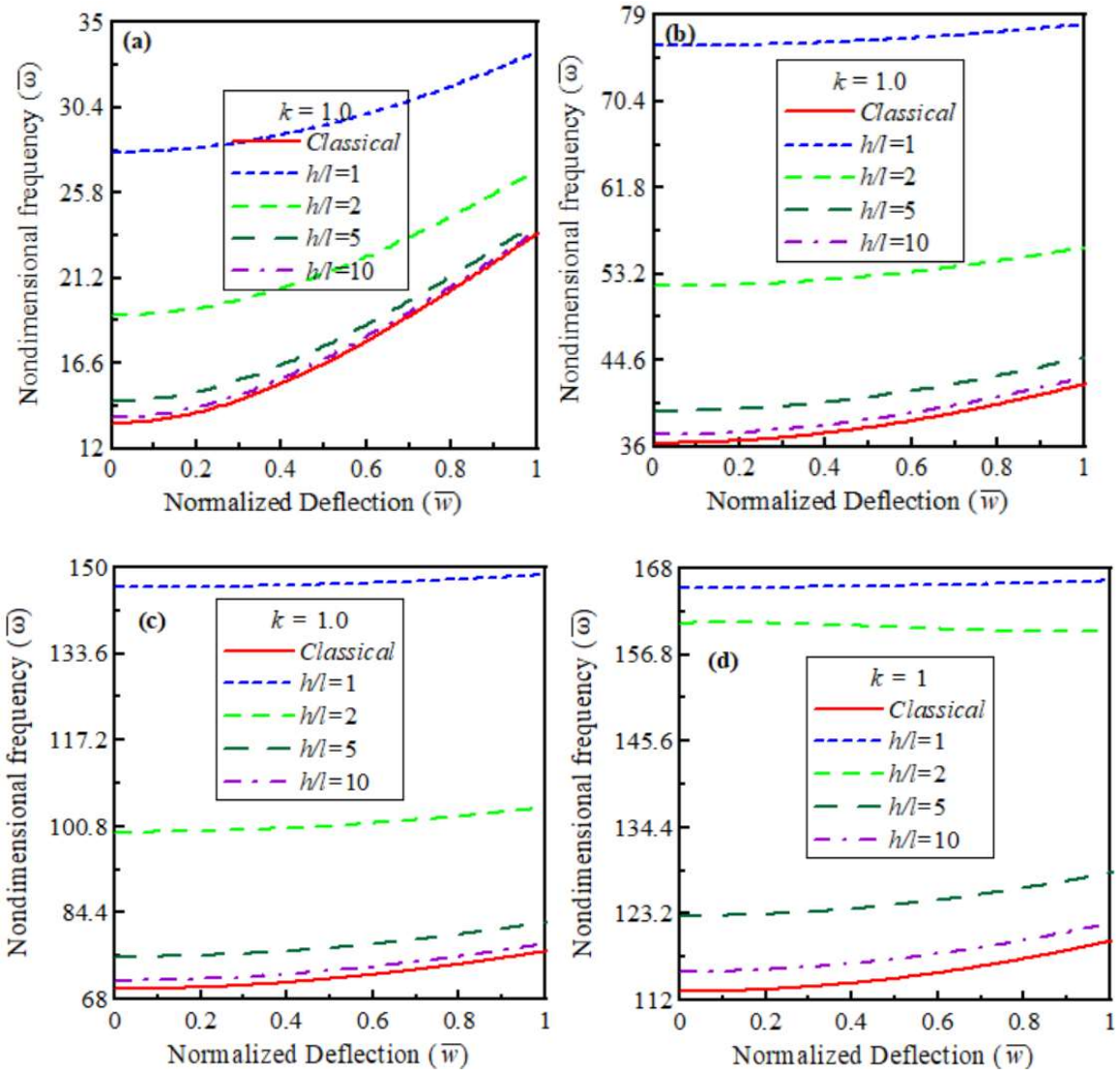

Fig. 4.2B: Effect of size on non-dimensional deflection-frequency curves for CC beams with *k*=1: (a) first mode, (b) second mode, (c) third mode, (d) fourth mode.

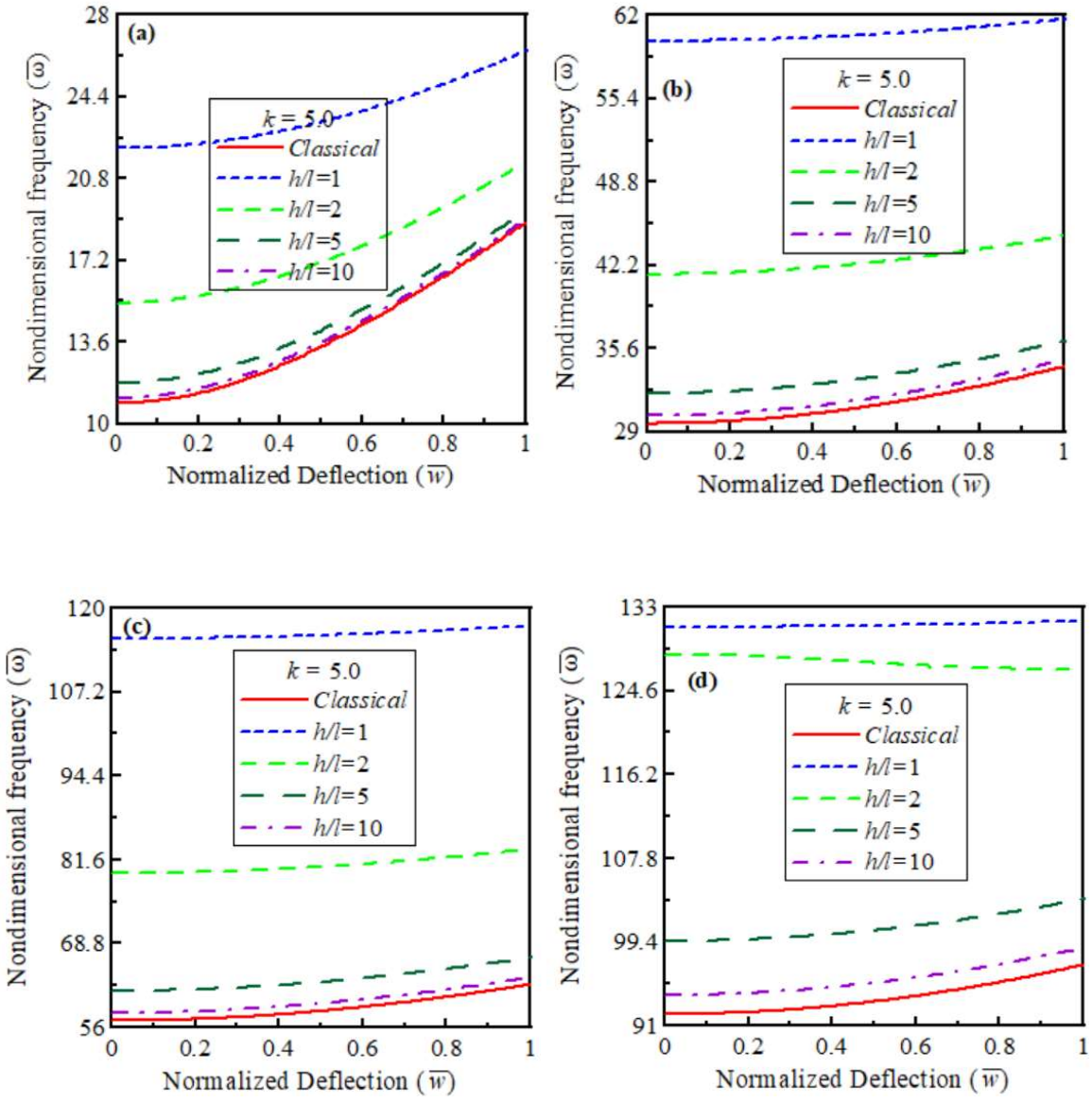

Fig. 4.2C: Effect of size on non-dimensional deflection-frequency curves for CC beams with k=5: (a) first mode, (b) second mode, (c) third mode, (d) fourth mode.

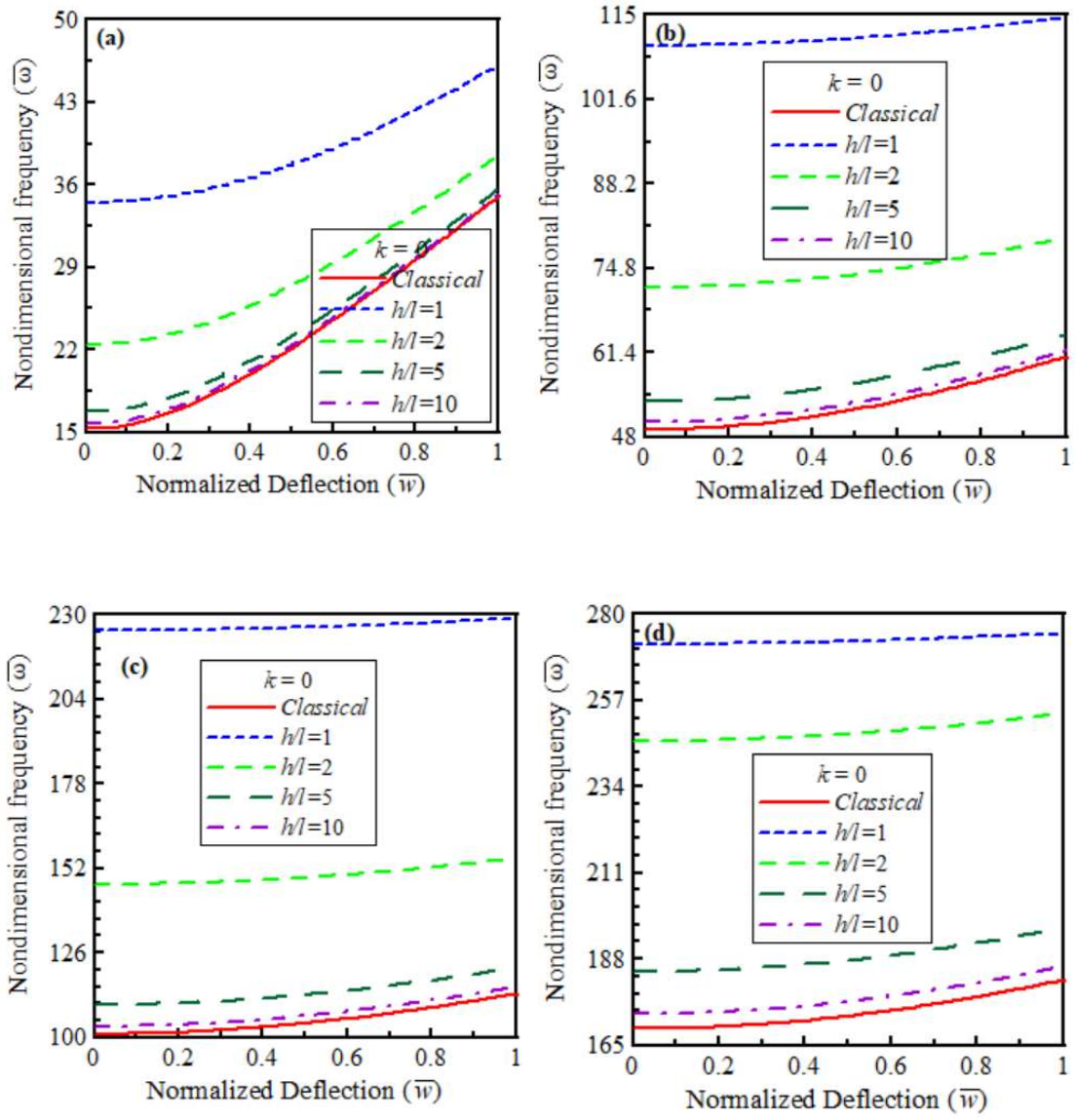

Fig. 4.3A: Effect of size on non-dimensional deflection-frequency curves for CH beams with k=0: (a) first mode, (b) second mode, (c) third mode, (d) fourth mode.

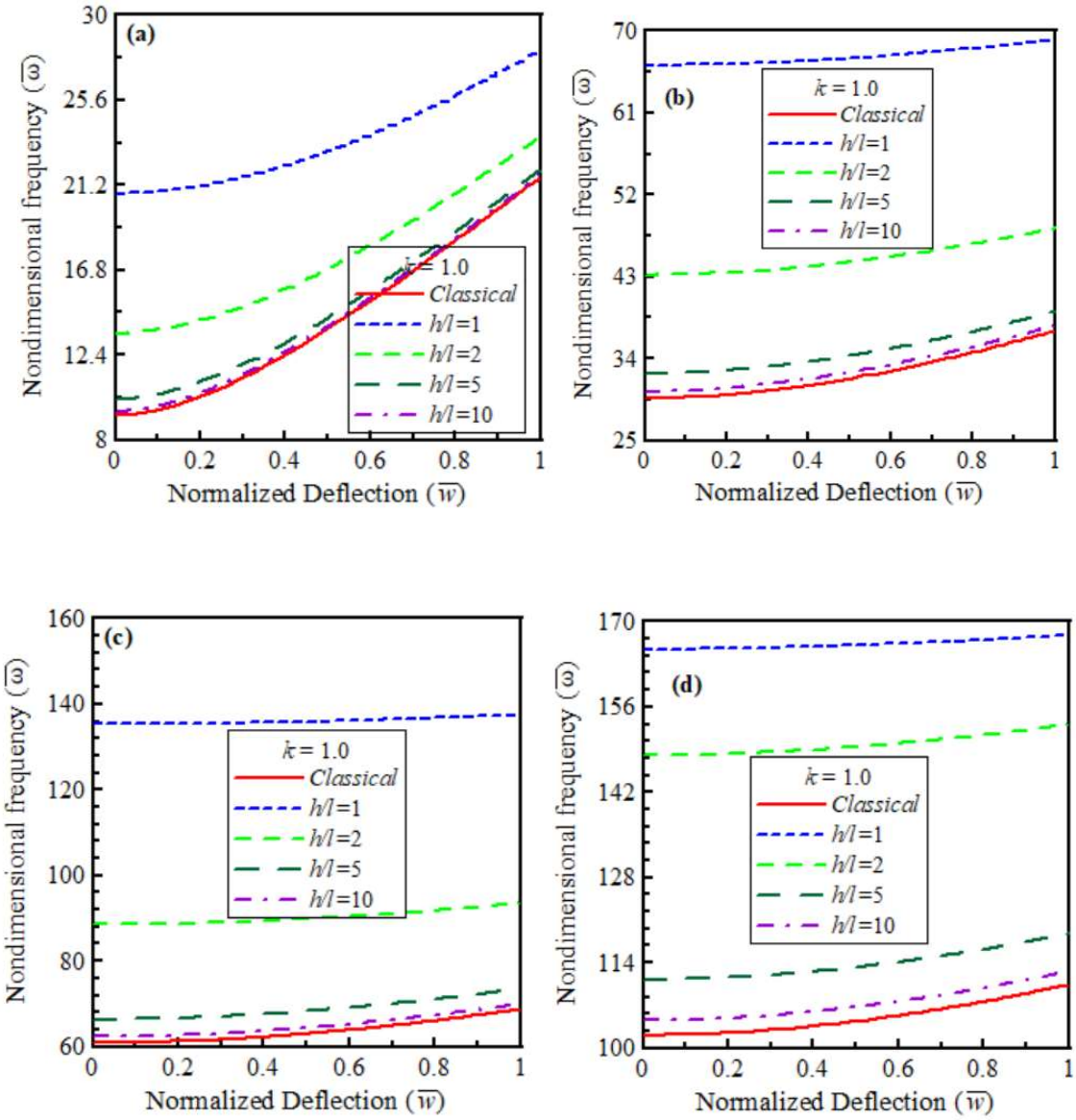

Fig. 4.3B: Effect of size on non-dimensional deflection-frequency curves for CH beams with k=1: (a) first mode, (b) second mode, (c) third mode, (d) fourth mode.

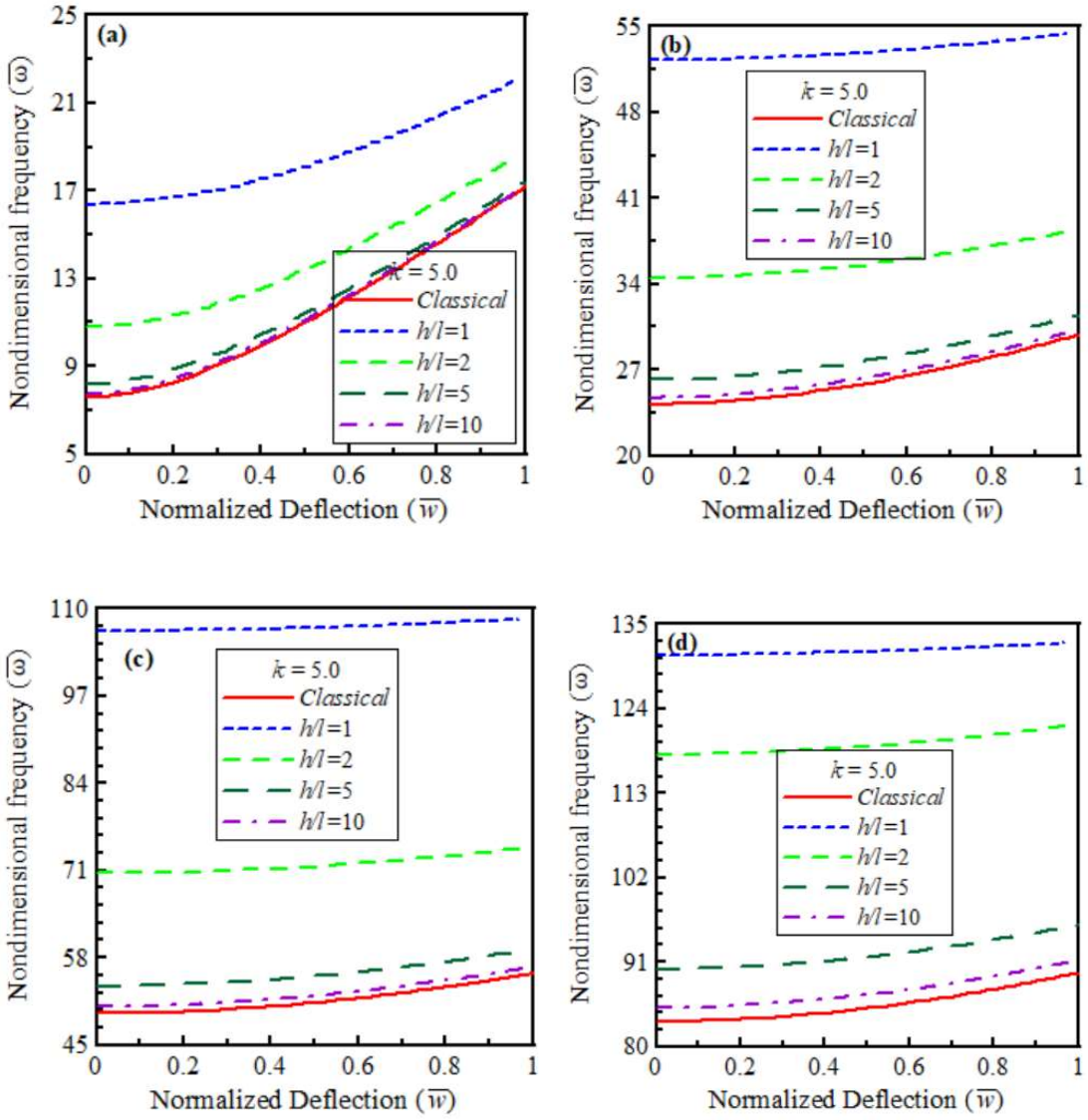

Fig. 4.3C: Effect of size on non-dimensional deflection-frequency curves for CH beams with *k*=5: (a) first mode, (b) second mode, (c) third mode, (d) fourth mode.

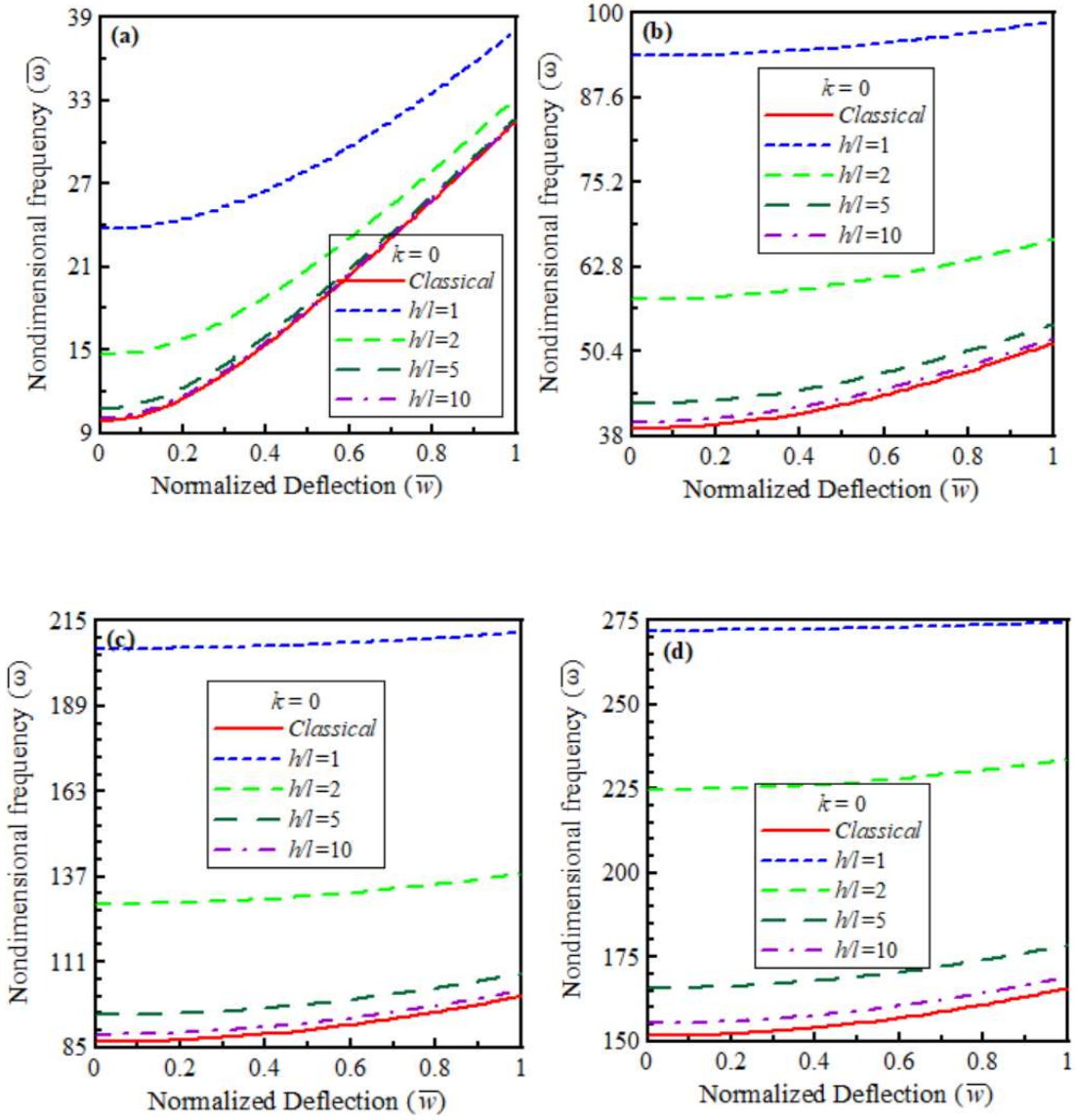

Fig. 4.4A: Effect of size on non-dimensional deflection-frequency curves for HH beams with k=0: (a) first mode, (b) second mode, (c) third mode, (d) fourth mode.

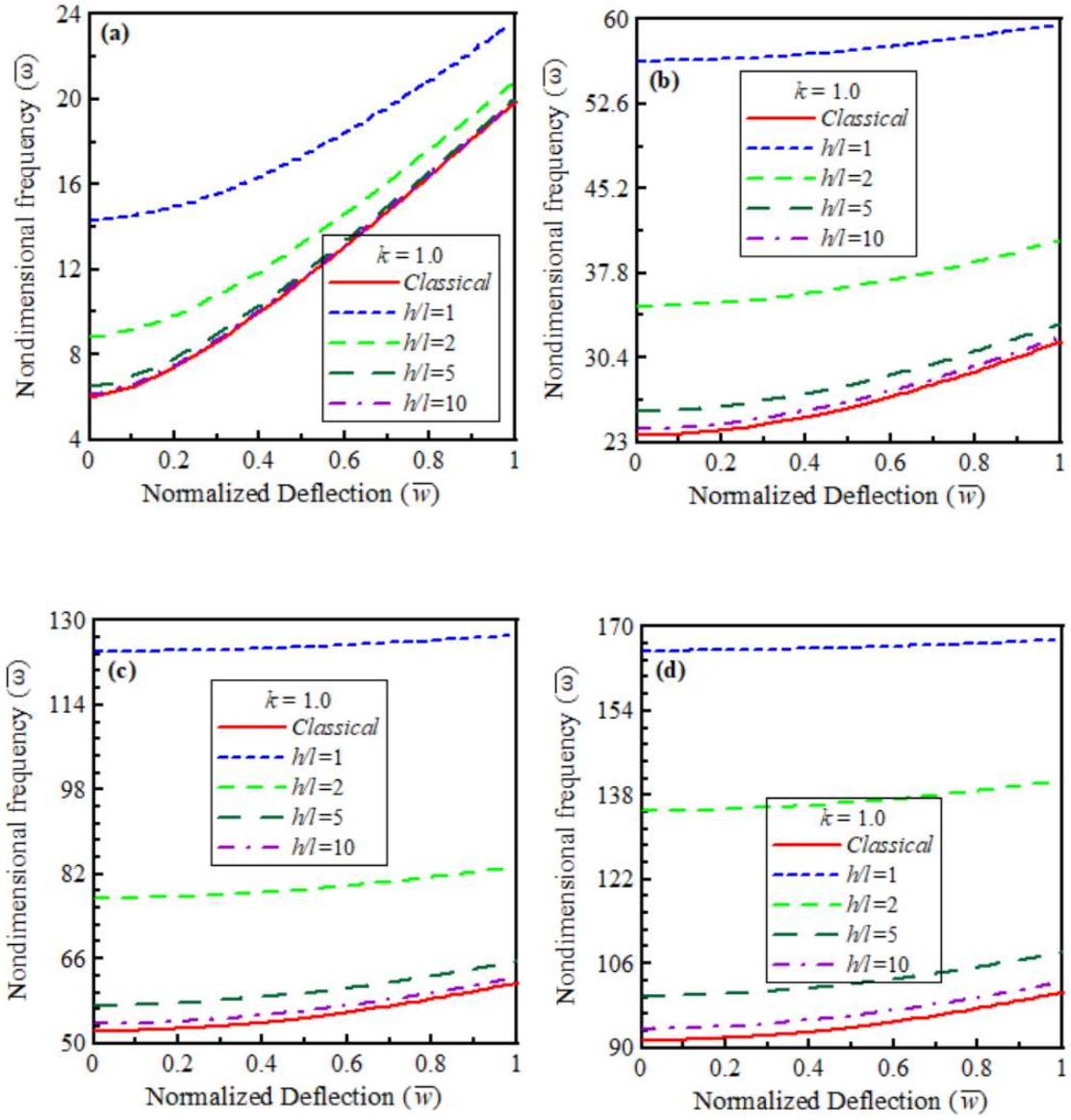

Fig. 4.4B: Effect of size on non-dimensional deflection-frequency curves for HH beams with k=1: (a) first mode, (b) second mode, (c) third mode, (d) fourth mode.

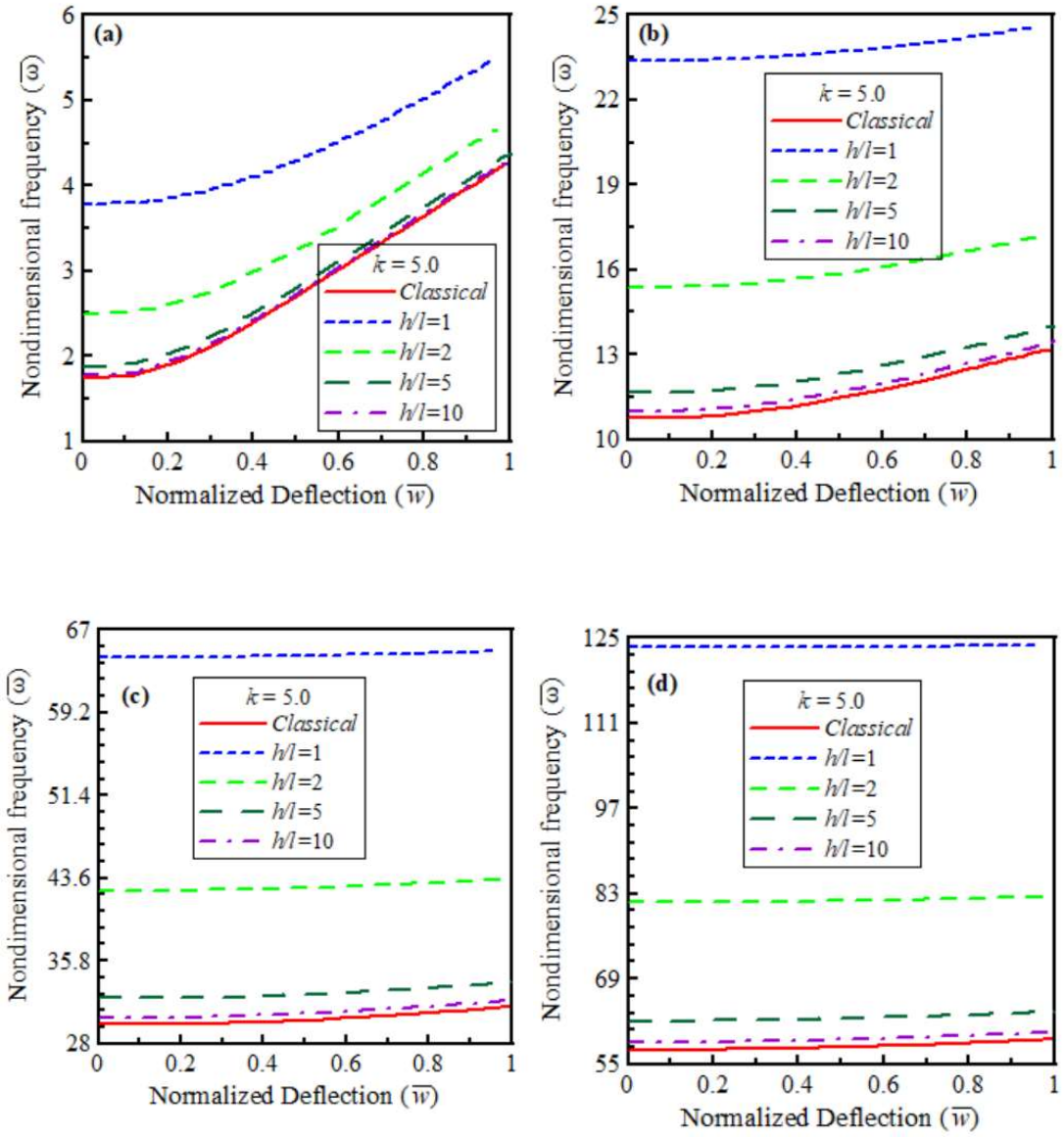

Fig. 4.4C: Effect of size on non-dimensional deflection-frequency curves for HH beams with *k*=5: (a) first mode, (b) second mode, (c) third mode, (d) fourth mode.

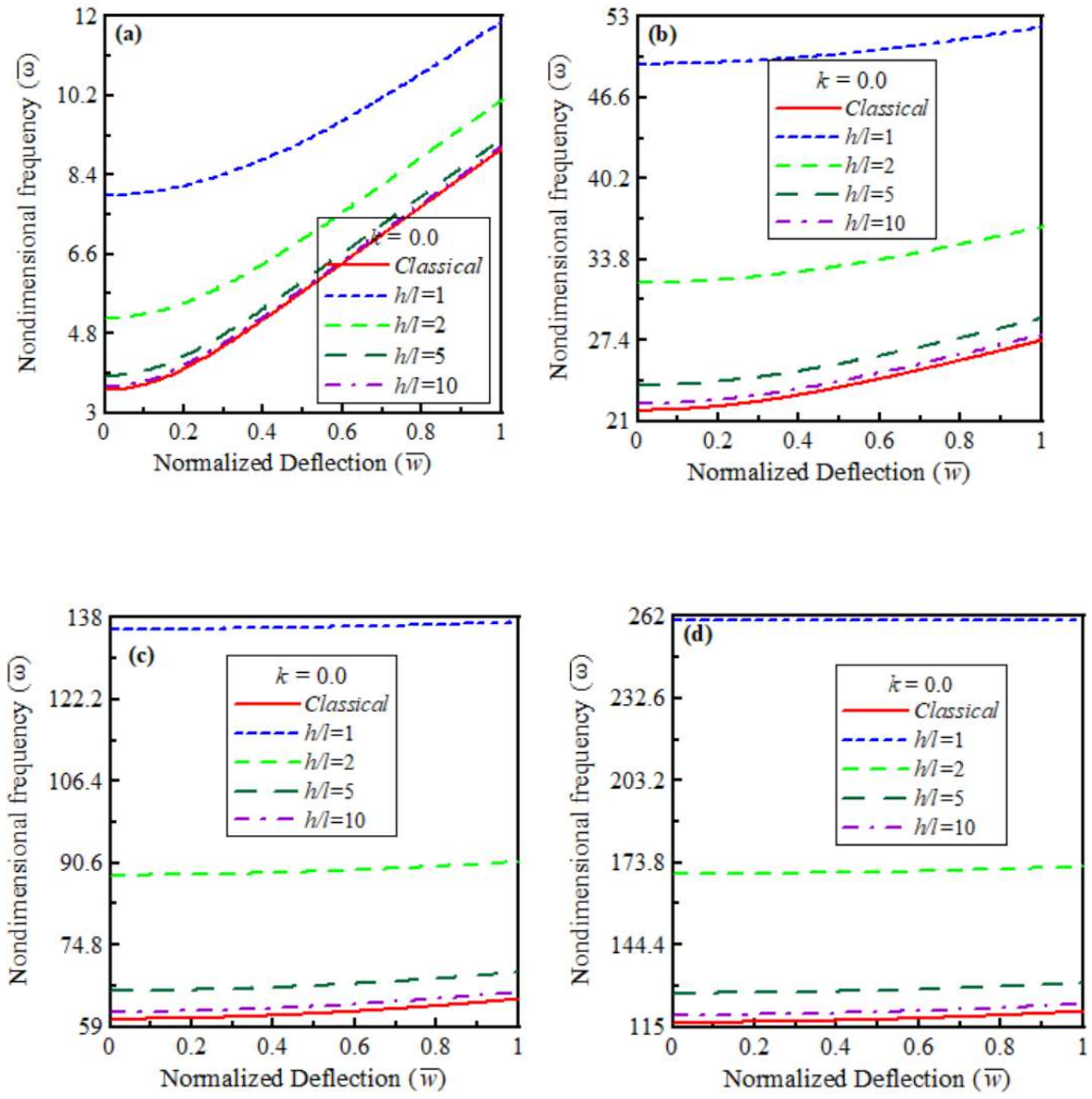

Fig. 4.5A: Effect of size on non-dimensional deflection-frequency curves for CF beams with k=0: (a) first mode, (b) second mode, (c) third mode, (d) fourth mode.

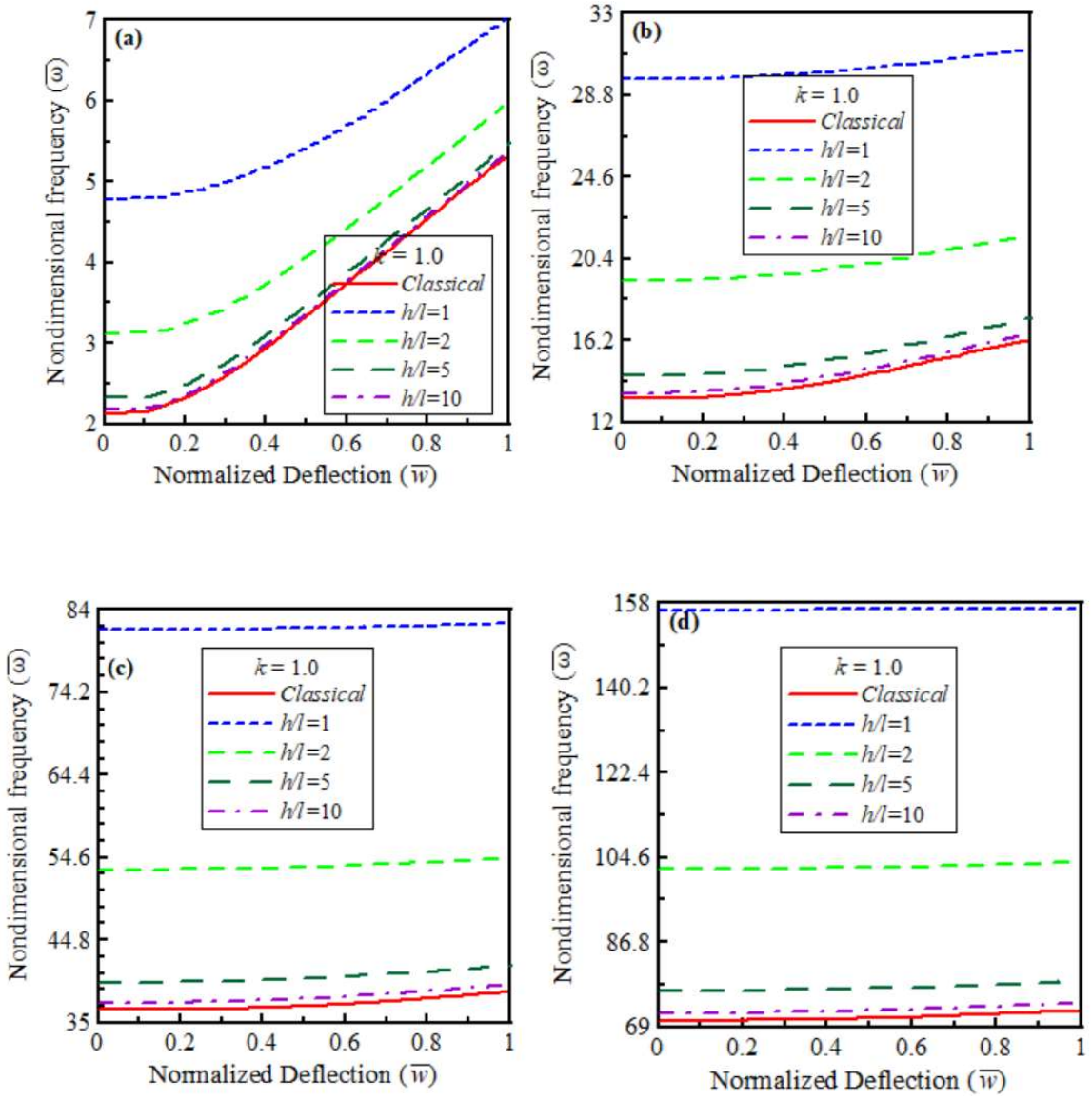

Fig. 4.5B: Effect of size on non-dimensional deflection-frequency curves for CF beams with k=1: (a) first mode, (b) second mode, (c) third mode, (d) fourth mode.

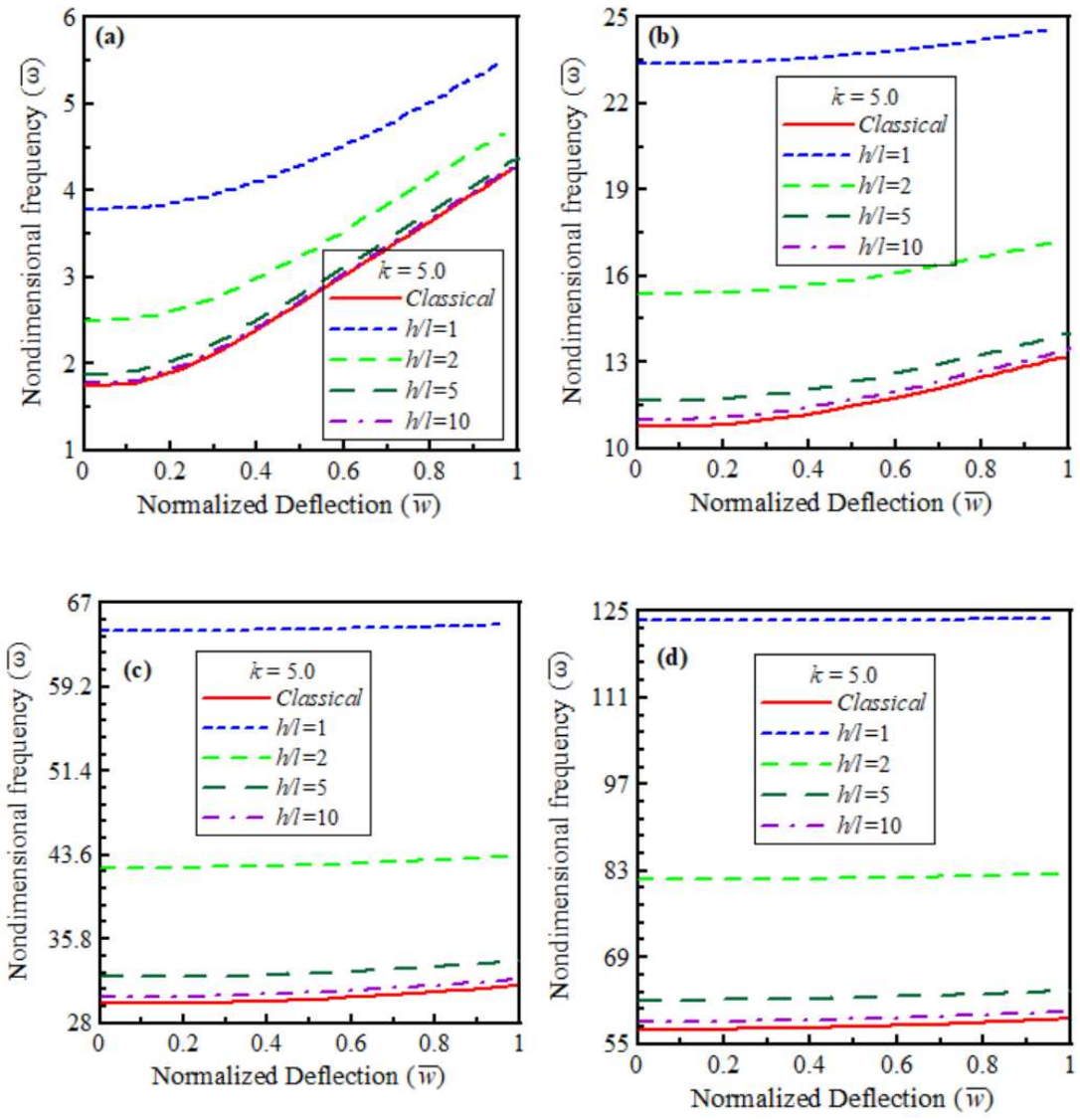

Fig. 4.5C: Effect of size on non-dimensional deflection-frequency curves for CF beams with k=5: (a) first mode, (b) second mode, (c) third mode, (d) fourth mode.

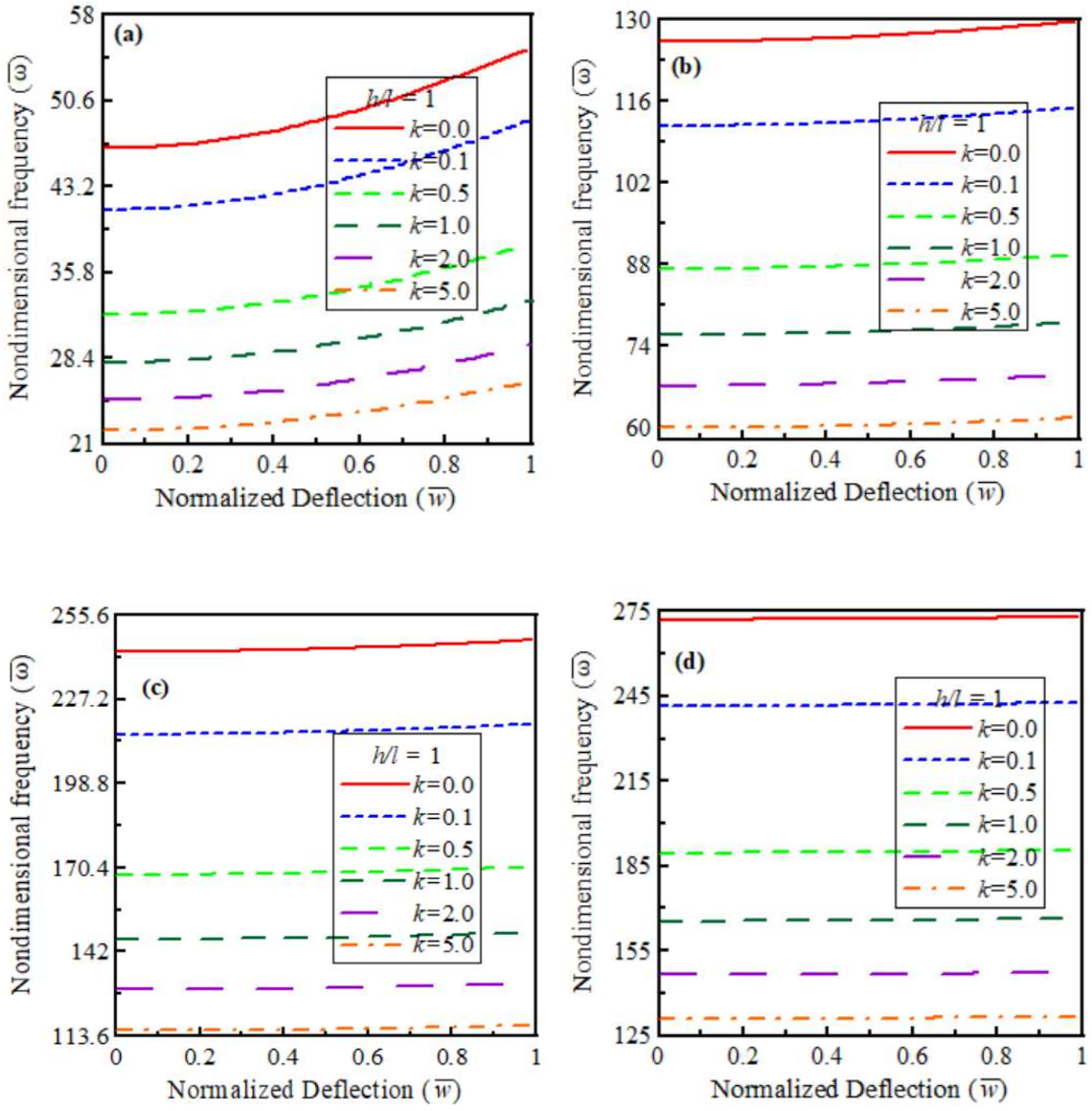

Fig. 4.6A: Effect of material gradation on non-dimensional deflection-frequency curves for CC beams with *h/l*=1.0: (a) first mode, (b) second mode, (c) third mode, (d) fourth mode.

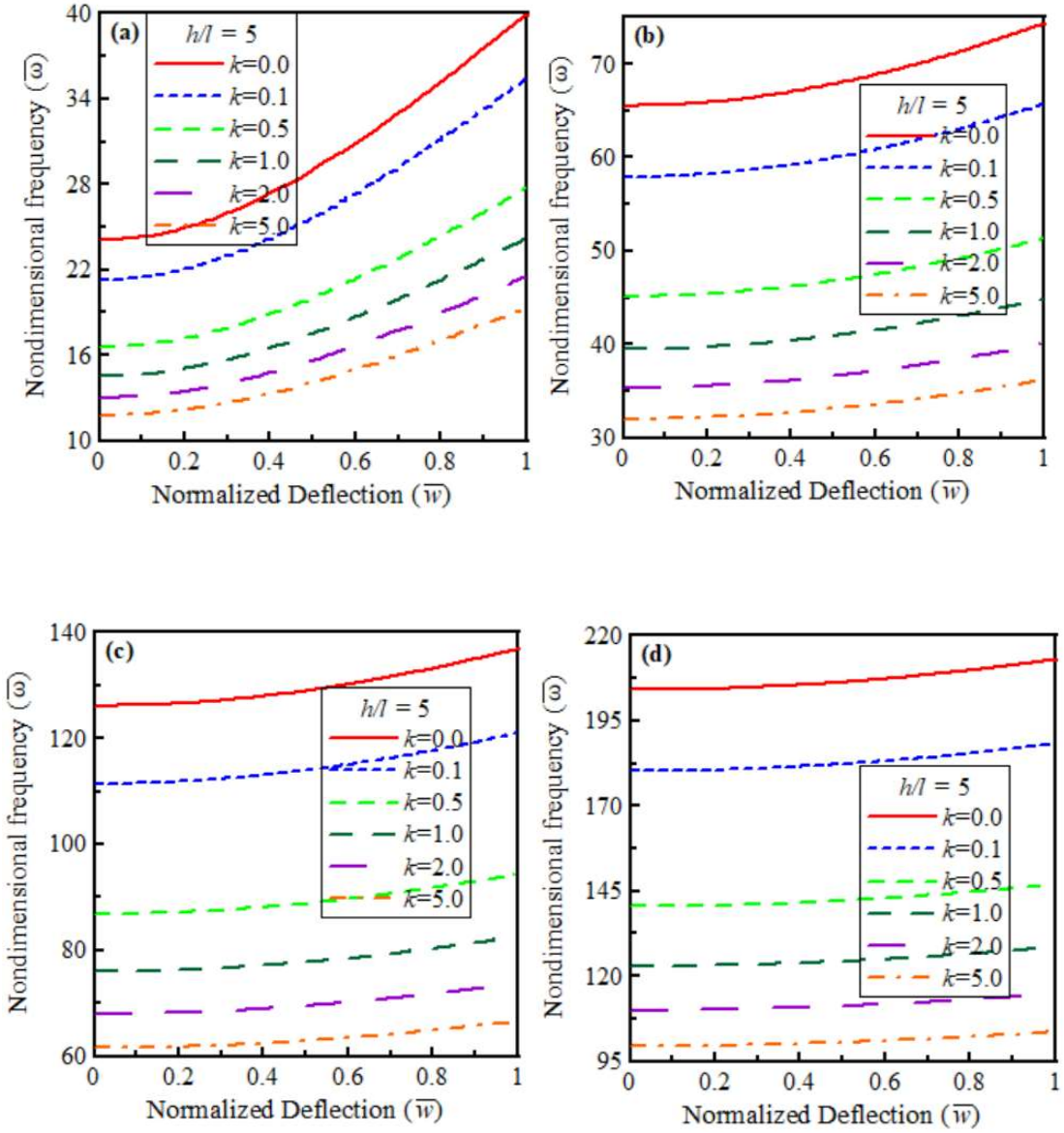

Fig. 4.6B Effect of material gradation on non-dimensional deflection-frequency curves for CC beams with *h/l*=5.0: (a) first mode, (b) second mode, (c) third mode, (d) fourth mode.

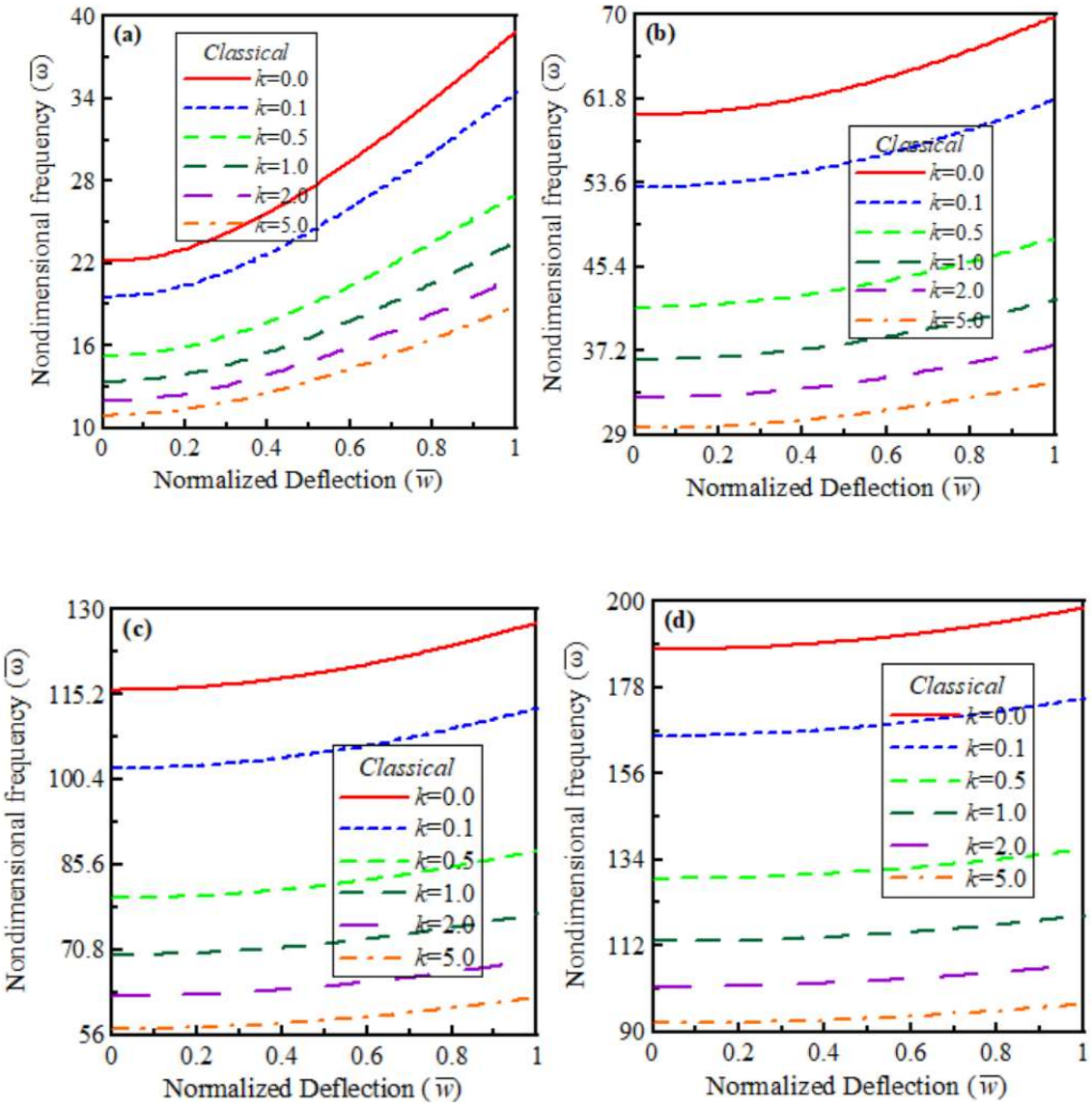

Fig. 4.6C: Effect of material gradation on non-dimensional deflection-frequency curves for CC beams with l=0 (classical): (a) first mode, (b) second mode, (c) third mode, (d) fourth mode.

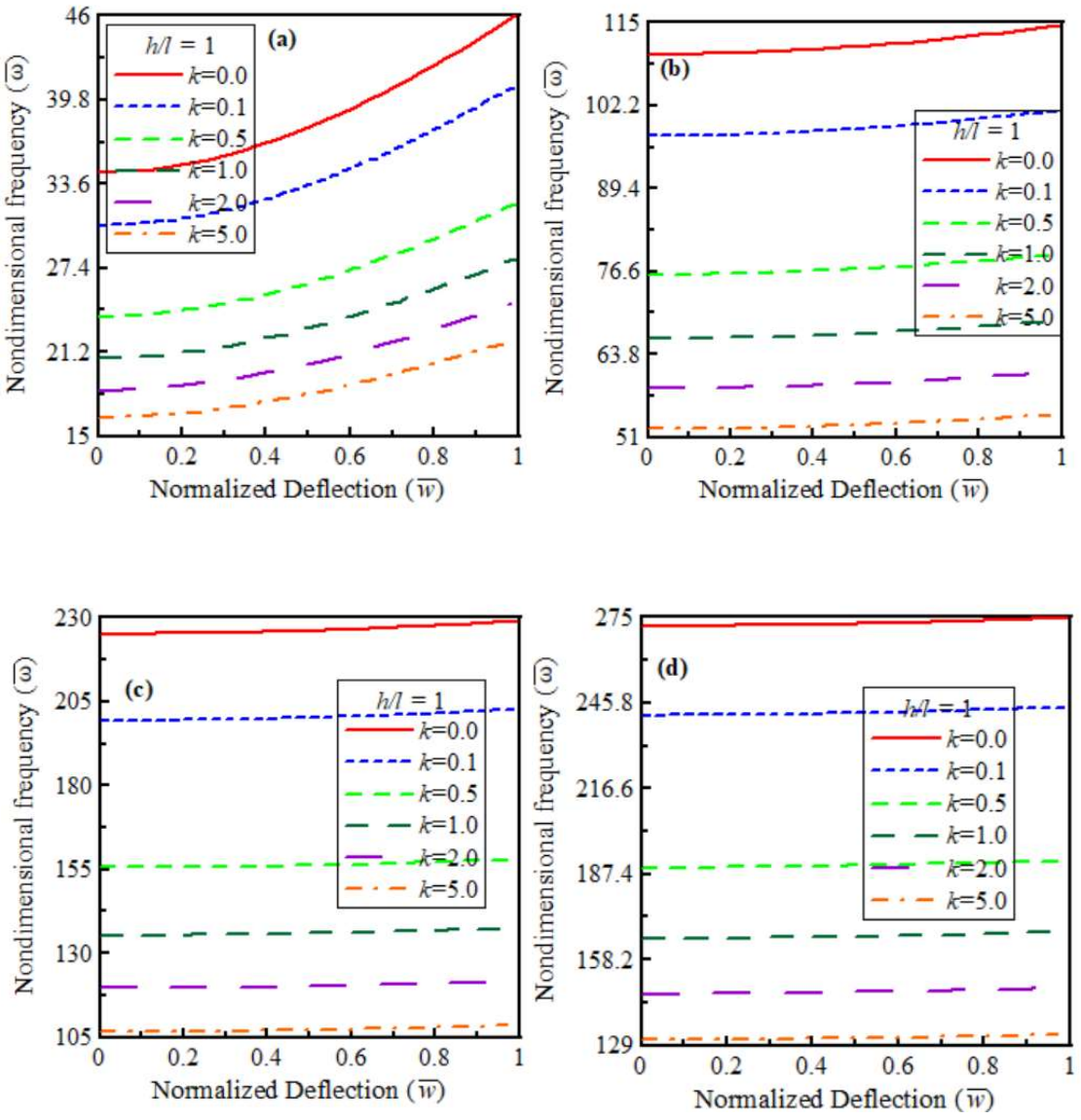

Fig. 4.7A: Effect of material gradation on non-dimensional deflection-frequency curves for CH beams with *h/l*=1.0: (a) first mode, (b) second mode, (c) third mode, (d) fourth mode.

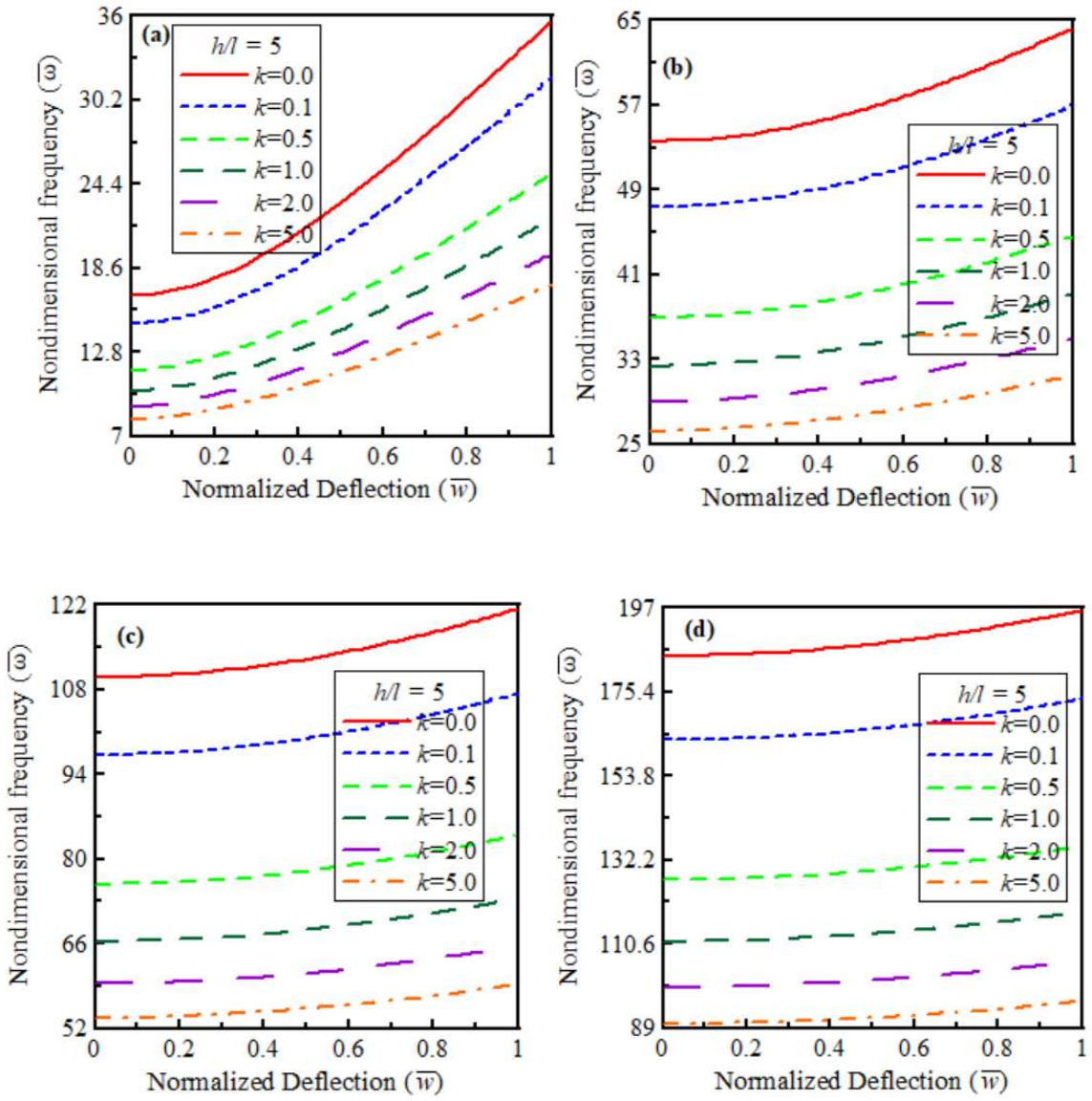

Fig. 4.7B Effect of material gradation on non-dimensional deflection-frequency curves for CH beams with *h/l*=5.0: (a) first mode, (b) second mode, (c) third mode, (d) fourth mode.

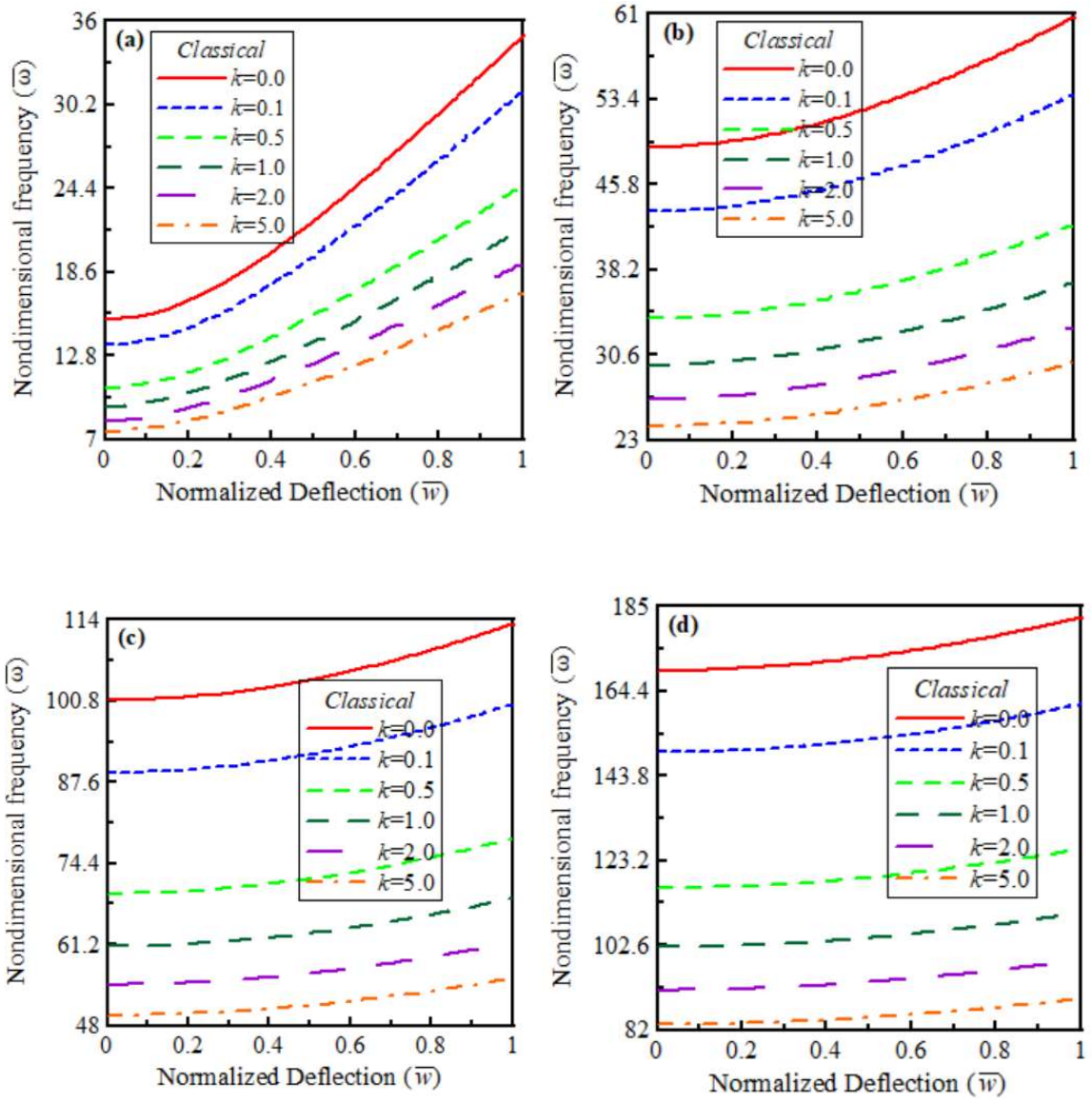

Fig. 4.7C: Effect of material gradation on non-dimensional deflection-frequency curves for CH beams with l=0 (classical): (a) first mode, (b) second mode, (c) third mode, (d) fourth mode.

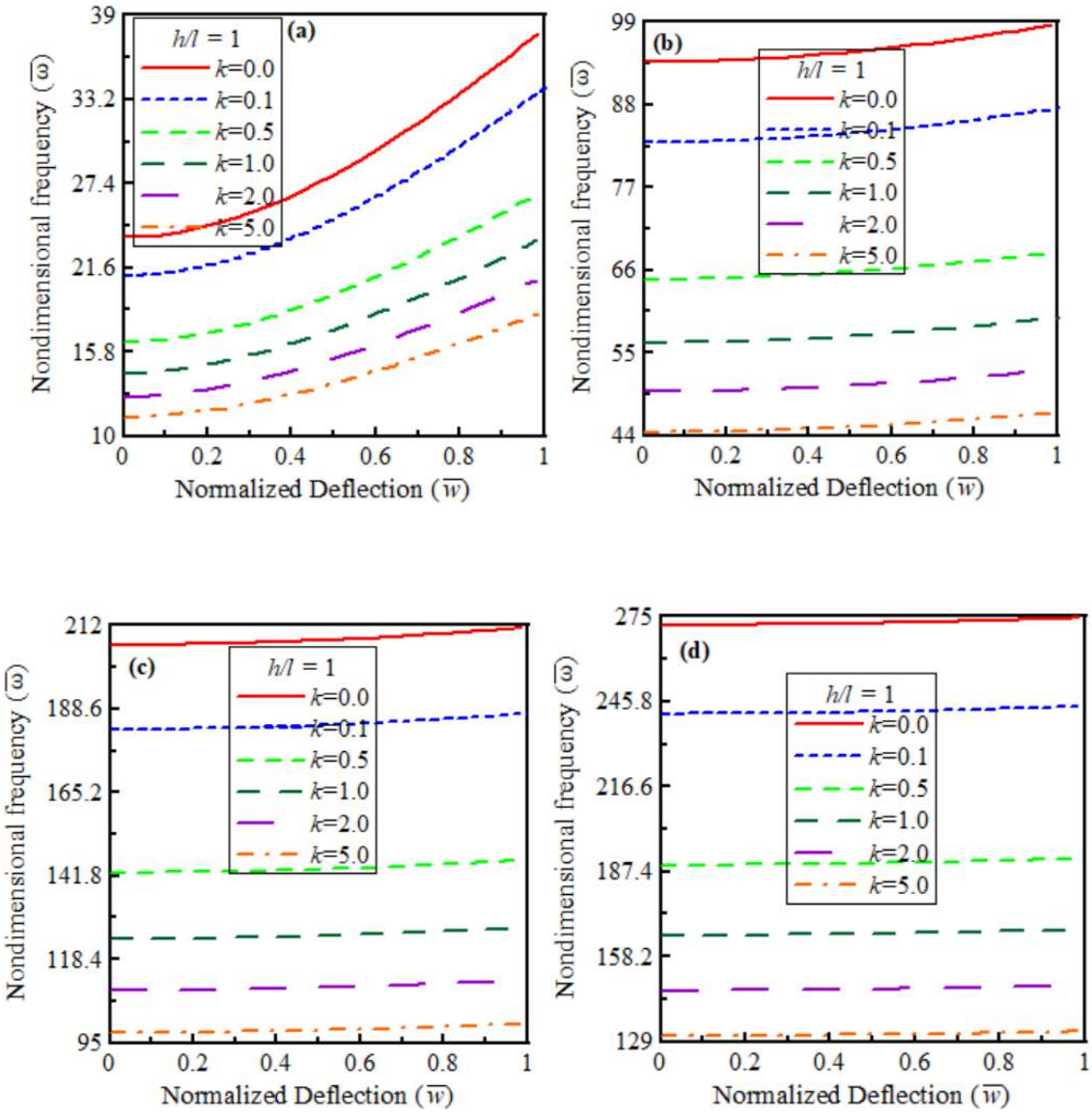

Fig. 4.8A: Effect of material gradation on non-dimensional deflection-frequency curves for HH beams with *h/l*=1.0: (a) first mode, (b) second mode, (c) third mode, (d) fourth mode.

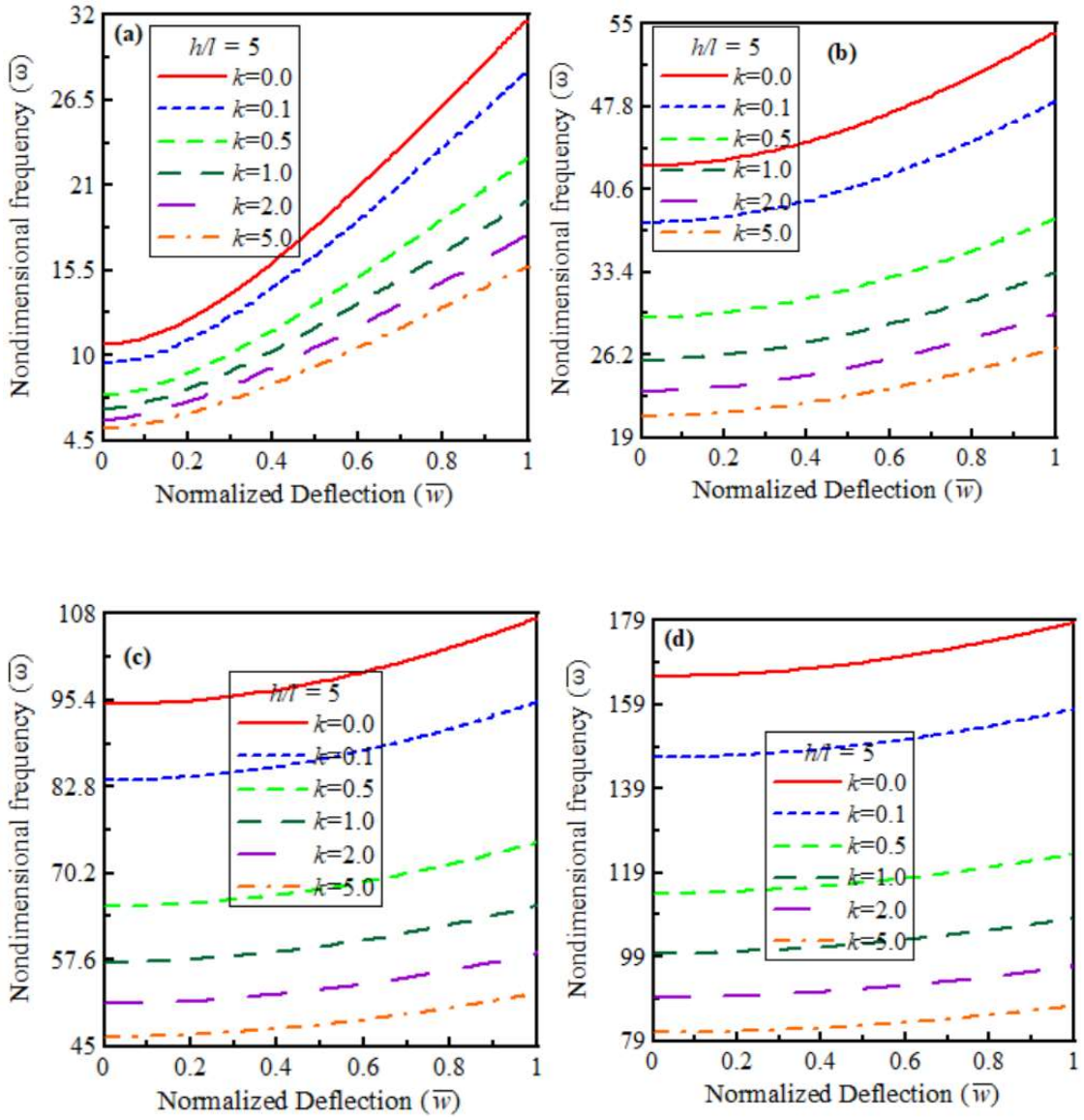

Fig. 4.8B Effect of material gradation on non-dimensional deflection-frequency curves for HH beams with *h/l*=5.0: (a) first mode, (b) second mode, (c) third mode, (d) fourth mode.

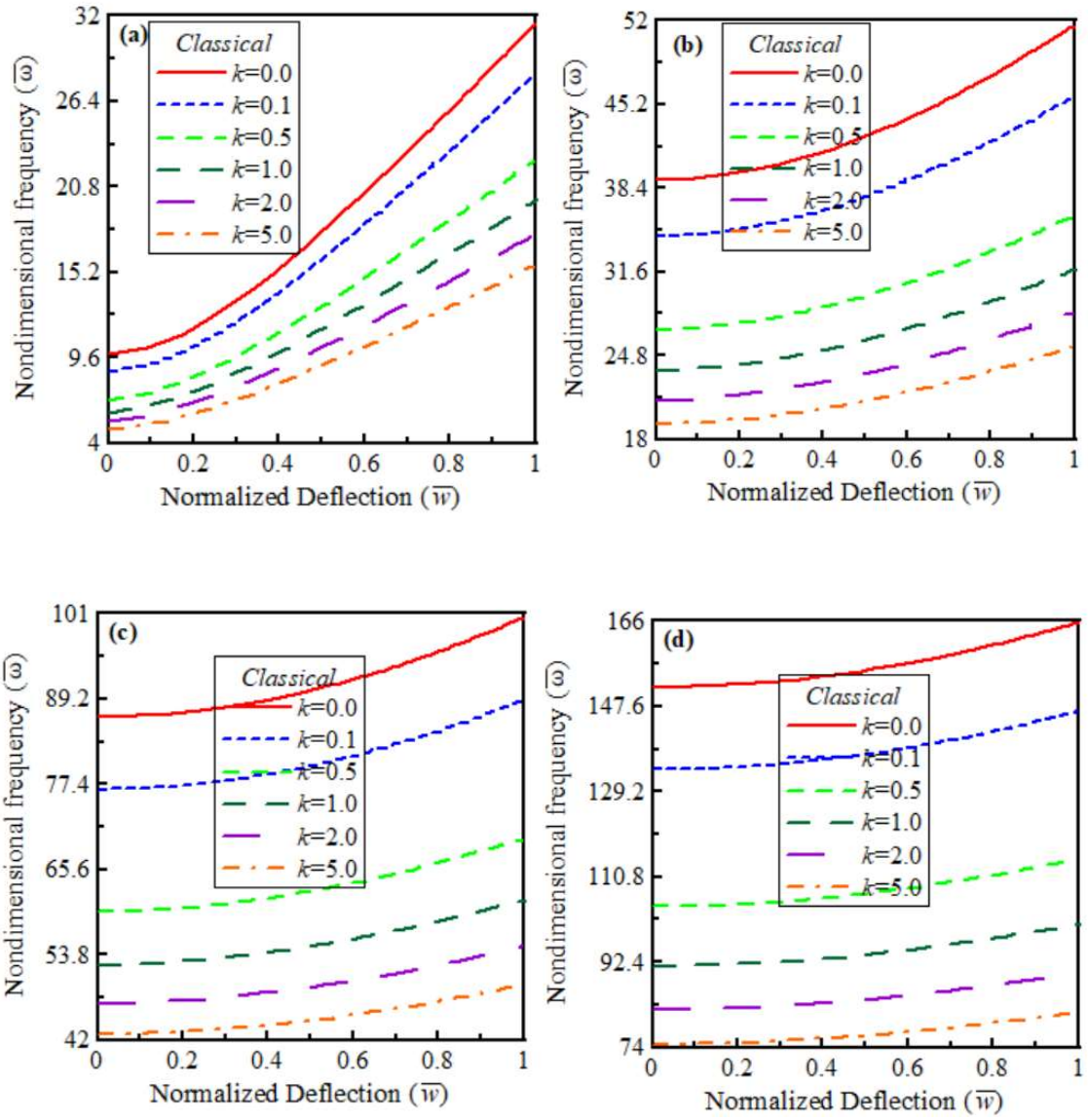

Fig. 4.8C: Effect of material gradation on non-dimensional deflection-frequency curves for HH beams with l=0 (classical): (a) first mode, (b) second mode, (c) third mode, (d) fourth mode.

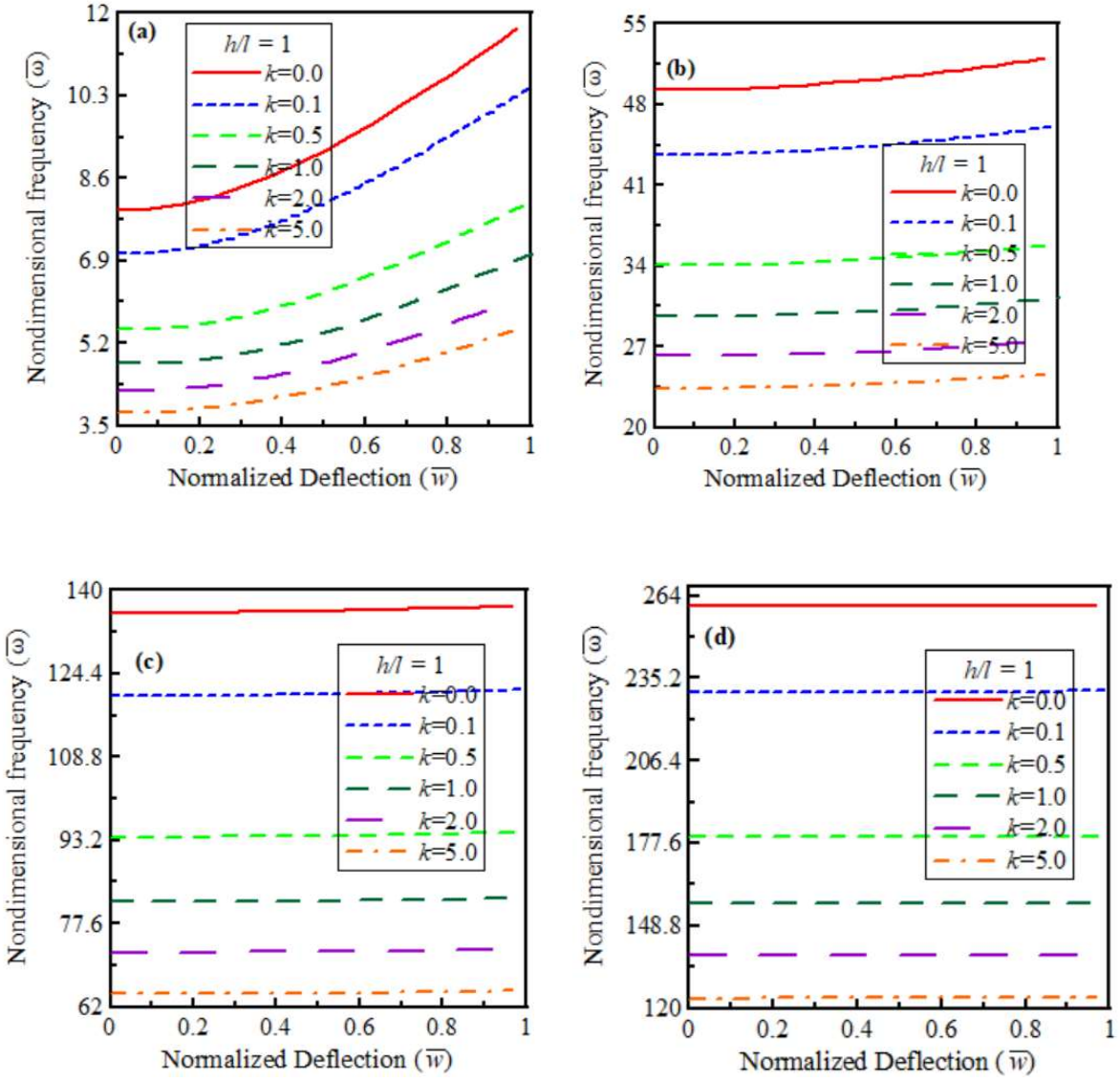

Fig. 4.9A: Effect of material gradation on non-dimensional deflection-frequency curves for CF beams with *h/l*=1.0: (a) first mode, (b) second mode, (c) third mode, (d) fourth mode.

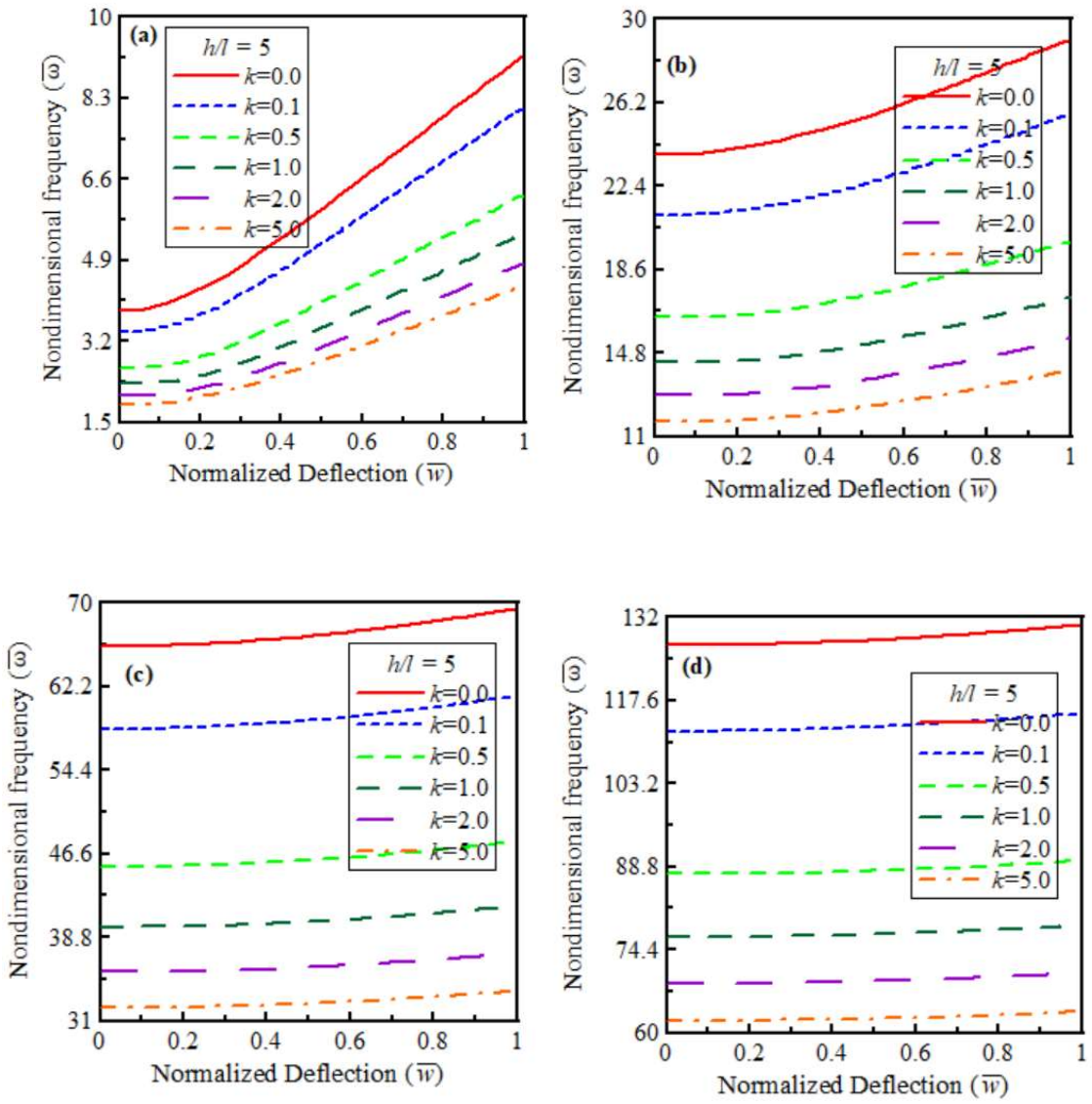

Fig. 4.9B Effect of material gradation on non-dimensional deflection-frequency curves for CF beams with *h/l*=5.0: (a) first mode, (b) second mode, (c) third mode, (d) fourth mode.

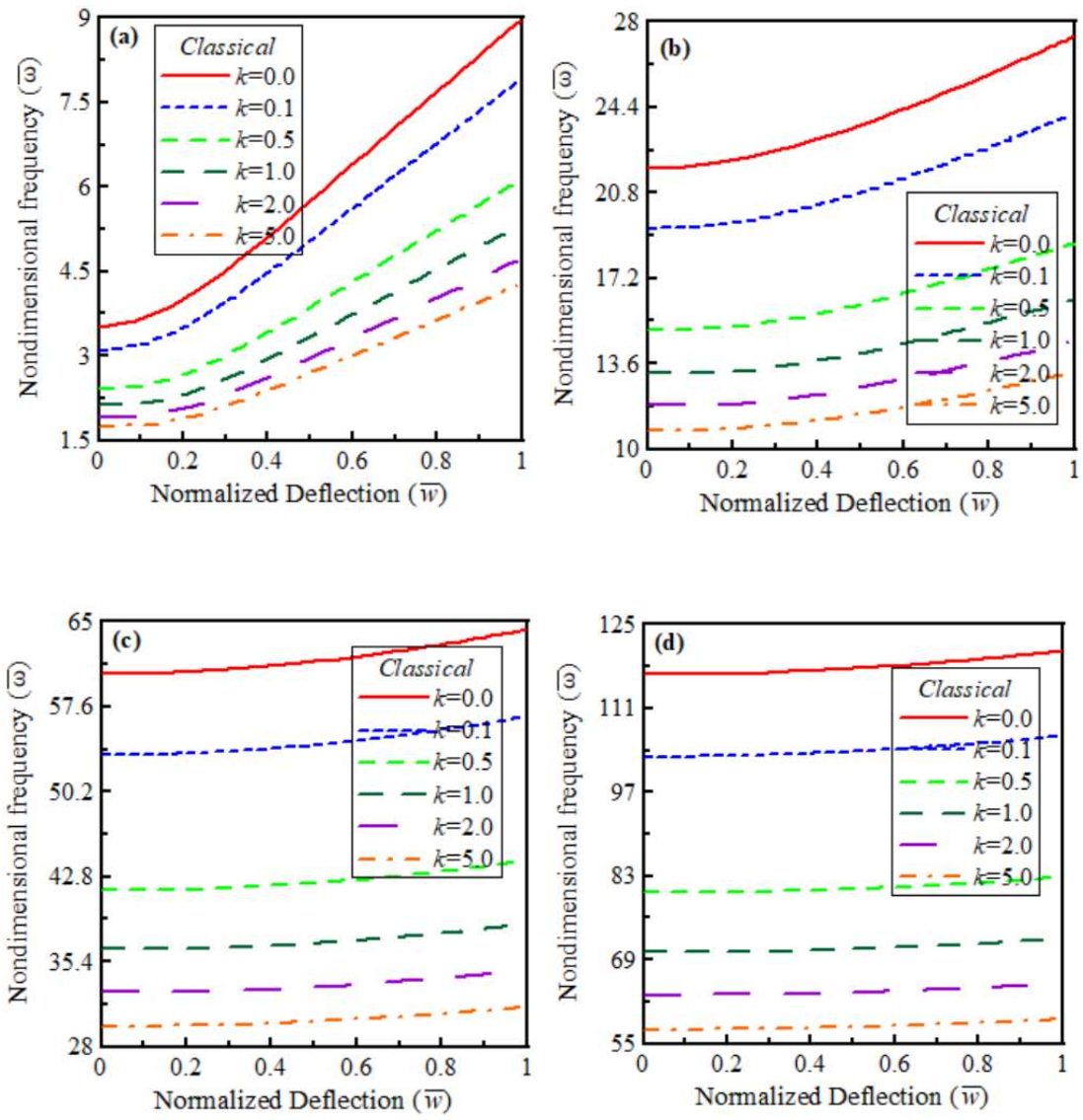

Fig. 4.9C: Effect of material gradation on non-dimensional deflection-frequency curves for CF beams with l=0 (classical): (a) first mode, (b) second mode, (c) third mode, (d) fourth mode.

The non-dimensional deflection-frequency curves for the first four modes of the CC, CH, HH and CF boundary conditions are shown in Figs. 4.10A-C, 4.11A-C, 4.12A–C and 4.13A–C respectively for k=1. Figures A-C correspond to different values of size-dependent thickness (h/l) such as: h/l=1.0, 5.0, and for classical FG beam (l = 0). In each of the figures A-C, plots are presented for the first four modes, indicated by (a)-(d) respectively. Each figure in Figs. 4.6-4.9 shows how different functionally graded materials affect the non-dimensional deflection-frequency behaviour.

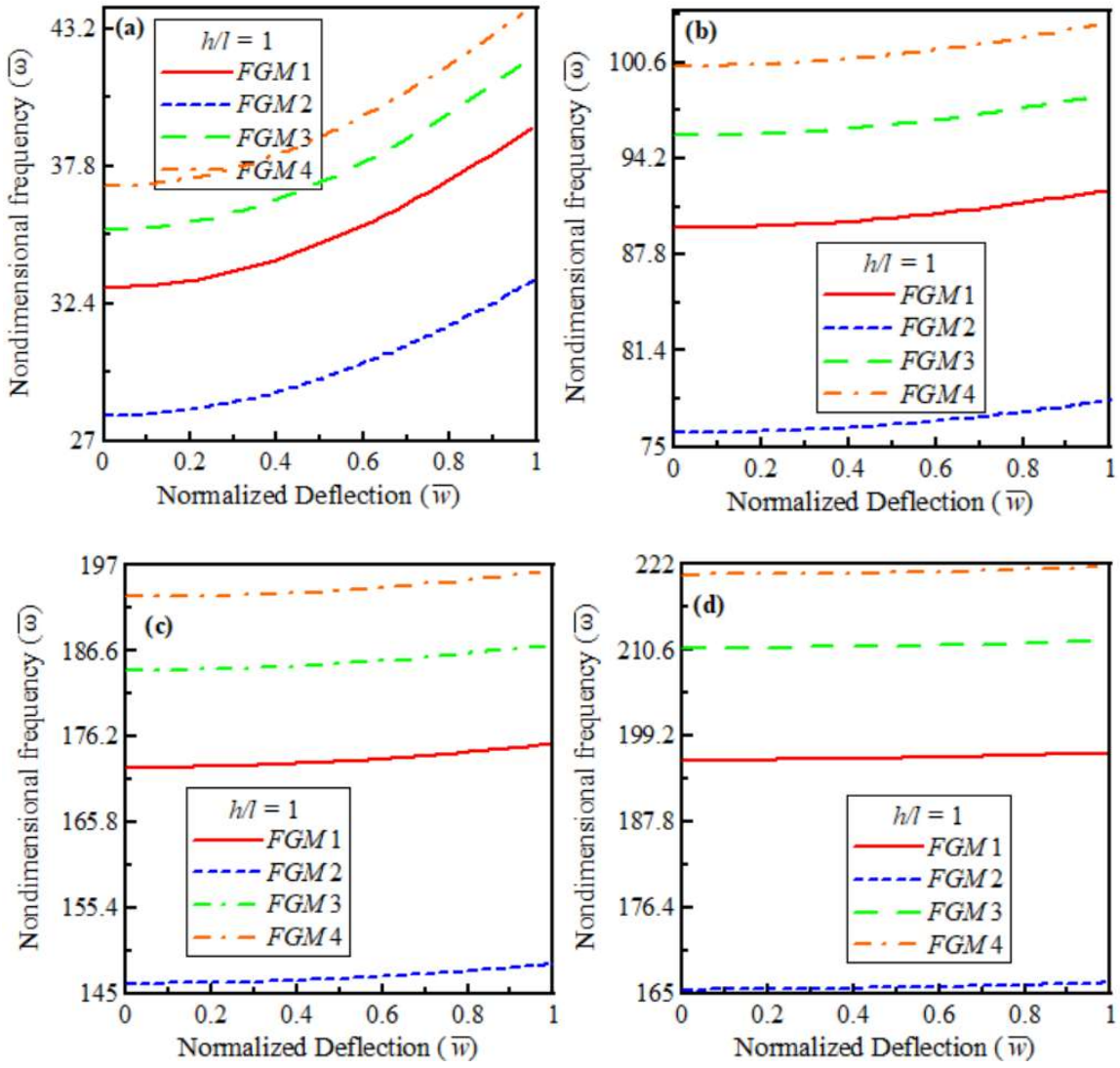

Fig. 4.10A: Effect of different FGM compositions on non-dimensional deflection-frequency curves for CC beams with h/l=1: (a) first mode, (b) second mode, (c) third mode, (d) fourth mode.

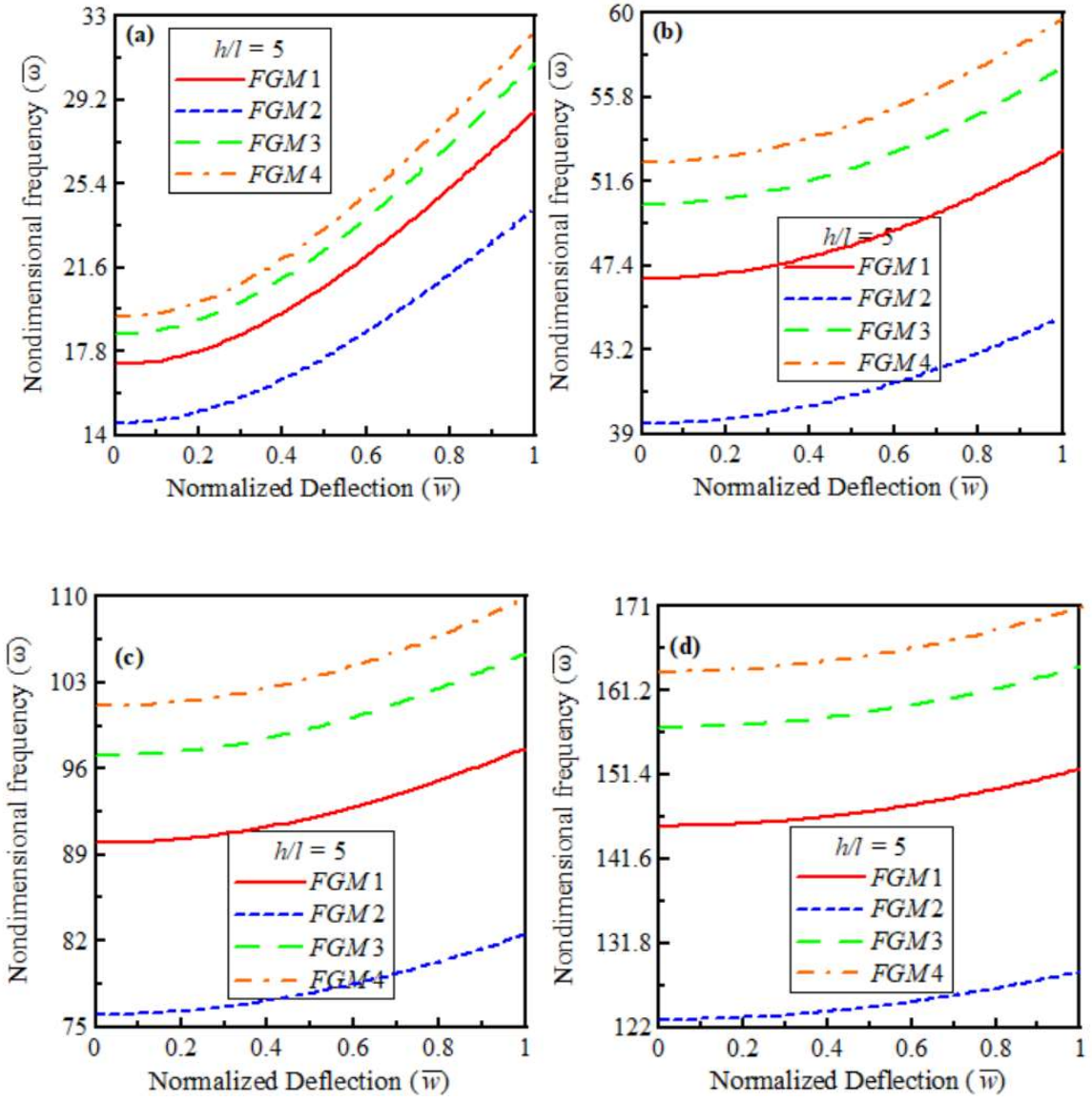

Fig. 4.10B: Effect of different FGM compositions on non-dimensional deflection-frequency curves for CC beams with *h/l*=5: (a) first mode, (b) second mode, (c) third mode, (d) fourth mode.

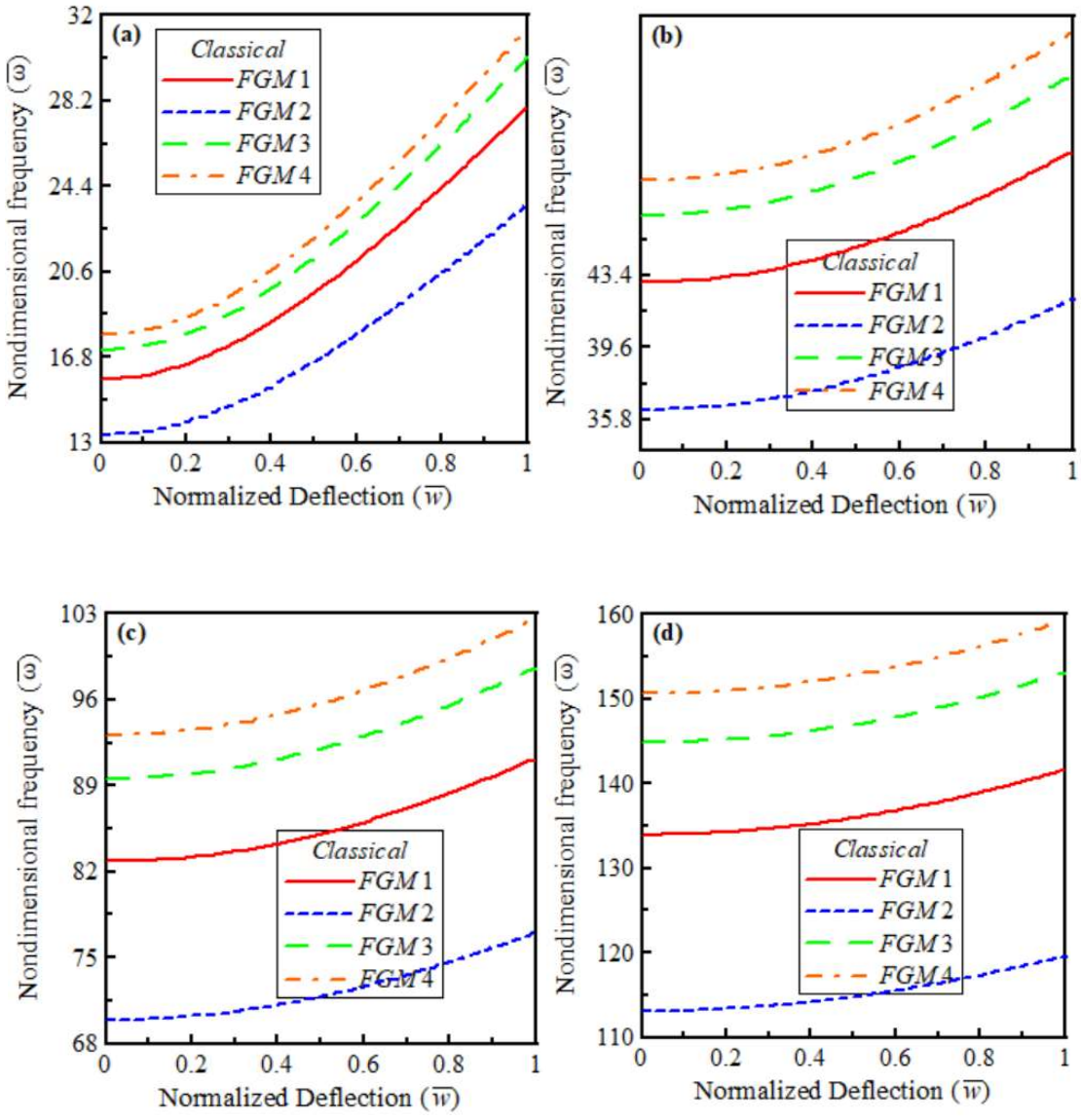

Fig. 4.10C: Effect of different FGM compositions on non-dimensional deflection-frequency curves for CC beams with l=0 (classical): (a) first mode, (b) second mode, (c) third mode, (d) fourth mode.

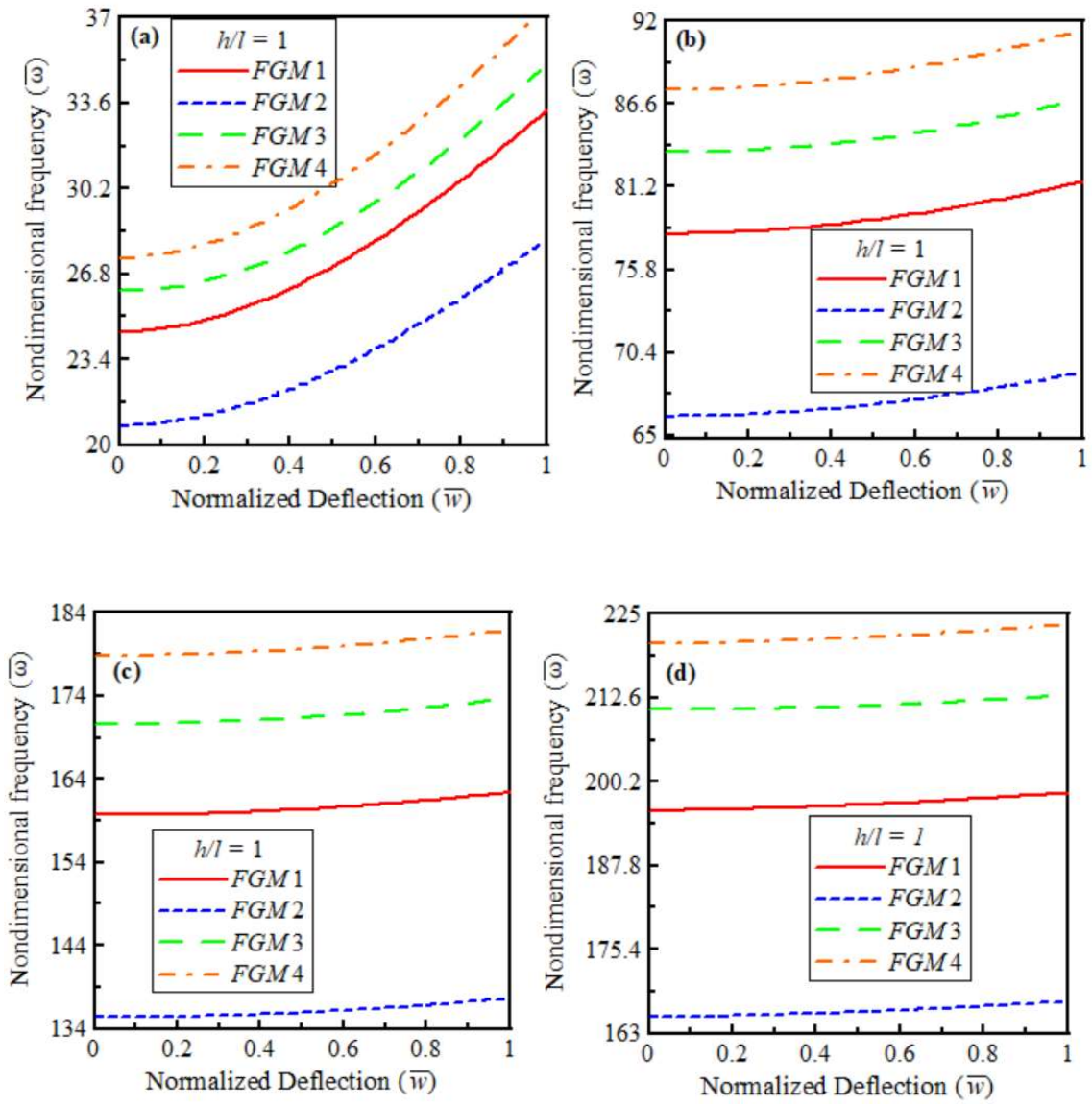

Fig. 4.11A: Effect of different FGM compositions on non-dimensional deflection-frequency curves for CH beams with h/l=1: (a) first mode, (b) second mode, (c) third mode, (d) fourth mode.

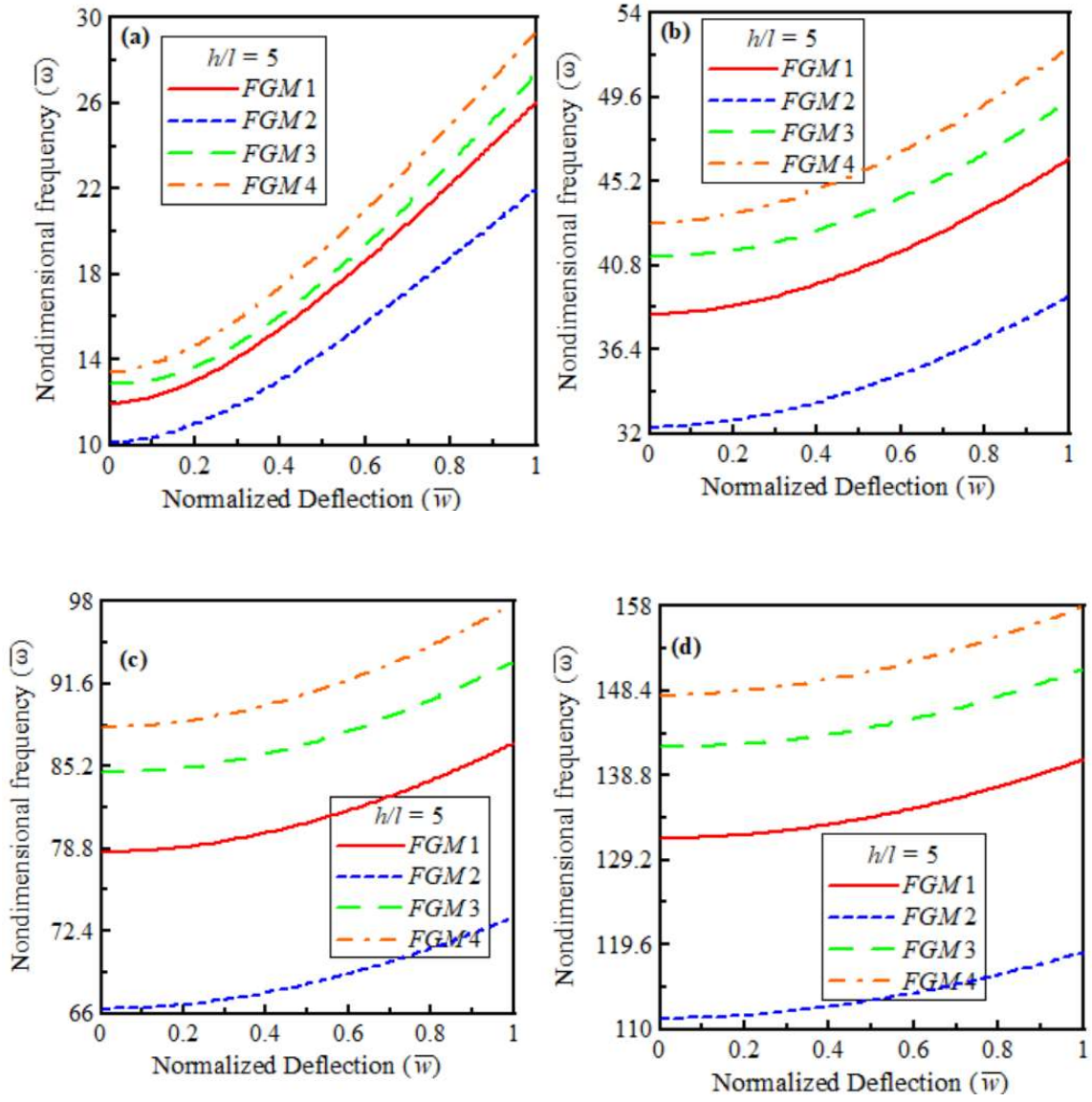

Fig. 4.11B: Effect of different FGM compositions on non-dimensional deflection-frequency curves for CH beams with *h/l*=5: (a) first mode, (b) second mode, (c) third mode, (d) fourth mode.

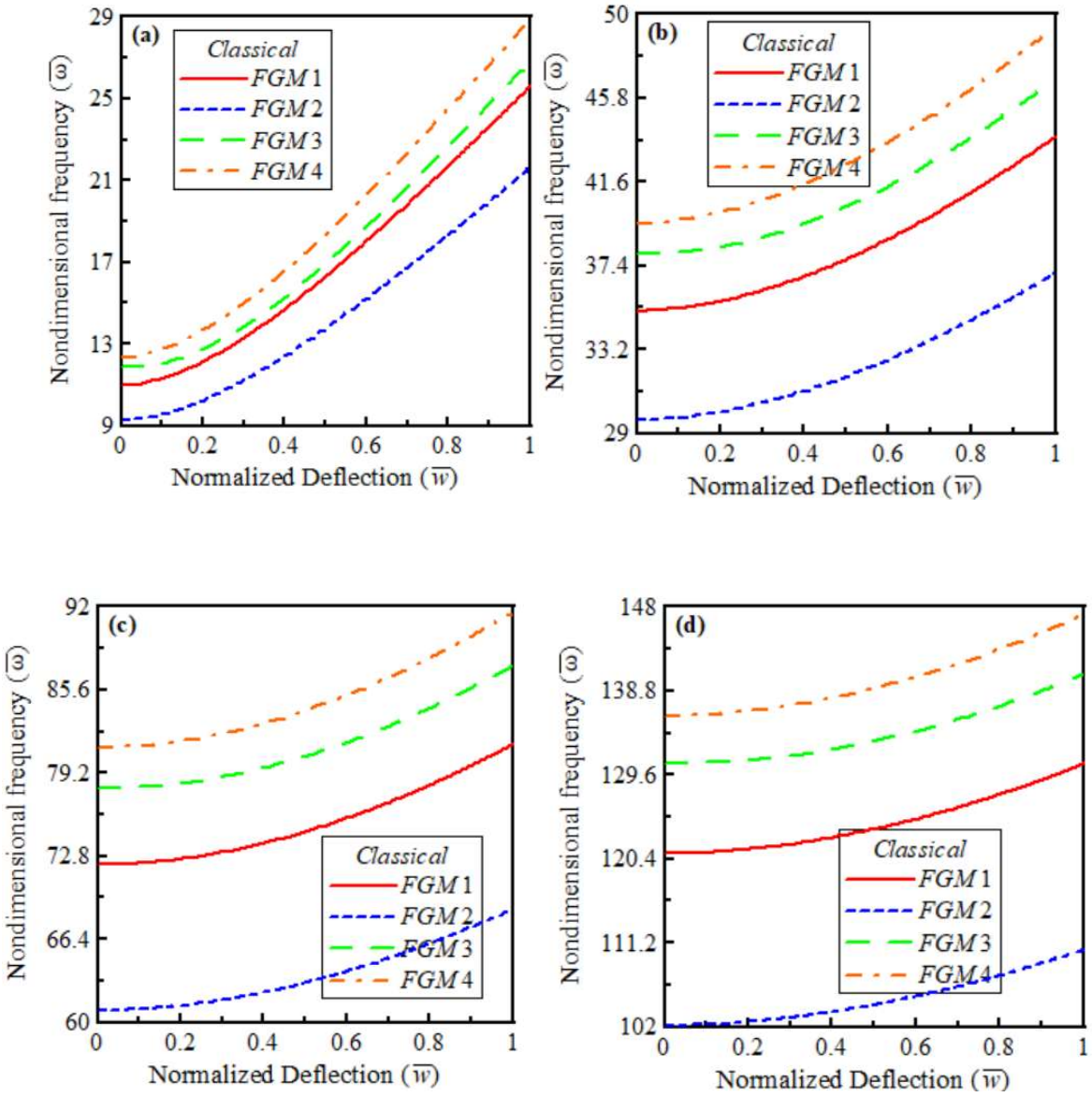

Fig. 4.11C: Effect of different FGM compositions on non-dimensional deflection-frequency curves for CH beams with l=0 (classical): (a) first mode, (b) second mode, (c) third mode, (d) fourth mode.

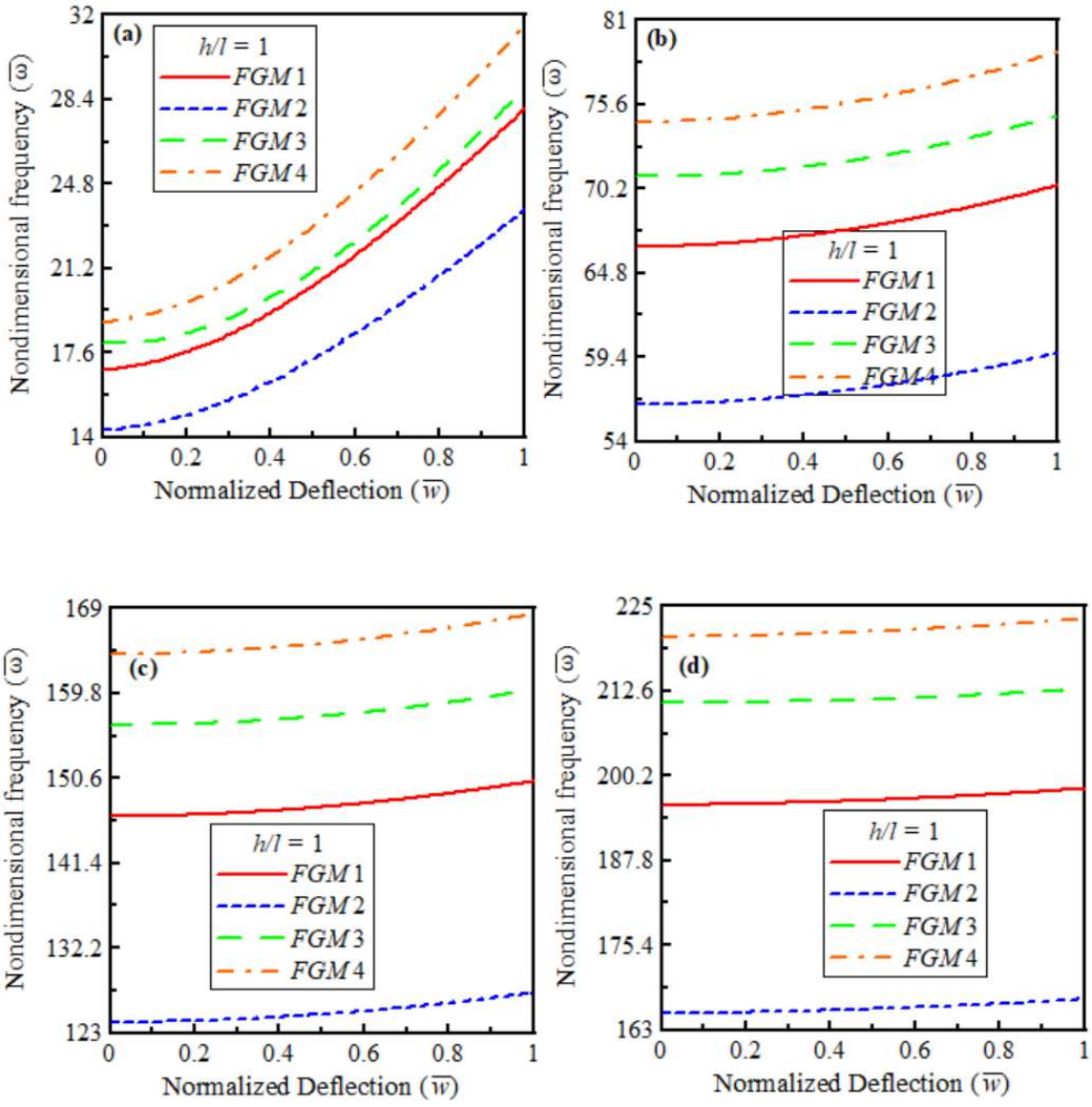

Fig. 4.12A: Effect of different FGM compositions on non-dimensional deflection-frequency curves for HH beams with *h*/*l*=1: (a) first mode, (b) second mode, (c) third mode, (d) fourth mode.

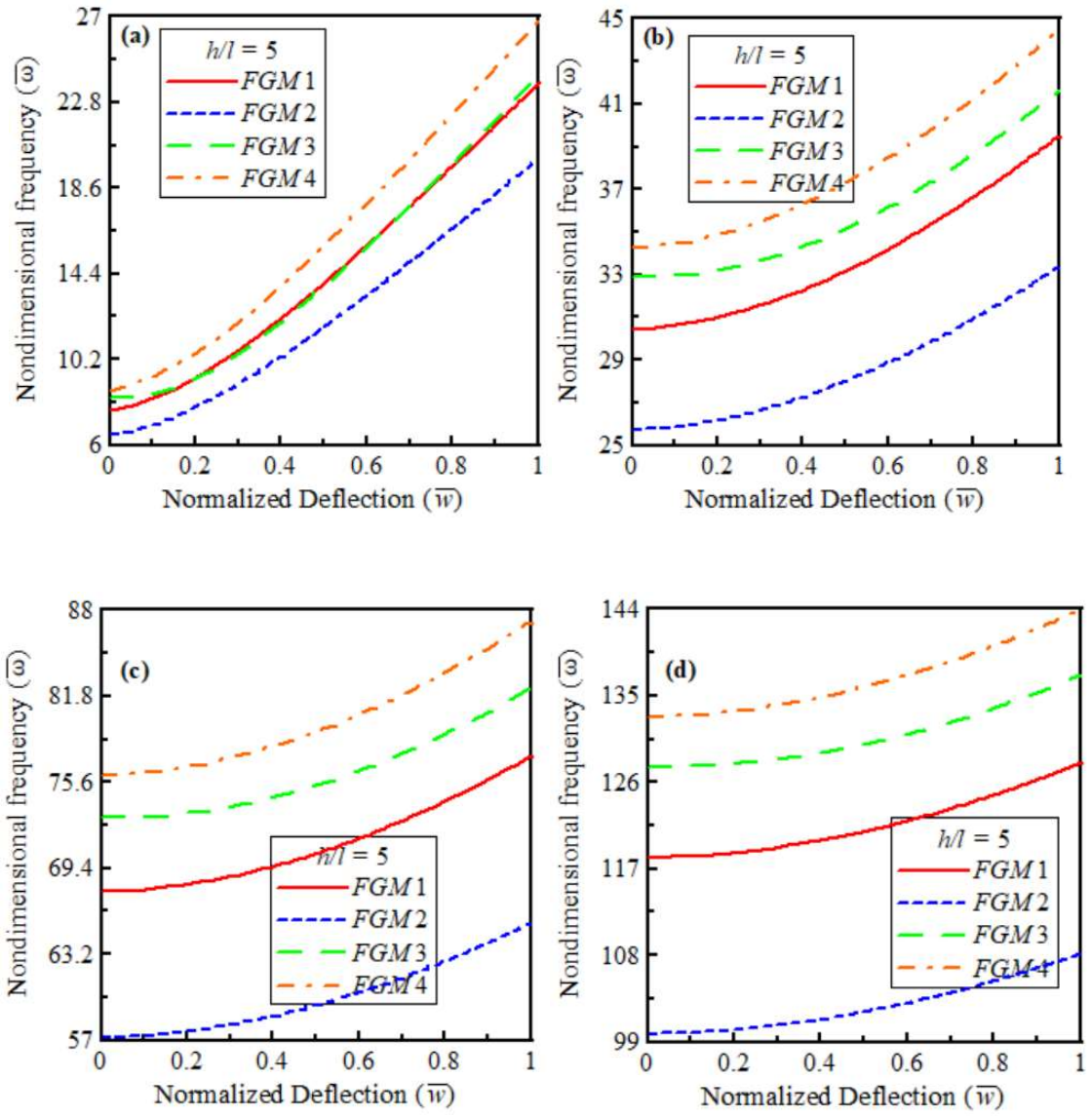

Fig. 4.12B: Effect of different FGM compositions on non-dimensional deflection-frequency curves for HH beams with *h/l*=5: (a) first mode, (b) second mode, (c) third mode, (d) fourth mode.

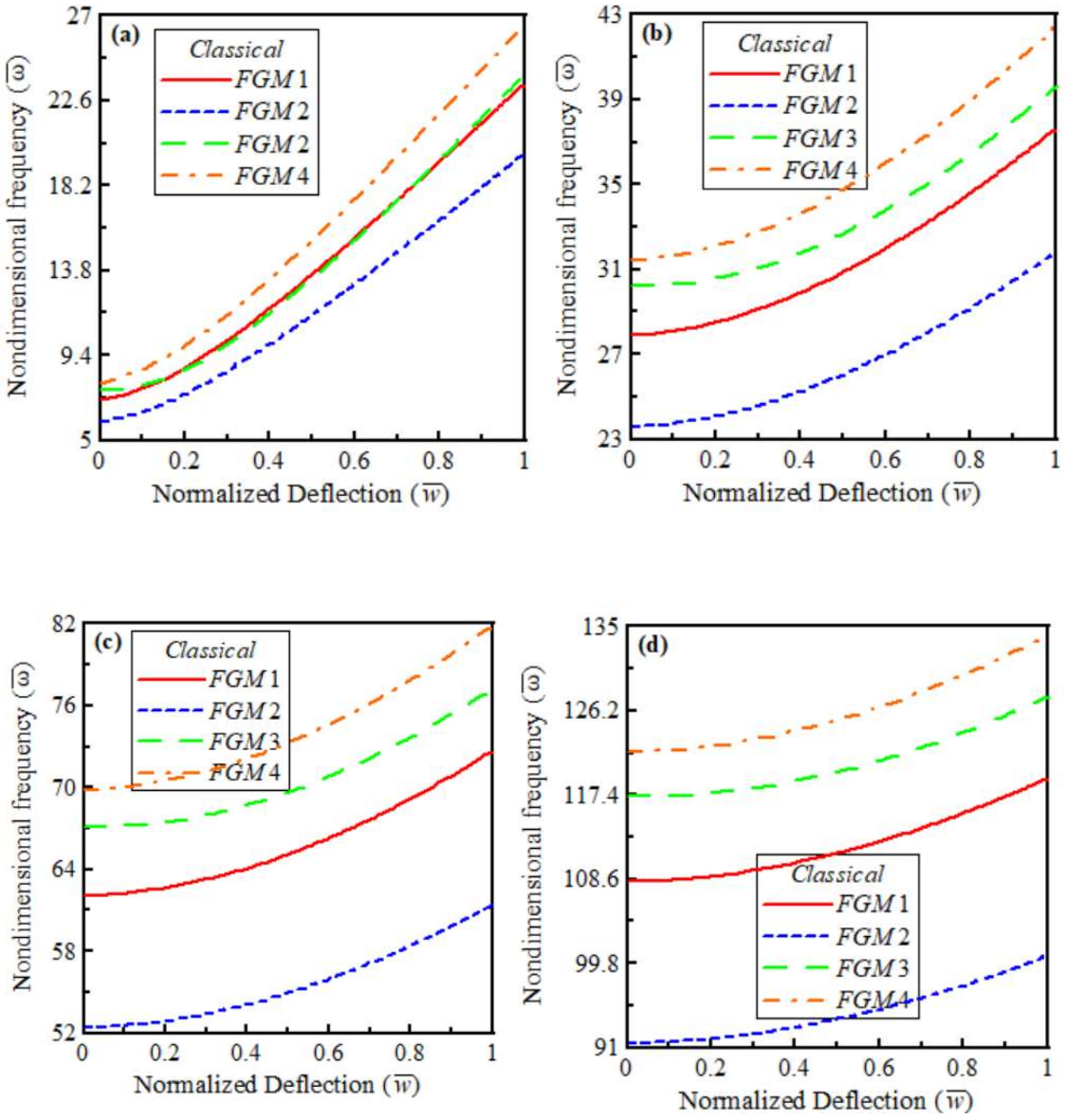

Fig. 4.12C: Effect of different FGM compositions on non-dimensional deflection-frequency curves for HH beams with l=0 (classical): (a) first mode, (b) second mode, (c) third mode, (d) fourth mode.

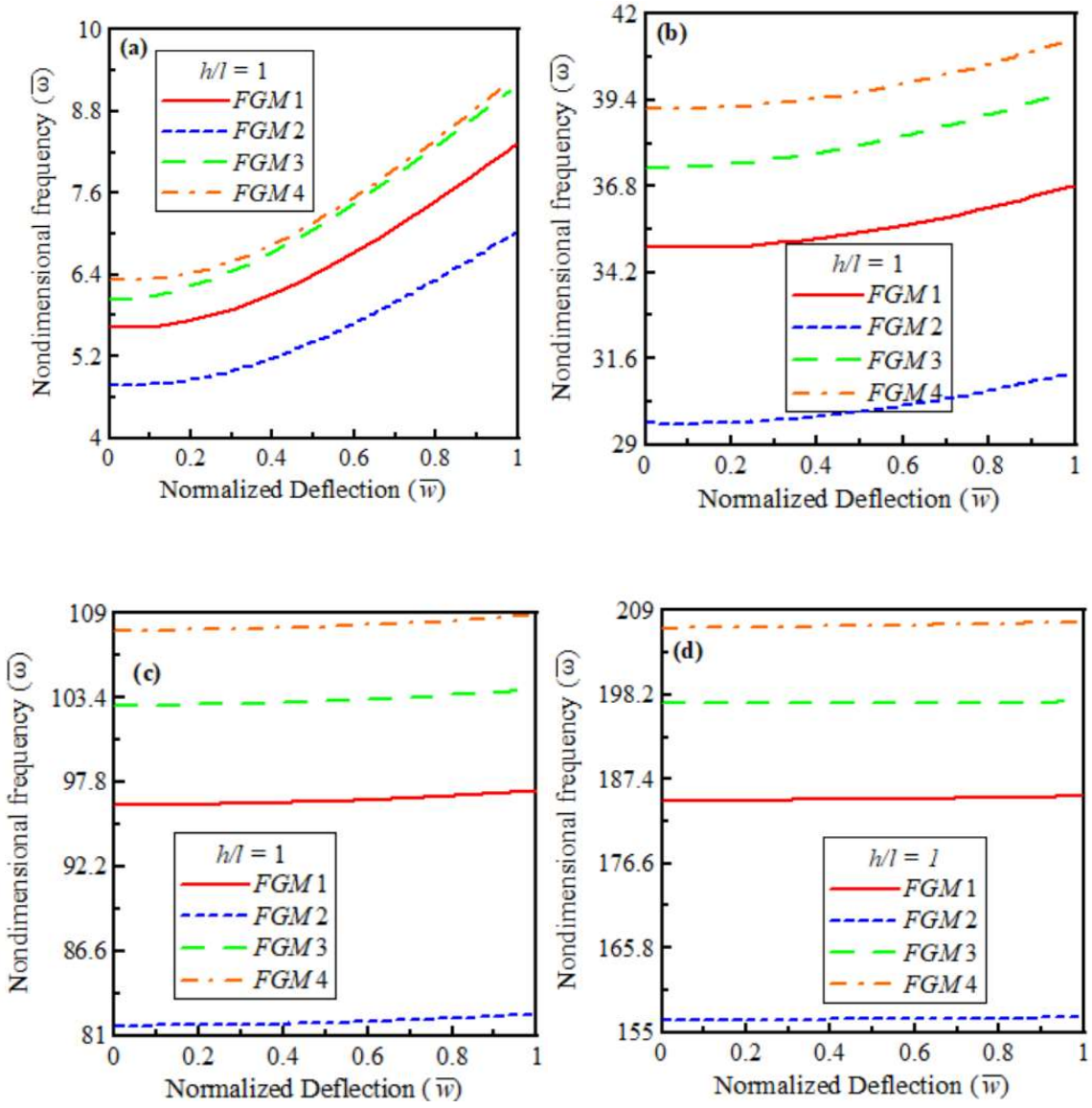

Fig. 4.13A: Effect of different FGM compositions on non-dimensional deflection-frequency curves for CF beams with h/l=1: (a) first mode, (b) second mode, (c) third mode, (d) fourth mode.

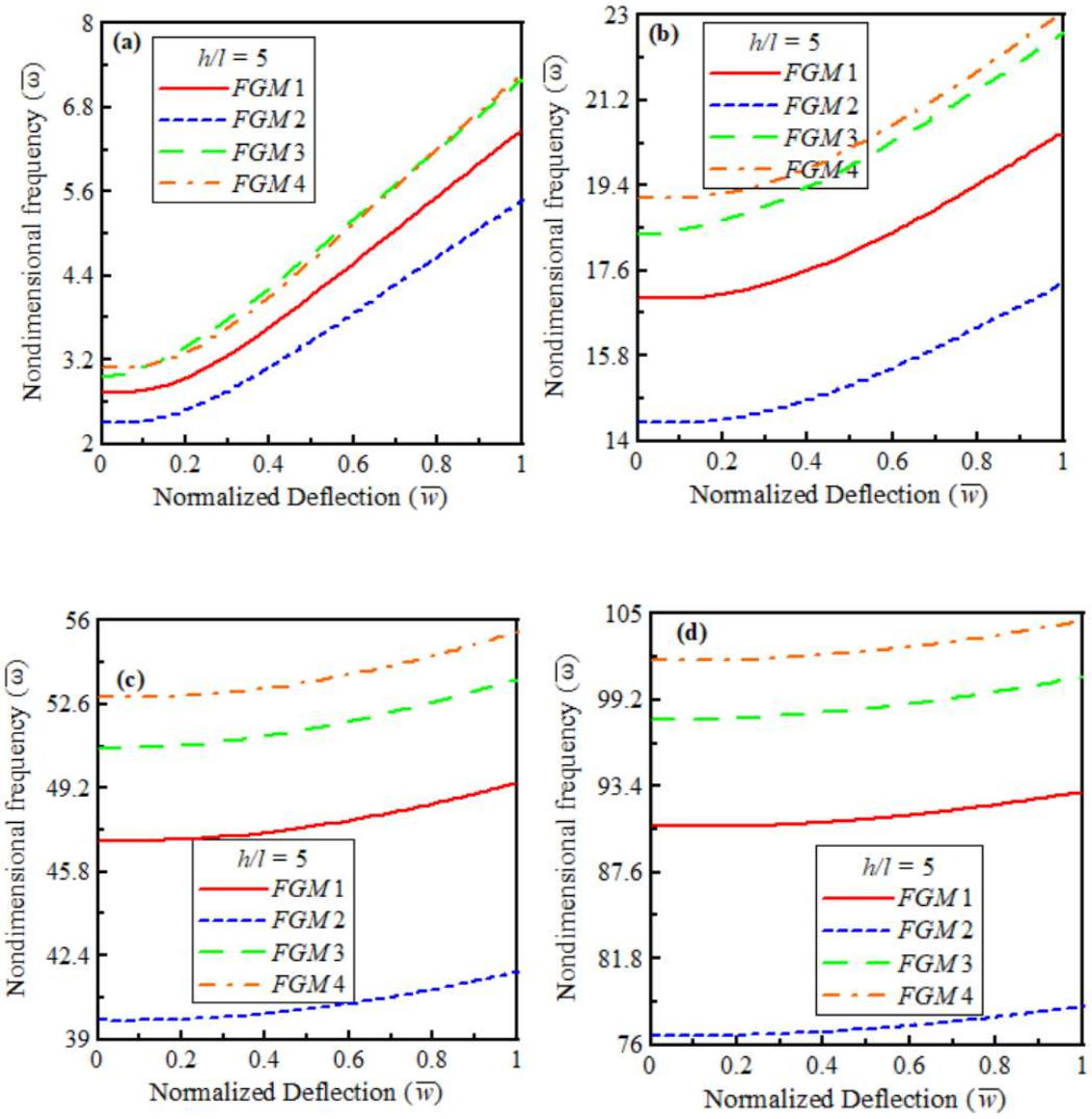

Fig. 4.13B: Effect of different FGM compositions on non-dimensional deflection-frequency curves for CF beams with *h/l*=5: (a) first mode, (b) second mode, (c) third mode, (d) fourth mode.

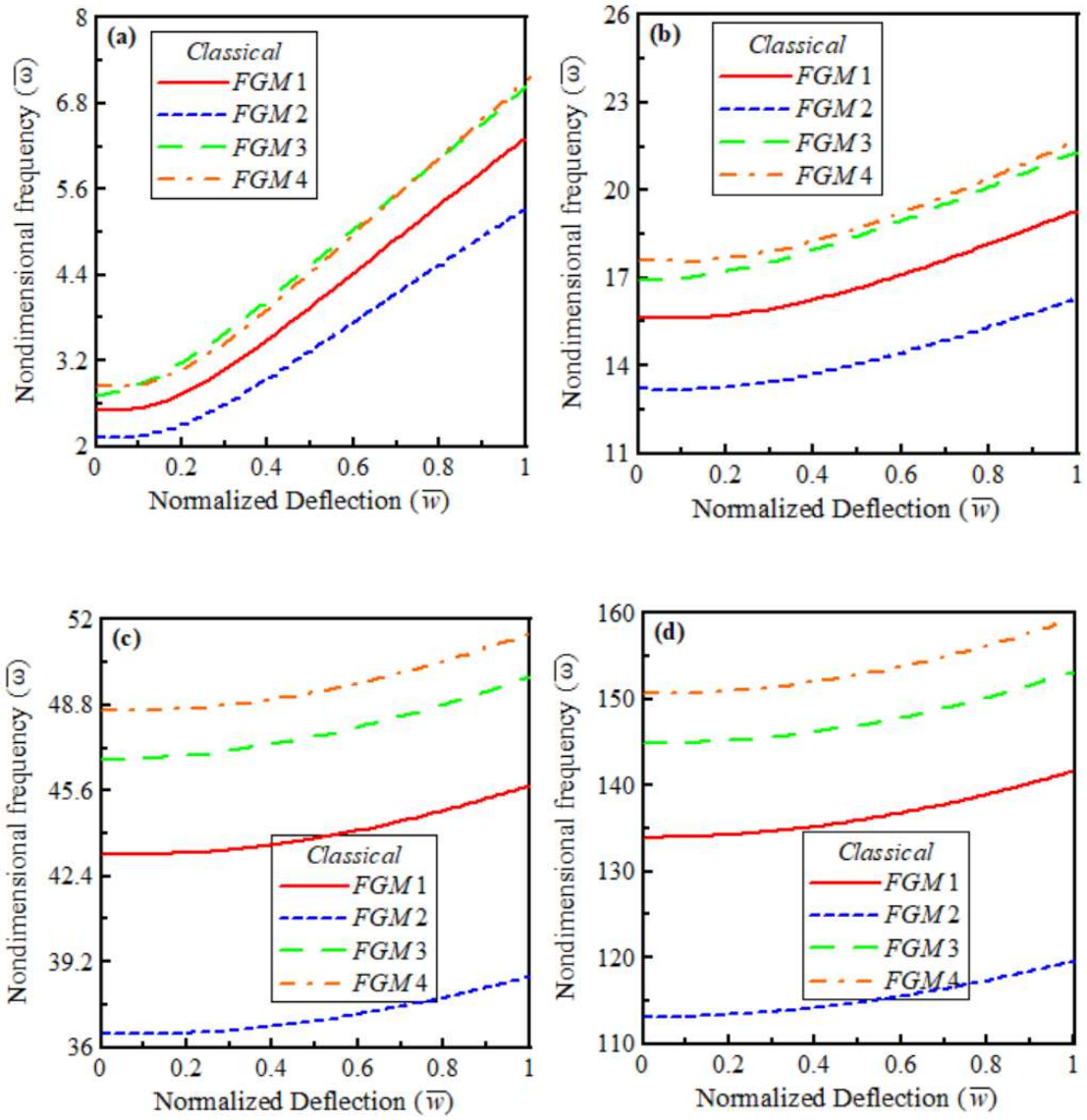

Fig. 4.13C: Effect of different FGM compositions on non-dimensional deflection-frequency curves for CF beams with l=0 (classical): (a) first mode, (b) second mode, (c) third mode, (d) fourth mode.

4.4 Chapter Summary

In this chapter we discussed the free vibration of Timoshenko microbeams made of functionally graded materials (FGMs). It presents a theoretical investigation using the von Kármán non-linear strain-displacement relationship and the Hamilton's principle to derive the governing equation for vibration. The study evaluates four different FGMs under various boundary conditions. The results are presented in normalized deflection-frequency plane for incorporating the size effect on natural frequency. Validation of the model is conducted against previous studies, demonstrating excellent agreement, and thereby validating the present model. The results are presented graphically as well as in tabulated form. The findings suggest that for any particular mode and h/l value, as material gradation index increases, the non-dimensional natural frequency deceases, and for any particular mode and particular material gradation index (k), natural frequency increases as size effect increases. The study provides valuable insights into the free vibration behaviour of FGM micro beams, elucidating the influence of material gradation, size-dependent thickness, and boundary conditions on the non-dimensional deflection-frequency behaviour.

"*This page is intentionally left blank*"

Chapter 5

CONCLUSIONS

5.1 Conclusions

Micro-beams, essential for high-precision measurements in technologies like atomic force microscopy (AFM) and various sensors, exhibit size-dependent behaviors that traditional continuum theories fail to capture. Non-classical continuum theories, such as modified couple stress theory (MCST) and nonlocal strain gradient theory, address these limitations. For micro- and nano-scale applications, functionally graded materials (FGMs) offer increased design flexibility, making them suitable for MEMS, micro-sensors, and micro-actuators.

Therefore, analyzing the static and dynamic behavior of functionally graded (FG) micro-beams is crucial for modeling and effectively using them in various microsystems. In this work, we have studied the nonlinear static deflection and free vibration behaviour of a Timoshenko FG micro-beam which is subjected to uniformly distributed load. In this analysis, we assumed that the beam follows the Timoshenko beam model and incorporated size effects using MCST. The governing equations for static behaviour are derived using the principle of minimum potential energy, while the governing equations for free vibration are derived using Hamilton's principle. These equations are nonlinear due to the incorporation of von Kármán-type nonlinearity in the classical strain expression. The solutions to the governing equations are obtained by approximating the displacement fields using the Ritz method. We have taken four different boundary conditions and four different FGMs into our consideration.

From our analysis, we have found that:

- For any given material gradation index (k) value, the micro-beam becomes more stiff with increasing size-effect, and that it is found to be maximum at h/l=1, but at h/l=10, the micro-effect almost disappears.

- When the material gradation index increases for a given value of the *h/l*, the stiffness of the beam decreases. This is because an increase in *k* results in a higher metal volume fraction within the beam. Since the metal component has a lower elastic modulus compared to the ceramic component, the beam becomes more elastically flexible.
- For a particular mode and particular material gradation index, natural frequency increases as size effect increases and it is maximum for *h/l* = 1, and deceases as the size effect decreases and approaches to the natural frequency of the classical beam at *h/l*=10.
- For a particular mode and given *h/l,* as the material gradation index increases, the non-dimensional natural frequency decreases. This decrease in natural frequency is due to the reduction in the beam's stiffness, which occurs because the material gradation leads to a higher proportion of the metal within the beam.
- As the material gradation index increases, the stiffness of the micro-beam decreases for most FGMs considered, except for FGM 3, where stiffness increases with the material gradation index.

5.2 Future Scope of Work

This study has shown that preloading the beam causes a hardening effect that raises the beam's natural frequency. The effects of temperature variations on the static and dynamic behaviour of micro-beams should be explored in future studies. To be more precise, examining the effects of temperature variations above and below room temperature on the mechanical characteristics and functionality of functionally graded micro-beams would offer a thorough grasp of how they behave in various thermal environments. This could entail examining the joint effects of preloading and thermal stresses on the natural frequency and stiffness, as well as investigating the possibility of thermally adjusting the properties of micro-beams in real-world applications. Furthermore, the study can be extended to include nonlocal theory of elasticity and strain gradient theory to address the size-effect.

Bibliography

Abadi M.M. and Daneshmehr A.R. (2014) An investigation of modified couple stress theory in buckling analysis of micro composite laminated Euler–Bernoulli and Timoshenko beams. *International Journal of Engineering Science* 75:40–53.

Abbasion S., Rafsanjani A., Avazmohammadi R. and Farshidianfar A. (2009) Free vibration of microscaled Timoshenko beams. *Applied Physics Letters* 95:143-122.

Akgöz B. and Civalek Ö.(2011) Strain gradient elasticity and modified couple stress models for buckling analysis of axially loaded micro-scaled beams. *International Journal of Engineering Science* 49:1268–1280.

Al-shujairi M. and Mollamahmutoğlu Ç. (2018) Dynamic stability of sandwich functionally graded micro-beam based on the nonlocal strain gradient theory with thermal effect. *Composite Structures* 201:1018–1030.

Ansari R., Gholami R. and Sahmani S. (2011) Free vibration analysis of size-dependent functionally graded microbeams based on the strain gradient Timoshenko beam theory. Composite Structures 94: 221-228.

Asghari M., Kahrobaiyan M.H. and Ahmadian M.T. (2010) A nonlinear Timoshenko beam formulation based on the modified couple stress theory. *International Journal of Engineering Science* 48:1749–1761.

Asghari M., Rahaeifard M., Kahrobaiyan M.H. and Ahmadian M.T. (2011) The modified couple stress functionally graded Timoshenko beam formulation. *Materials and Design* 32:1435–1443.

Babaeia H. and Eslamib M.R. (2022) Nonlinear bending analysis of size-dependent FG porous microtubes in thermal environment based on modified couple stress theory. *Mechanics Based Design of Structures and Machines* 50:2714-2735

Bhattacharya S. and Das D. (2019) Free vibration analysis of bidirectional-functionally graded and double tapered rotating micro-beam in thermal environment using modified couple stress theory. *Composite Structures* 215:471–492.

Cannizzaro F., Fiore I., Caddemi S. and Calio I. (2023) The exact distributional model for free vibrations of shear-bending multi-cracked Timoshenko beams. *European Journal of Mechanics/A Solids* 101:105-039.

Chen W., Li L. and Xu M. (2011) A modified couple stress model for bending analysis of composite laminated beams with first order shear deformation. *Composite Structures* 93:2723–2732.

Das D. (2018) A new tangent stiffness based formulation to study the free vibration behavior of transversely loaded Timoshenko beam with geometric non-linearity. *Journal of Vibration and Control* 24:1716-1728.

Das D., Sahoo P. and Saha K. (2008) Large-amplitude dynamic analysis of simply supported skew plates by a variational method. Journal of Sound and Vibration 313:246–267.

Esen I. (2020) Dynamics of size-dependant Timoshenko micro beams subjected to moving loads. *International Journal of Mechanical Sciences* 175:105-501.

Fu Y., Du H. and Zhang S. (2003) Functionally graded TiN/TiNi shape memory alloy films. *Materials Letters* 57:2995–2999.

Ghasemi A.R. and Mohandes M. (2020) Free vibration analysis of micro and nano fiber-metal laminates circular cylindrical shells based on modified couple stress theory. *Mechanics of Advanced Materials and Structures* 27:43-54.

Gul U. and Aydogdu M. (2021) Dynamic analysis of functionally graded beams with periodic nanostructures. *Composite Structures* 257:113-169.

Habibi B., Benib Y.T. and Mehraliana F. (2019) Free vibration of magneto-electro-elastic nanobeams based on modified couple stress theory in thermal environment. *Mechanics of Advanced Materials and Structures* 26:601-613.

Hariz M., Marrec L.L. and Lerbet J. (2022) Buckling of Timoshenko beam under two-parameter elastic foundations. *International Journal of Solids and Structures* 244-245:111-583.

Hemmatnezhad M., Ansari R. and Rahimi G.H. (2013) Large-amplitude free vibrations of functionally graded beams by means of a finite element formulation. *Applied Mathematical Modelling* 37:8495–8504.

Hendou R.H. and Mohammadi A.K. (2014) Transient analysis of nonlinear Euler–Bernoulli micro-beam with thermoelastic damping, via nonlinear normal modes. *Journal of Sound and Vibration* 333:6224–6236.

Jia X.L., Ke L.L., Feng C.B., Yang J. and Kitipornchai S. (2015) Size effect on the free vibration of geometrically nonlinear functionally graded micro-beams under electrical actuation and temperature change. *Composite Structures* 133:1137–1148.

Karparvarfard S.M.H., Asghari M. and Vatankhah R. (2015) A geometrically nonlinear beam model based on the second strain gradient theory. *International Journal of Engineering Science* 91:63–75.

Ke L.L. and Wang Y.S. (2011) Size effect on dynamic stability of functionally graded microbeams based on a modified couple stress theory. *Composite Structures* 93:342–350.

Ke L.L., Wang Y.S. Yang J. and Kitipornchai S. (2012) Nonlinear free vibration of size-dependent functionally graded microbeams. *International Journal of Engineering Science* 50:256–267.

Khorshidi M.A. (2018) The material length scale parameter used in couple stress theories is not a material constant. *International Journal of Engineering Science* 133:15-25.

Kong S., Zhou S., Nie Z. and Wang K. (2008) The size-dependent natural frequency of Bernoulli–Euler micro-beams. *International Journal of Engineering Science* 46:427–437.

Kong S., Zhou S., Nie Z. and Wang K. (2009) Static and dynamic analysis of micro beams based on strain gradient elasticity theory. *International Journal of Engineering Science* 47:487–498.

Li T., Tang J., Hu Z., wand Z. and Fu Z. (2023) Three-dimensional vibration investigation of the thin web gear pair based on Timoshenko beam. *Thin-Walled Structures* 184:110-507.

Li Z., He Y., Lei J., Han S., Guo S. and Liu D. (2018) A standard experimental method for determining the material length scale based on modified couple stress theory. *International Journal of Mechanical Science* 141:198–205.

Liu Y., Nguyen L.T.K., Li X. and Feene A. (2024) A Timoshenko-Ehrenfest beam model for simulating Langevin transducer dynamics. *Applied Mathematical Modelling* 131:363–380.

Loya J.A., Aranda-Ruiz J. and Zaera R. (2022) Natural frequencies of vibration in cracked Timoshenko beams within an elastic medium. *Theoretical and Applied Fracture Mechanics* 118-103:257.

Ma H.M., Gao X.L. and Reddy J.N. (2008) A microstructure-dependent Timoshenko beam model based on a modified couple stress theory. *Journal of the Mechanics and Physics of Solids* 56:3379–3391.

Mao Y.Q., Ai S.G., Fang D.N., Fu Y. M. and Chen C.P. (2013) Elasto-plastic analysis of micro FGM beam basing on mechanism-based strain gradient plasticity theory. *Composite Structures* 101:168–179.

Mindlin R.D. (1964) Micro-structure in linear elasticity. *Archive for Rational Mechanics and Analysis* 16:51–78.

Mindlin R.D. and Tiersten H.F. (1962) Effects of couple-stresses in linear elasticity. *Archive for Rational Mechanics and Analysis* 11:415–448.

Mohammadabadi M., Daneshmehr A.R. and Homayounfard M. (2015) Size-dependent thermal buckling analysis of micro composite laminated beams using modified couple stress theory. *International Journal of Engineering Science* 92:47–62.

Mohanty M., Maity R., Pradhan M. and Dash P. (2023) Parametric stability of Timoshenko taper sandwich beam on Pasternak foundation. *Materials Today: Proceedings* DOI: 10.1016/j.matpr.2023.03.735.

Molina-Villegas J.C., Ortega J.E.B. and Soto S.B. (2024) Closed-form solutions for axially non-uniform Timoshenko beams and frames under static loading. *Composite Structures* 337:118-078.

Nguyen H.X, Lee J., Vo T.P. and Lanc D. (2016) Vibration and lateral buckling optimisation of thin-walled laminated composite channel-section beams. *Composite Structures*143:84–92.

Nguyen N.D., Nguyen T.K., Thai H.T. and Vo T.P. (2018) A Ritz type solution with exponential trial functions for laminated composite beams based on the modified couple stress theory. *Composite Structures* 191:154–167.

Noori J., Fariborz S.J. and Vafa J.P. (2016) A higher-order micro-beam model with application to free vibration. *Mechanics of Advanced Materials and Structures* 23:443-450

Park S. K. and Gao X. L. (2006) Bernoulli–Euler beam model based on a modified couple stress theory. *Journal of Micromechanics and Microengineering* 16:2355–2359.

Patil R., Joladarashi S. and Kadoli R. (2023) Effect of porosity and viscoelastic boundary conditions on FG sandwich beams in thermal environment: Buckling and vibration studies. *Structures* 56:105-001.

Paul A. and Das D. (2016) Free vibration analysis of pre-stressed FGM Timoshenko beams under large transverse deflection by a variational method. *Engineering Science and Technology, an International Journal* 19:1003–1017.

Rahimi G.H., Gazor M.S., Hemmatnezhad M. and Toorani H. (2013) On the postbuckling and free vibrations of FG Timoshenko beams. *Composite Structures* 95:247–253.

Reddy J.N. (2011) Microstructure-dependent couple stress theories of functionally graded beams. *Journal of the Mechanics and Physics of Solids* 59:2382–2399.

Rodríguez-Cruz W., Torres-Guzmán J.C. and Díaz-de-Anda A. (2023) Degenerate normal-mode states above the cutoff frequency as analogs of the thickness-shear mode for finite Timoshenko–Ehrenfest beams with free end. *Journal of Sound and Vibration* 554:117-661.

Romanoff J., Reddy J.N. and Jelovica J. (2016) Using non-local Timoshenko beam theories for prediction of micro- and macro-structural responses. *Composite Structures* 156:410–420.

Sabzehzar S., Noorollah M., Ali S. and Tajmir R.H. (2024) Proposing a practical equivalent Timoshenko beam for analysis of truss structures. *Structures* 63:106-401.

Sahmani S., Aghdam M.M. and Rabczuk T. (2018) Nonlinear bending of functionally graded porous micro/nano-beams reinforced with graphene platelets based upon nonlocal strain gradient theory. *Composite Structures* 186:68–78.

Saimi A., Bensaid I. and Civalek O. (2023) A study on the crack presence effect on dynamical behaviour of bi-directional compositionally imperfect material graded micro beams. *Composite Structures* 316:117-032.

Salamat-talab M., Nateghi A. and Torabi J. (2012) Static and dynamic analysis of third-order shear deformation FG micro beam based on modified couple stress theory. *International Journal of Mechanical Sciences* 57:63–73.

Shafiei N. and Kazemi M. (2017) Nonlinear buckling of functionally graded nano-/micro-scaled porous beams. *Composite Structures* 178:483–492.

Shafiei N., Kazemi M. and Ghadiri M. (2016) Nonlinear vibration of axially functionally graded tapered Microbeams. *International Journal of Engineering Science* 102:12–26.

Shames I.H. and Dym C.L. (2009) *Energy and Finite Element Methods in Structural Mechanics*. Delhi:New Age International Publishers.

Shan J., Zhuang C. and Loong C.N. (2023) Parametric identification of Timoshenko-beam model for shear-wall structures using monitoring data. *Mechanical Systems and Signal Processing* 189:110-100.

Sharma J.N. and Grover D. (2011) Thermoelastic vibrations in micro-/nano-scale beam resonators with voids. *Journal of Sound and Vibration* 330:2964–2977.

Sharma J.N. and Kaur R. (2014) Transverse vibrations in thermoelastic-diffusive thin micro-beam resonators. *Journal of Thermal Stresses*37:1265–1285.

Shen H.S. (2009) *Functionally Graded Materials Nonlinear Analysis of Plates and Shells*. USA:CRC Press.

Shen J.P. and Li C. (2017) A semi-continuum-based bending analysis for extreme-thin micro/nano-beams and new proposal for nonlocal differential constitution. *Composite Structures* 172:210–220.

Simsek M. (2016) Nonlinear free vibration of a functionally graded nanobeam using nonlocal strain gradient theory and a novel Hamiltonian approach. *International Journal of Engineering Science* 105:12–27.

Sobhy M. and Zenkour A.M. (2020) The modified couple stress model for bending of normal deformable viscoelastic nanobeams resting on visco-Pasternak foundations. *Mechanics of Advanced Materials and Structures* 27:525-538.

Stolken J.S. and Evans A.G. (1998) Microbend test method for measuring the plasticity length scale. *Journal of Acta Materialia* 46:5109–5115.

Taati E. (2018) On buckling and post-buckling behavior of functionally graded micro-beams in thermal environment. *International Journal of Engineering Science* 128:63–78.

Tajalli S.A., Rahaeifard M., Kahrobaiyan M.H., Movahhedy M.R., Akbari J. and Ahmadian M.T. (2013) Mechanical behavior analysis of size-dependent micro-scaled functionally graded Timoshenko beams by strain gradient elasticity theory. *Composite Structures* 102:72–80.

Torres-Guzmán J.C., Díaz-de-Anda A., Martínez-Argüello A.M. and Arriaga J. (2024) Exact closed forms for the transfer matrix of free oscillations in finite periodic Timoshenko–Ehrenfest beams. *Results in Physics* 59:107-569.

Toupin R.A. (1962) Elastic materials with couple stresses. *Archive for Rational Mechanics and Analysis* 11:385–414.

Wriggers P. (2023) A locking free virtual element formulation for Timoshenko beams. *Computer Methods Applied Mechanics Engineering* 417:116-234.

Xu L. and Yang Q. (2015) Multi-field coupled dynamics for a micro beam. *Mechanics Based Design of Structures and Machines* 43: 57–73.

Xu Z., Zhang L., Xu R., Chen W. and Wang G. (2024) Static, dynamic and buckling behavior of functionally graded beams with tunable inclusions. *International Journal of Solids and Structures* 288:112-620.

Yang F, Chong A.C.M., Lam D.C.C. and Tong P (2002) Couple stress based strain gradient theory for elasticity. *International Journal of Solids and Structures* 39:2731–2743.

Yang W., He D. and Chen W. (2017) A size-dependent zigzag model for composite laminated micro beams based on a modified couple stress theory. *Composite Structures* 179:646–654.

Yassopoulos C., Reddy J.N. and Mortari D. (2023) Analysis of nonlinear Timoshenko–Ehrenfest beam problems with von Kármán nonlinearity using the Theory of Functional Connections. *Mathematics and Computers in Simulation* 205:709–744.

Yee K., Khaniki H.B., Ghayesh M.H. and Ng Ching-Tai. (2023) Free vibrations of cracked functionally graded graphene platelets reinforced Timoshenko beams based on Hu-Washizu-Barr variational method. *Engineering Structures* 293:116-587.

Yue Y.M., Xu K.Y. and Chen T. (2016) A micro scale Timoshenko beam model for piezoelectricity with flexoelectricity and surface effects. *Composite Structures* 136:278–286.

Zandekarimi S., Asadi B. and Rahaeifard M. (2018) Size dependent thermal buckling and postbuckling of functionally graded circular microplates based on modified couple stress theory. *Journal of Thermal Stresses* 41:1-16.

Zhang L., Xu Z., Gao M., Xu R. and Wang G. (2023) Static, dynamic and buckling responses of random functionally graded beams reinforced by graphene platelets. *Engineering Structures*. 291:116-476.

“This page is intentionally left blank”

Publications

- Samrat and Das D. (2024) Non-linear static deflection analysis of a functionally graded micro-beam based on modified couple stress theory. *2nd International Conference on Mechanical Engineering (INCOM 24)*, Paper Id: INCOM 221, 5-6 January 2024, Jadavpur University, Kolkata.